Modeling and Optimization of Energy Pile Systems for Enhanced Efficiency in Sustainable Building Applications

How can the efficiency and reliability of energy pile system be enhanced?

A.Maras

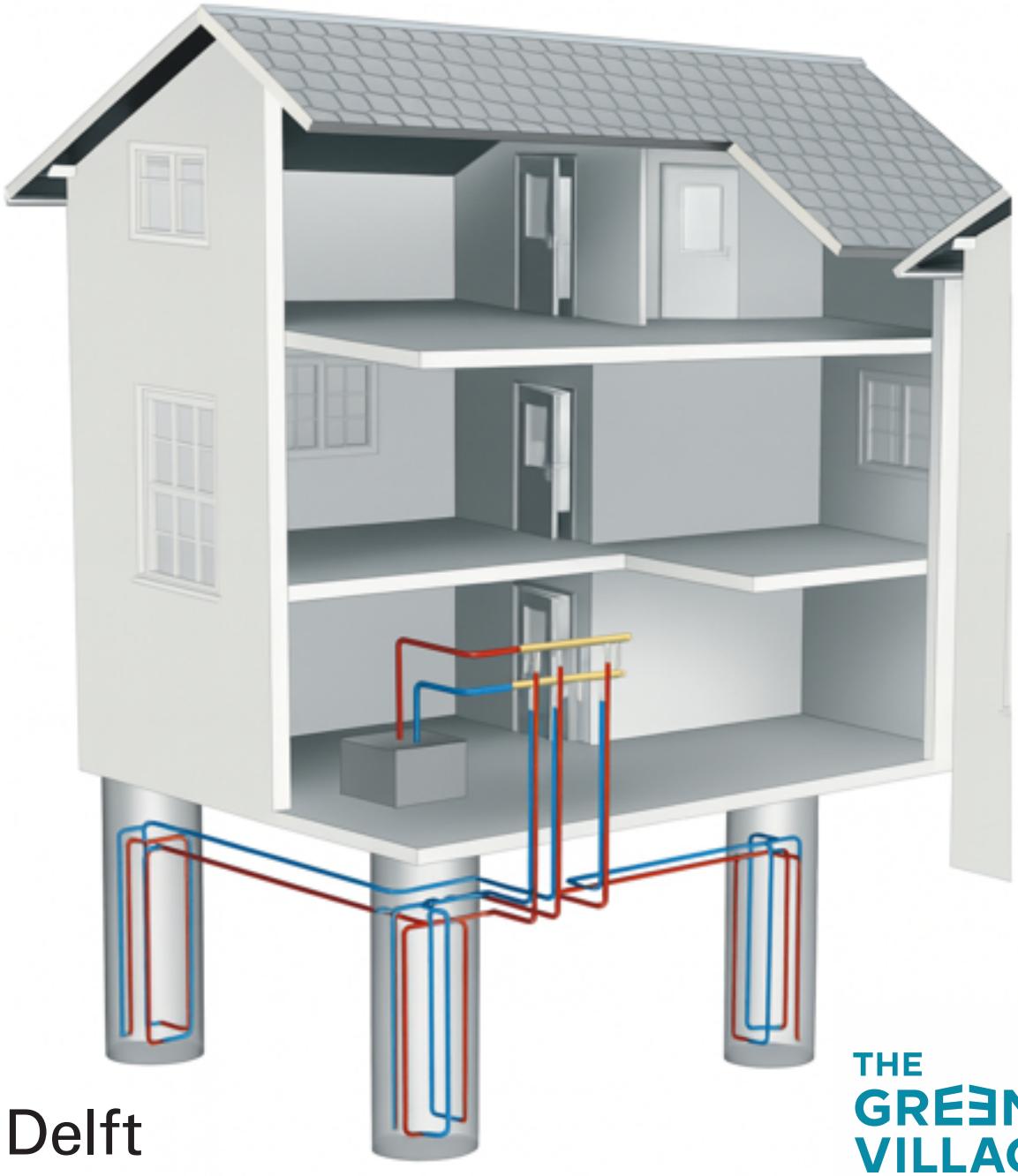

TU Delft

THE GREEN VILLAGE

Modeling and optimization of energy pile systems for enhanced efficiency in sustainable building applications

How can the efficiency and reliability of energy pile system be enhanced?

by

A.Maras

Student Number:	5862175
Chairman of Thesis Committee:	Prof. dr. ir. P. J. Vardon
Daily Supervisor:	Dr. A. Daniilidis
Thesis Committee Member:	Dr. ir. J. M. Bloemendal
Daily Advisor :	Dr. S. Hashemi
Project Duration:	December 2024 – September 2025
Faculty:	Faculty of Civil Engineering and Geosciences

TU Delft

THE GREEN VILLAGE

Preface

This thesis presents the results of my graduation project for the Master of Science in Sustainable Energy Technology at Delft University of Technology, carried out in collaboration with The Green Village at the TU Delft Campus.

Over the past eight months, I have conducted research on a promising technology that can contribute significantly to the decarbonization of heating and cooling systems, while also reducing their electricity consumption. This technology addresses critical challenges faced today and highlights the growing need for solutions that prioritize environmental sustainability and preservation.

From TU Delft, I would like to sincerely thank the members of my graduation committee. Without their guidance and feedback, this research would not have reached the same quality and depth, nor would I have gained the knowledge and results achieved throughout this project.I am especially grateful to Prof. Phil Vardon, who served as Chairman of my thesis committee. Phil, thank you for giving me the opportunity to work with you on such an interesting topic and, more importantly, for the valuable guidance you provided on how to conduct thorough and detailed research. Your constructive feedback greatly improved both my work and my academic development.I would also like to extend my gratitude to Prof. Alexandros Daniilidis, who generously shared his expertise in numerical modelling and dedicated time to discuss the model and its various aspects with me. Moreover, I would like to thank Prof. Martin Bloemendal for his constructive feedback and for kindly accepting to serve as a member of my examination committee.A very special thanks goes to Dr. Amirhossein Hashemi. Amir, our weekly collaboration was an essential part of this research, and without it, the quality of this work would not have been the same. I deeply appreciate your effort, support, and the help you provided throughout the process. I truly enjoyed our collaboration—not only because of your knowledge, but also because of the excellent communication and connection we developed. It was a joy working with you.

This project would not have been possible without the contribution of my colleagues at The Green Village. Thank you all for welcoming me and making me feel comfortable in the working environment. In particular, I would like to thank Marijn Leeuwenberg, who supported my research by providing essential documentation and assistance that enabled me to continue and advance my work.

Finally, I am deeply grateful to my family for supporting me throughout this journey and for giving me the opportunity to pursue my MSc at TU Delft. I also wish to thank my friends in Delft and in Greece for standing by me in moments of joy and in times of difficulty.

I sincerely hope you enjoy reading this thesis as much as I enjoyed conducting the research

A.Maras
Delft, September 2025

Abstract

The energy crisis and climate change, is creating an urgent need for sustainable and energy-efficient solutions. A significant portion of global energy consumption comes from households. Within this sector, the largest share is used for space heating and cooling. Therefore, efforts to reduce energy usage and cut carbon emissions should primarily target heating and cooling systems. A promising solution to this challenge lies in harvesting shallow geothermal energy through technologies such as energy piles, which have a multifunctional role to the building.

Energy piles are a specialized form of Borehole Thermal Energy Storage (BTES) systems that utilize shallow geothermal energy by taking advantage of the ground's stable temperature throughout the year. They are gaining popularity as an efficient solution for both heating and cooling, primarily because they serve a dual function within a building. On the one hand, they act as heat exchangers, enabling the transfer of thermal energy to and from the ground. On the other hand, they provide structural support, as they are typically constructed from reinforced concrete. This multifunctional role makes them a cost-effective choice and reduces the initial costs investments. These systems are commonly integrated with Ground Source Heat Pumps (GSHPs), which facilitate the exchange of thermal energy between the energy piles and the circulating fluid within the system. Their high Coefficient of Performance (COP) and environmentally friendly operation contribute positively to the transition towards more sustainable energy solutions.

This research focuses on an existing energy pile system located beneath a building on the TU Delft campus, which is responsible for covering the building's heating and cooling demands. The main objective of this research is to assess how the efficiency and reliability of this system can be improved through the implementation of advanced control strategies. To achieve this, a precise simulation model was developed to capture the underlying physical processes and monitor key performance indicators.Energy balance is a key metric and evaluation point for the system that secures the efficiency and sustainability of it. Additionally, various scenarios with different operational parameters were designed to evaluate the system's capabilities and performance.

The main findings initially indicated that the heating load is higher than the cooling load, revealing a significant imbalance. By creating various scenarios with different temperature setpoints, heating and cooling months, and durations of heating and cooling modes, an energy balance was achieved. However, the system was still unable to adequately cover the energy needs of the building during winter. Scenarios that utilized solar gains —by opening the building's sunblinds— enabled the heating and cooling system to supply the majority of the heating load during winter. This aligns with one of the main goal of the system while maintaining energy balance throughout the year. Among the scenarios evaluated, scenario 5 demonstrated the highest heating and cooling energy delivery. According to performance evaluations, it also consumed the least electricity among the compared scenarios. Additionally, Scenario 5 provided the highest levels of visual and thermal comfort for occupants, as the sunblinds remained open during non-operational months. The system was found capable of operating under loads 50% higher than normal, although these levels push its operational limits. Moreover, it was observed that the energy piles system can store surplus energy during summer and completely cover the heating demand of a neighboring apartment of 60 m^2.

The thermal plume interaction is investigated thoroughly and shows the rate and the magnitutude of the expansion or contraction of those. It was observed that energy is lost due to the open boundary with the ambient air temperature but varies between the scenarios. More details will be discussed in the following sections.

Contents

List of Figures

List of Tables

Nomenclature

Abbreviations

Abbreviation	Definition
ASHP	Air Source Heat Pumps
BTES	Borehole Thermal Energy Storage System
CCC	Co-Creation Center
COP	Coefficient of Performance
EP	Energy Piles
GHE	Ground Heat Exchanger
GSHP	Ground Source Heat Pumps
HDPE	High Density Polyethylene
ILS	Infinite Line Source
SPF	Seasonal Performance Factor
TES	Thermal Energy Storage
TIR	Thermal Imbalance Ratio

Symbols

Symbol	Definition	Unit
V	Velocity	[m/s]
T	Temperature	[$\circ$C]
T_0	Initial ground temperature	[$\circ$C]
k	Hydraulic Conductivity	[W/m/K]
c_p	Specific Heat Capacity	[J/kg/K]
$c_{\text{p,fluid}}$	Specific Heat Capacity of fluid	[J/kg/K]
$c_{\text{p,HDPE}}$	Specific Heat Capacity of HDPE	[J/kg/K]
$c_{\text{p,ground}}$	Specific Heat Capacity of ground	[J/kg/K]
$c_{\text{p,concrete}}$	Specific Heat Capacity of concrete	[J/kg/K]
T_in	Inlet temperature of working fluid	[$\circ$C]
T_{Out}	Outlet Temperature of working fluid	[$\circ$C]
Q	Power Demand	[W]
$Q_{\text{Extracted}}$	Power extracted from the subsurface ground	[W]
Q_{Injected}	Power injected to the subsurface ground	[W]
l	Length of borehole	[m]
C	Volumetric heat capacity of the ground	[J/(m^3·K)]
U	Overall heat transfer coefficient	[W/(m^2·K)]
$U_{\text{triple-glazed facades}}$	Triple-glazed facades Overall heat transfer coefficient	[W/(m^2·K)]
U_{Ceiling}	Ceiling Overall heat transfer coefficient	[W/(m^2·K)]
A	Heat transfer surface area of building	[m^2]
ΔT	Temperature difference	[K]
ρ	Density	[kg/m^3]
ρ_{fluid}	Density of working fluid	[kg/m^3]
ρ_{HDPE}	Density of Polyethylene pipe	[kg/m^3]
ρ_{ground}	Density of ground	[kg/m^3]
ρ_{concrete}	Density of concrete	[kg/m^3]

Symbol	Definition	Unit
μ_{fluid}	Dynamic Viscosity [Pa*s]	
λ	Thermal Conductivity	[W/m/K]
λ_{fluid}	Thermal Conductivity of working fluid	[W/m/K]
λ_{HDPE}	Thermal Conductivity of HDPE	[W/m/K]
λ_{ground}	Thermal Conductivity of ground	[W/m/K]
$\lambda_{concrete}$	Thermal Conductivity of concrete	[W/m/K]

1

Introduction

1.1. Sustainable Energy and the Role of Energy Piles

The global energy crisis, coupled with concerns about climate change and fossil fuel depletion, has created the need for sustainable energy solutions. Traditional energy sources, such as fossil fuels, are major contributors to the increase in carbon dioxide (CO_2) emissions, which contribute significantly to climate change and environmental degradation. The built environment plays an important role in energy consumption, with households in the European Union(EU) alone accounting for 25.8% of the final energy use [9]. A remarkable 63.5 % of this household energy demand is dedicated to heating, cooling and hot water production. This signifies the urgent need for efficient and sustainable solutions for heating and cooling to reduce energy consumption and carbon footprint in buildings. The following graph provides a visual representation of household energy consumption, illustrating the huge amount of energy needed for heating and cooling purposes and the growing need for a sustainable energy solution in this particular sector.

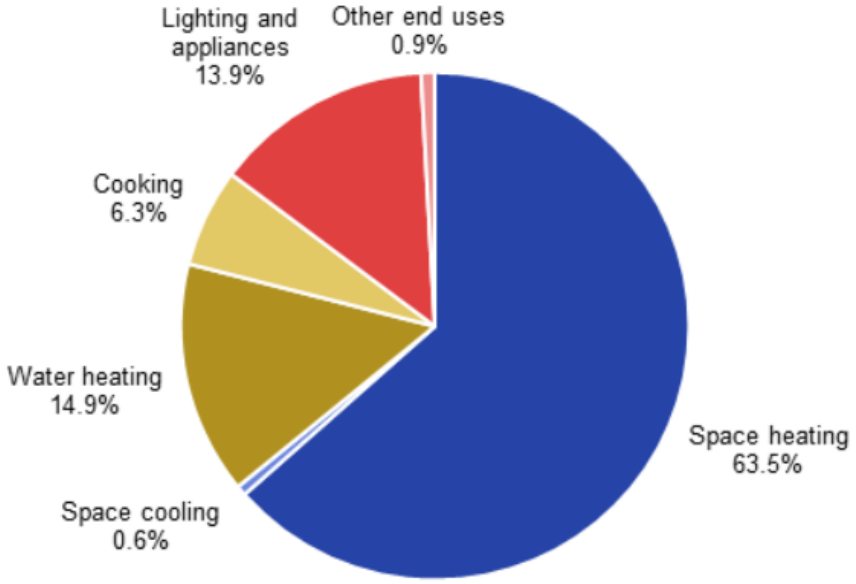

Figure 1.1: Final energy consumption in households EU at year 2022(Source: Eurostat)

A promising sustainable solution to address the high energy demand for heating and cooling is the geothermal energy. Geothermal energy is an efficient, reliable and low-carbon alternative that could replace the fossil-fuel operating systems. Furthermore, has a continuous and stable thermal output unlike the wind and solar energy which are depending from the weather conditions. Therefore these characteristics making it suitable for delivering heating and cooling in buildings. Among geothermal technologies, ground source heat pumps (GSHPs) have gained recognition due to their high energy efficiency and the ability to significantly reduce CO_2 emissions. They have a higher coefficient of performance (COP) compared with the air-source heat pumps (ASHP) because of the temperature of the ground, which is relatively stable throughout the year [1]. The GSHPs rely on ground heat exchangers (GHEs) to extract or inject thermal energy either from or to the earth, providing sustainable thermal regulation throughtout the year.

One of the most innovative and efficient application of geothermal energy in buildings is the energy pile system. Energy piles integrate geothermal heat exchangers into foundation piles and simultaneously offer structural stability and operate as a heat transfer medium.They are an evolved version of borehole heat exchangers (BHEs) and their dual-purpose make them particularly advantageous especially in urban environments where the space is limited.Researches have shown that the energy pile can reach higher heat transfer efficiency under heating and cooling conditions compared to a borehole heat exchanger [35].Moreover, the capital costs are reduced compared with the common borehole heat exchangers (BHEs) as they utilize the pre-existing foundation infrastructure avoiding the need for additional drilling. The image below illustrates an energy pile system underneath a building to visualize the operational and structural configuration of it.

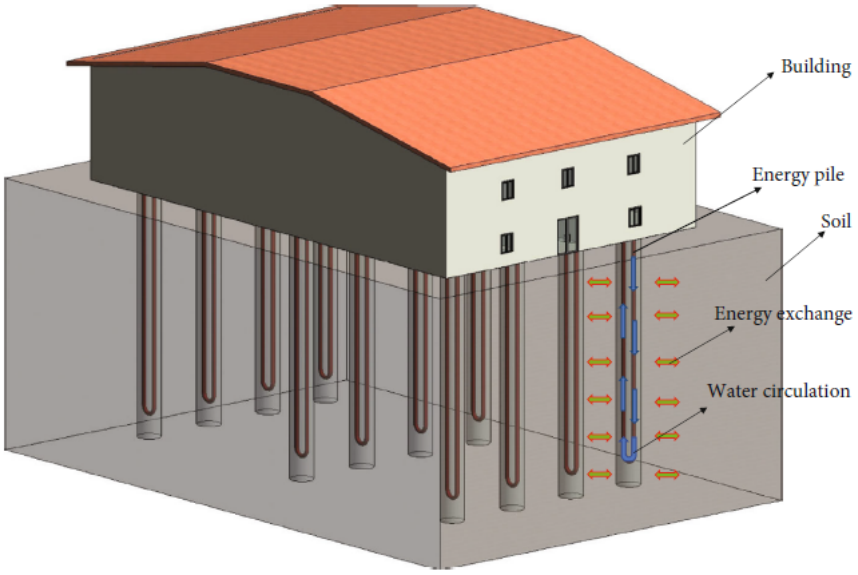

Figure 1.2: Energy pile system configuration [36]

The technology of energy pile systems is evolving and the number of projects worldwide is the evidence. The scientific community along with the governments have recognized the potential of energy piles and the benefits that they offer. According to recent studies, the number of projects that energy piles are involved is increasing worldwide in the past two decades. Figure 1.3 depicts the increasing trend of energy pile projects and the CO_2 savings that derive from those projects.

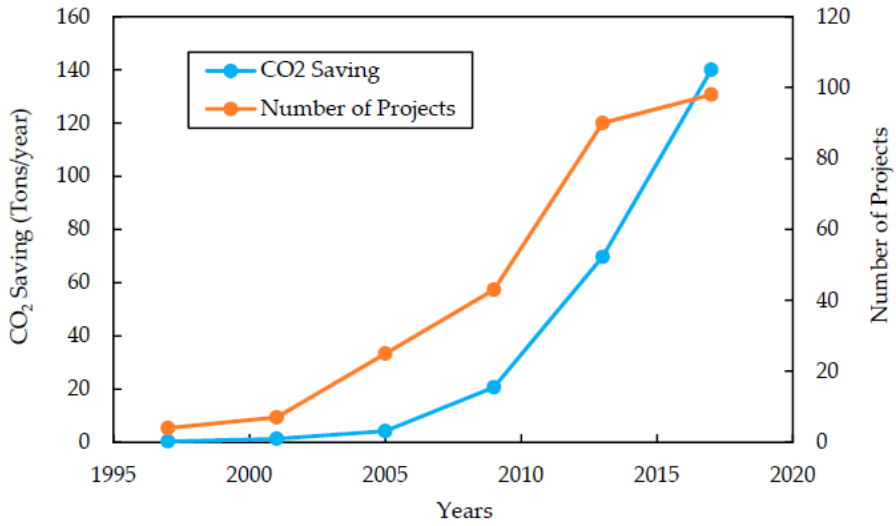

Figure 1.3: Number of projects and CO_2 reductions the past two decades [15]

1.2. Research Scope

Despite the fact that geothermal projects and especially the energy pile applications are constantly increasing and contributing to the decarbonization of energy, several crucial factors need to be further investigated and analyzed in order to enhance the efficiency and reliability of these systems within sustainable energy infrastructures. This research focuses on an existing energy pile system located in The Green Village at the TU Delft Campus, which is used to cover the heating and cooling demand of the Co-Creation Center. The initial scope is to develop a tool that represents this energy storage system and based on that numerical model, to create different operational scenarios in order to investigate the system's capabilities, limitations, and overall behavior through simulations. From the objective stated, the following main research questions derives.

Main Research Question

How the efficiency and reliability of energy pile systems can be enhanced for sustainable heating and cooling applications in modern buildings through advanced control strategies ?

In order to reach this research objective, the following supporting sub-questions need to be answered :

1. How can the pre-existing configuration of energy piles be modeled to represent the realistic phenomena occurring?
2. How the numerical model can be verified based on the analytical model ?
3. How do thermal plumes interact between energy piles?
4. What control strategies should be used based on the energy demand, weather conditions and seasonality ?
5. How much energy is lost to the atmosphere?
6. Can the surplus energy from the system be distributed to neighboring buildings?

1.3. Approach

In order to answer the main objective of the research and the sub-questions that presented, a detailed approach was designed and will be described in detail.

Initially, the existing borehole thermal energy storage configuration that is used to cover the heating and cooling loads of the Co-Creation Center that is located in The Green Village (TU Delft Campus) will be modeled using COMSOL Multiphysics. The geometry of the energy piles and the surrounding soil will be accurately defined, and the relevant material parameters will be implemented accordingly. Subsequently, the numerical model will be verified against an analytical solution based on the Infinite Line Source (ILS) theory. This step will be essential to ensure that the COMSOL model accurately simulates the heat transfer phenomena under investigation. Before running the simulations, it will be necessary to establish a realistic thermal gradient in the soil, accounting for seasonal and depth-dependent temperature variations. To achieve this, a preconditioning phase will be introduced for a period of two years, during which the only active heat transfer mechanism will be conduction, driven by the temperature difference between the ambient air and the top boundary of the soil domain. Having finalized the modeling section, the research will now focus on the second part of it, which is the optimization of the system.

In this part of the research, different scenarios based on multiple variables will be designed in order to identify the optimal configuration that achieves high efficiency and energy balance within the system. The heating and cooling demands of the building will be calculated, and corresponding load profiles will be developed for a five-year simulation period. Initially, the operational scenarios will explore the impact of varying indoor temperature setpoints. In addition, different durations and seasonal periods for heating and cooling operation will be investigated.

Subsequently, more advanced operational strategies will be examined, incorporating real-time weather conditions—specifically, solar gains. Scenarios will be developed that enable the system to store excess energy when solar gains are high. These will be structured in relation to the operation schedule of the building's solar blinds. Finally, the potential for the system to store surplus energy and distribute it to a neighboring small building, with an area of approximately 60 m^2, will be evaluated.

2

Literature Review

In that chapter, initially, the variety of thermal energy storage systems will be presented, while afterward the focus will be directed on borehole energy storage systems (BTES). Energy piles (EP), which is a sub-category of BTES, will be the main focus of this chapter. The main characteristics and different configurations of them will be presented. Additionally, modelling advancements on EPs will be discussed.

2.1. Sensible Thermal Energy Storage Systems

There are many ways to store thermal energy, with the most widely used approach being the increase of a material's temperature by storing heat as internal energy.This process is one of sensible heat storage when there is no chemical change or phase change of the material during the heating or cooling process. The amount of heat retained in a sensible heat storage system depends directly on the material's heat capacity and mass. The aim is to increase the amount of heat that can be stored, therefore solids (e.g., rock, concrete) and liquids (e.g., water,glycol) are usually used for that specific reason. Heat transfer fluid is frequently water mixed with ethylene glycol for antifreeze effect due to its high volumetric heat capacity, broad availability and affordability.

There are many important reasons that define the design of a thermal energy storage system (TES).These include total capacity,energy density,heat loss, space requirements and hydrogeological restrictions. Hence, the optimum design and sizing of the thermal storage system will be influence by several factors such as the distribution and the temperature of the energy supply, the temperature requirements, the necessary charging and discharging rates and the temporal variation of the load throughout the day or season [7].

Several short and long-term sensible heat storage solutions exist and they can be divided into six main categories in terms of storage medium : tank, aquifer, borehole, pit, cavern and fracture where the last two are rarely used [27]. Each of the aforementioned systems has its own advantages and disadvantages, and as previously mentioned, the most feasible solution tha offers the greatest balance of cost-effectiveness and performance is chosen. In the following sections, the literature will delve deeper into borehole thermal energy storage systems (BTES), exploring their key characteristics, and subsequently analyze a sub-category relevant to the case study presented in this thesis.

2.2. Borehole Thermal Energy Systems (BTES)

The first BTES actions started back at 1970s when the oil crises striked and initiated the search for alternatives to fossil fuels [24]. Large scale storage of heat was the main objective and these systems were supposed to work without heat pump assistance. By the late 1980s there was growing interest in utilizing thermal energy storage at lower temperatures for heating and cooling applications. Those systems often used heat pumps for heating while cooling could be done without them. This technology has shown high efficiency and practicality, especially with the improved insulation of the buildings [10].

One of the earliest multiple-borehole BTES system is believed to be a 12-borehole installation in Jura Mountains of France in 1976, designed for seasonal solar energy storage [12]. Early BTES systems in clay and soil were installed in Sweden,Switzerland and the Netherlands in the 1980s. In 1979, a family in Utby,Sweden constructed a BTES system of 37 vertical tubes which were inserted into clay soil at a depth of 10 meters. During the summer, the system utilized an air-to-fluid heat exchanger to capture low-temperature heat from the ambient air which was then stored in the ground [25].

2.2.1. Working Principles and Characteristics

In Borehole Heat Exchangers (BHE) systems, heat is transfered mainly through conduction, raising the temperature of the surrounding soil and rocks around the boreholes. The other heat process that takes part is convection due to the circulating fluid inside the pipes. This whole process is accomplished by circulating the working fluid -typically water mixed with ethylene glycol to prevent freezing- down vertically drilled boreholes, which usally ranges from 30 to 200 meters in depth.The specific drilling depth is influenced by the presence and depth of suitable soil or rock formations as well as the overall design of the system [23]. The key geotechnical characteristics that support the effectiveness of BHE system include :

- Drillable soil or rock
- Hydrogeological conditions - Low groundwater flow
- High thermal conductivity
- High heat capacity

The main components of the system is the borehole heat exchanger (BHE) containting U-tubes (single or double) where the working fluid is circulating and the grout material filling the space between the surrounding ground and the U-tubes.A simplified schematic of a single borehole is presented in Figure 2.1 .

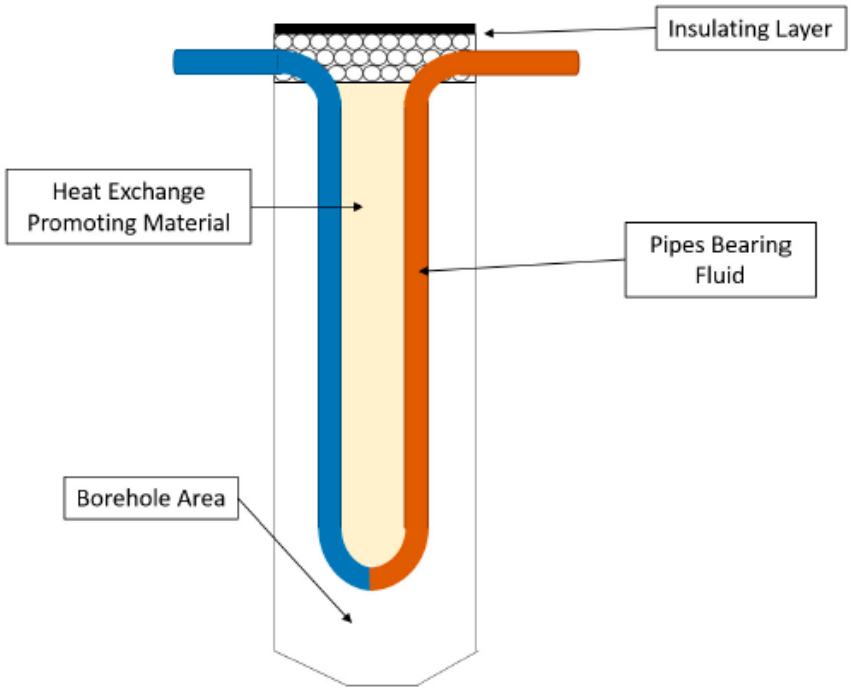

Figure 2.1: Single borehole schematic [16]

BTES systems can be coupled with ground source heat pumps (GSHPs) and they form closed-loop systems. In a closed loop system the heat carrier fluid is circulated within the heat exchanger in contrast

to the open loop system where the fluid is the ground water and is not circulated in the system. These systems can be divided into two categories the horizontal and the vertical systems. On both of those the pipes are buried underground. Figure 2.2 depicts those two systems.

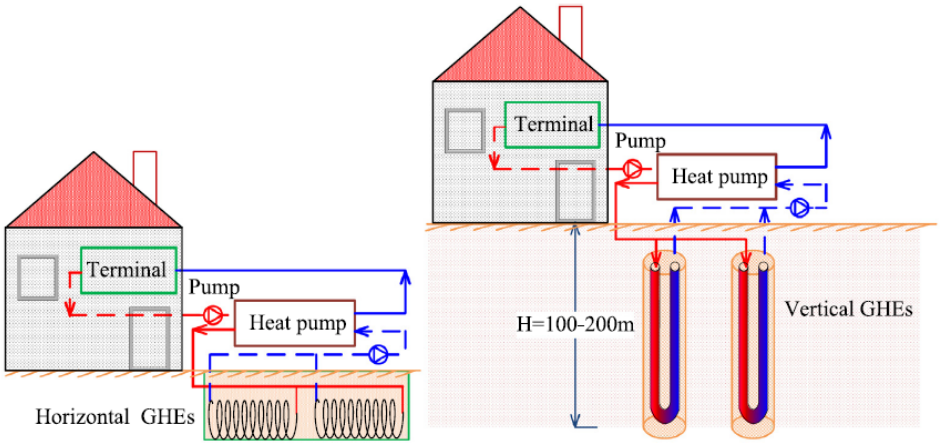

Figure 2.2: Horizontal GHE's and Vertical (single U-pipe) GHE's [8]

GSHP's extract energy from the ground when heating is needed, using the higher ans stable ground temperatures during the winter season. On the other hand, during the summer season the ground works as a heat sink. When the building needs cooling, energy is rejected to the working fluid which circulates into the ground and energy is stored in the subsurface and the surrounding soil. This method can act as a charging source for the system and is a crucial procedure to maintain soil temperature balances which secure higher COPs over the lifetime of the system.

The efficieny of the system mainly depends by the heat losses.The range of the heat losses is determined by various parameters such as the storage geometry, the average store temperature, soil properties and the borehole spacing which is an important factor and further details will be given in the following sections.

Borehole Spacing

Borehole thermal energy storage (BTES) systems tend to shape horizontal temperature stratification, with heat accumulating towards the center of the borehole field. This pattern occurs because conduction is the primary mechanism of heat transfer within the system. The depth and number of wells are determined by the geological characteristics of the site and the required storage capacity.

Studies have identified borehole spacing as the most influential factor which affects both storage efficiency and temperature distribution in the field. Wider spacing improves storage efficiency but results in a lower temperature density [37].Research by Wells et al.[33] evaluated the effects of borehole spacing,length,quantity and inlet temperature on medium-depth BTES systems. The study showed that increasing the borehole number enhanced both initial storage performance and long-term efficiency while increasing the spacing had better efficiency and heat extraction.

Additionally, Gultekin et al.[13] analyzed severak borehole arrays with spacing from 1 to 10 m. Heat transfer rates were compared between a single, isolated borehole and the same borehole within an array. Individual boreholes reached 42.7 W/m and 41 W/m. They found that performance loss decreased as spacing increased. Furthermore, a 4.5 m spacing kept overall system heat losses under 10% indicating that the optimal borehole spacing fluctuates around those values. As it can be seen from the Figure 2.3 which is based on six cases the efficiency of a borehole system maximizes approximately at 4 m spacing. Furthermore, the efficiency increases when more energy is injected into the system.

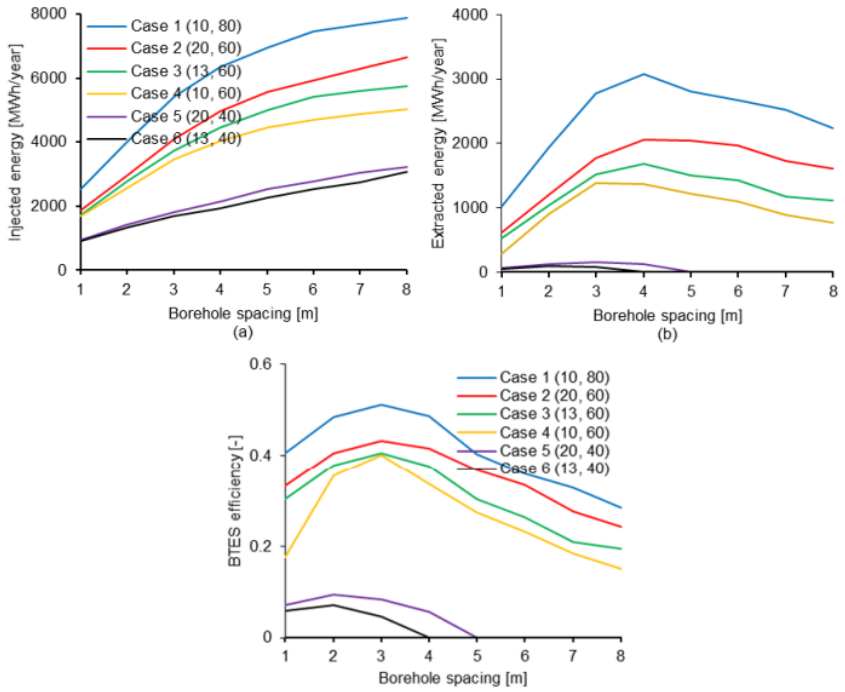

Figure 2.3: (a) Injected Energy (MWh), (b) Extracted Energy (MWh), (c) BTES Efficiency [21].

Configurations

There are various configurations of BHE, the most commmon are single and double U-tube, W shaped, coaxial shaped and complex coaxial. Each of these configurations have been widely used and have their advantages and disadvantages and they are applied based on the purpose of the system. In the Figure 2.4 is depicted the top view and front view of those configurations with only missing the W-shaped one which will be thoroughly discussed and shown on the following chapters as it is implemented on the case study of that research.

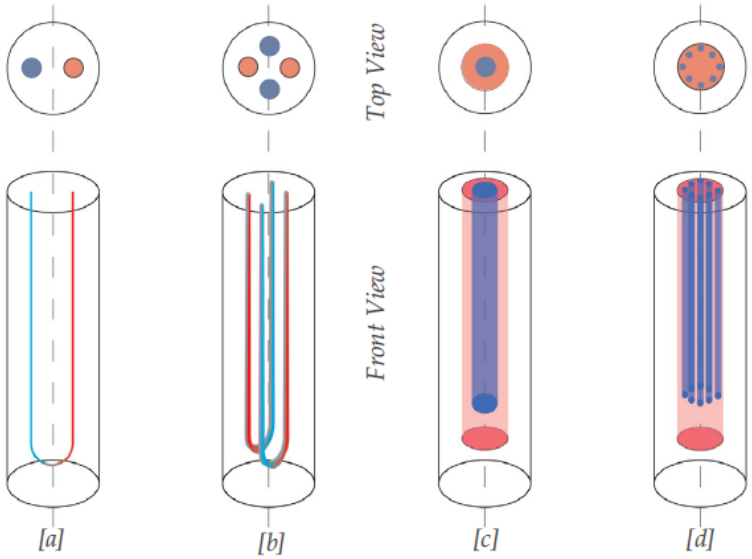

Figure 2.4: (a) Single U-tube, (b) Double U-tube, (c) Simple coaxial, (d) complex coaxial [2]

Energy Balance
In order the BTES to be used sustainably every one of these systems need to maintain an energy balance throughout the year of operation. In other words, the heat extracted from the ground must meet the heat injected into the ground and maintained to a balance. Soil thermal imbalance occurs when there is a significant difference between the amount of heat extracted from the soil and the amount returned to it, resulting in either excessive cooling or heating of the ground over time. In order to evaluate the imbalance degree,the thermal imbalance ratio (TIR) can be used and represents the ratio of the difference between the extracted and injected heat to their maximum value, which is directly influenced by the load profile [34].

The cold regions suffer from this phenomenon more frequently as they extract far more energy during the winter from the soil compared to the energy that they inject into the summer. Those imbalances cause two main problems. Initially, the soil thermal imbalance in short and long term operations can lead to soil temperature decrease which means that a large amount of energy is deducted every year from the soil and make the system not sustainable for long term operations. Additionally, this decrease in soil temperature will cause the decrease of the outlet temperature in the ground heat exchanger year by year. Subsequently, the performance of the ground source heat pump (GSHP) unit will deteriorate which means that the Coefficient of Performance (COP) will decline causing the increase in the electricity consumption of the system. Hence, the energy balance dictates the longevity and sustainability of the system and is the key factor that secures the high efficiency of it.

2.3. Energy Piles (EP)

Energy Piles (EP) are closed-loop ground energy system in which small diameter pipes are cast into the pilled foundations of a building to allow circulation of a heat transfer fluid.This method which is a subcategory of borehole heat exchangers (BHE) can dramatically decrease the drilling and backfill material cost of the system. Additionally, it is beneficial where the land is limited and the building occupies large areas. Energy Piles are thicker in diameter and shorter in length compared to boreholes. They serve simultaneously two purposes as they are used for heating/cooling applications and offer structural stability to the building. The heat transfer mechanisms in an energy pile are similar to this in a borehole heat exchanger. Heat is transferred through the ground by conduction through pile concrete and pipes and by convection in the fluid due to its movement [20].

Foundation piles generally have diameters ranging from 0.3 to 1.5 meters and are typically installed at depths between 15 and 40 meters. These piles are constructed from reinforced concrete, while the embedded pipes—used for thermal exchange—are made of High-Density Polyethylene (HDPE) [4]. These probes are attached to the pile's steel reinforcement frame using plastic brackets.

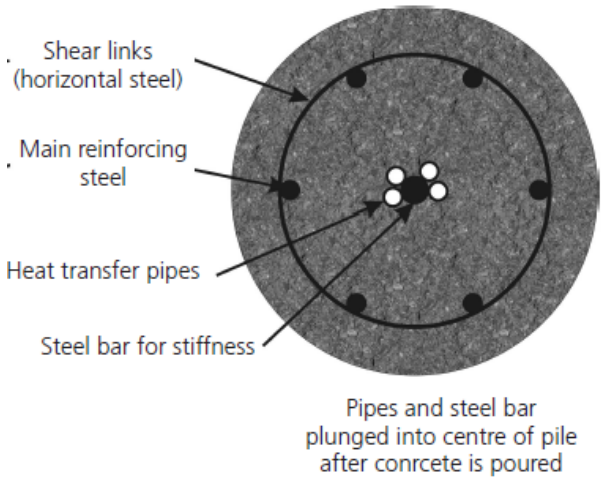

Figure 2.5: Pipes and steel bars are inserted into the center of the pile after the concrete has been poured [17]

Various configurations are possible, including single, double, W-shaped and spiral coils and they are illustrated in Figure 2.6.

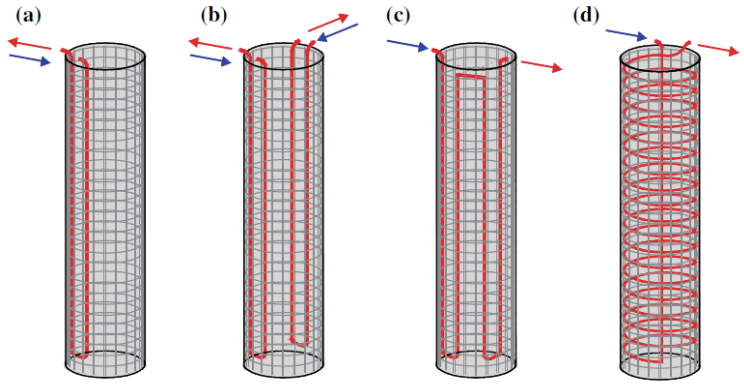

Figure 2.6: (a) Single U-tube, (b) Double U-tube, (c) W-type, (d) Helix [4]

Thermomechanical Behaviour

Energy piles are exposed to heating and cooling loads which tend to expand or contract the pile. This phenomenon can not occur because the pile is constrained both by the surrounding soil and the adjacent structure. Subsequently, a portion of the theoretical strain will be expressed instead as a change in longitudinal stress within the pile and transferred to the ground by skin friction or end bearing. This phenomenon is important because it raises concerns including overstressing the cross-section and development of negative (downward) skin friction which can cause deterioration of the external load carrying capacity. Many experiments on the thermo-mechanical response of energy piles have been conducted from Bourne-Webb et al. [3] showing that the contraction and expansion of an energy pile is around a null point. This null point is defined as the point that the pile does not experience displacements.The location of that point depends on the stiffness of the boundaries and the friction developed at the shaft. The response mechanism to thermal load is depicted in Figure 2.7. The graphs for the axial strain, axial load and shaft friction can be seen.

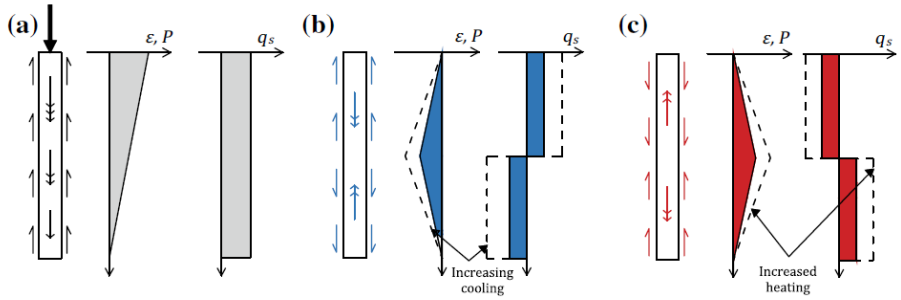

Figure 2.7: Thermal response of an energy pile in heating and cooling mode [11]

3

Methodology

3.1. Introduction

In this chapter, the research approach is outlined. The approach consists of two main parts. The first part involves developing a numerical model that accurately represents the pre-existing configuration and the physical phenomena occurring within the system. This model serves as a tool to simulate the energy pile system and to investigate its behavior and capabilities. The second part focuses on creating operational scenarios based on the heating and cooling demand of the system. By applying different setpoints for key variables and testing advanced control strategies, these scenarios aim to explore the system's limits, capabilities, and overall behavior. This chapter will present the case study and the governing equation of the problem. Additionally, the detailed procedure followed to construct the model, the model verificatio and the scenarios that were created to investigate the system will be presented.

3.2. Case Study

The model developed in this study represents a real, pre-existing Borehole Thermal Energy Storage (BTES) system. The building that this heating and cooling system serves the Co-Creation Center (CCC),a building that it is located within The Green Village at the TU Delft campus [31]. This system is coupled with a ground source heat pump (GSHP) which supplies the building with the required heating and cooling loads throughout the year. Given that the system already exists, the model follows closely the actual configuration, including the geometric dimensions, material properties, and technical specifications provided by the system's design documentation. These details are further elaborated in the subsequent chapters.

The Co-Creation Centre is supported by 22 foundation piles, 9 of which function as energy piles (EPs). These energy piles serve a dual purpose: they provide structural stability to the building while also operating as components of the thermal energy storage system. Depending on seasonal conditions and building energy demands, the energy piles either extract or store heat within the subsurface, thereby enhancing the overall efficiency of the heating and cooling system. The Figure 3.1 illustrates the foundation piles and the energy piles of the building.

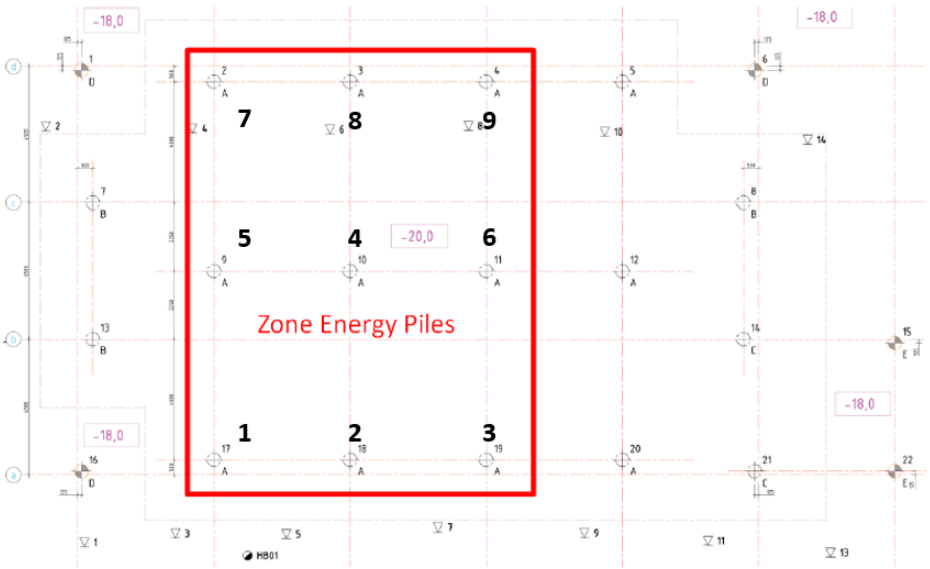

Figure 3.1: Energy Piles configuration

The energy pile spacing is 5 meters and the diameter of the concrete pile is 0.38 meters.The configuration of the pipes inside each pile is W-shaped. The system is divided into piles of 3, that means that 3 circuits are created. Each circuit consists of 3 energy piles which are connected to each other. The working fluid is injected to the inlet of first pile and flows through the second and third pile where it is extracted from the outlet of the third pile. Based on the Figure 3.1, Circuit 1 : Energy Piles 1,2,3 , Circuit 2 : Energy Piles : 5,4,6 and Circuit 3 : Energy Piles 7,8,9. The total pipe length of a circuit is 266 meters while the pipe length in a single energy pile is 74 meters. The inner pipe diameter is 0.028 meters and the maximum flowrate per loop is 0.75 m^3/h. In the Appendix A the detailed characteristics of a single energy pile and the location of those are presented.

3.3. Governing Equations

The software that is being used for the analysis is able to simulate heat transfer processes in Borehole heat excahnger (BHE) systems using computational fluid dynamics (CFD). The heat transfer processes in energy piles and surrounding soil include heat conduction between soil,concrete and pipe material and heat convection due to the fluid flow inside the pipes between the pipe walls and the fluid. In Figure 3.2 those mechanisms are explicitly depicted for better understanding.

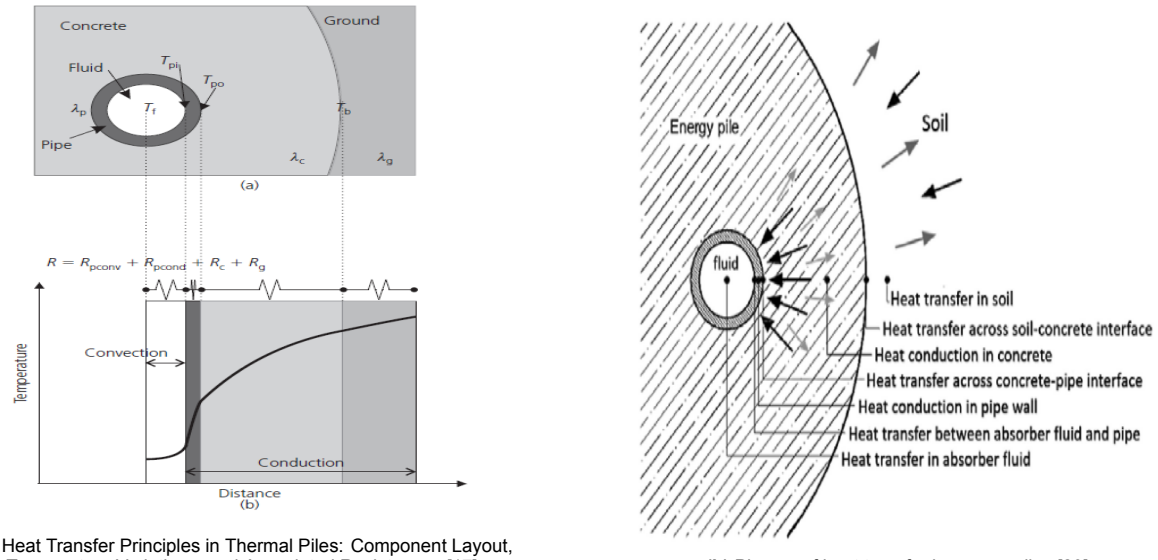

(a) Heat Transfer Principles in Thermal Piles: Component Layout, Temperature Variations, and Associated Resistances [17]

(b) Phases of heat transfer in energy piles [20]

Figure 3.2: Heat transfer mechanisms

The following governing equations for heat conduction and convection will be presented below.

Continuity

This equation for continuity is used for incompressible flows. It states that the fluid velocity field divergence is zero. This means that the fluid entering is equal to volume with the fluid that exiting, no compressions or expansions occurs. This happens due to the constant density that has been assumed.

$$\rho \nabla \cdot \mathbf{u} = 0 \tag{3.1}$$

Where:

- ρ is the fluid **density** (kg/m^3).
- $\mathbf{u}$ is the **velocity vector field** of the fluid (m/s), usually expressed as:

$$\mathbf{u} = (u, v, w)$$

  for flow in the x, y, and z directions respectively.

Momentum Equation

The momentum equation is also known as Navier-Stokes equation and describes how the velocity field changes due to the effects of viscosity, pressure and external forces such as gravity.This equations is fundamental in calculating how the fluids move and interact with the boundaries. In incompressible flows the density is assumed to be constant and the model simplifies based on that.

$$\rho(\mathbf{u} \cdot \nabla)\mathbf{u} = \nabla \cdot (-p\mathbf{I} + \mathbf{K}) + \mathbf{F} \tag{3.2}$$

Where:

- ρ is the **fluid density** (kg/m^3)
- $\mathbf{u}$ is the **velocity vector field** (m/s), with components:

$$\mathbf{u} = (u, v, w)$$

- μ is the **dynamic viscosity** (Pa·s)
- $\mathbf{F}$ is the **body force per unit volume** (e.g., gravity)

Energy Equation
The energy equation insures the the conservation of energy within the system by accounting all forms of thermal input and output. It is important for calculating temperature fields accurately for both fluids and solids under various thermal conditions. It captures the effects of transient heat accumulation, heat carried by moving fluid, and thermal conduction based on Fourier's law.Finally, the equation takes into account heat generated by internal sources and mechanical eenrgy converted into heat through viscous dissipation.

$$\rho C_p \frac{\partial T}{\partial t} + \rho C_p \mathbf{u} \cdot \nabla T + \nabla \cdot \mathbf{q} = Q + Q_{\text{ted}} \tag{3.3}$$

Where:

- ρ is the **fluid density** (kg/m^3)
- C_p is the **specific heat capacity at constant pressure** (J/kg·K)
- T is the **temperature** (K)
- k is the **thermal conductivity** (W/m·K)
- ∇T is the temperature gradient
- Q is a **volumetric heat source** (W/m^3)
- Q_{ted} is the **thermal energy from viscous dissipation** (W/m^3)

Fourier's Law
Fourier's law describe how heat is conducted through a material and mentions that the heat flux is proportional to the negative gradient of temperature which means that heat naturally flow from hotter to colder regions. In the model it is used to to calculate the thermal conduction both in solids and fluids of the domain.

$$\mathbf{q} = -k \nabla T \tag{3.4}$$

- $\mathbf{q}$ is the **heat flux vector** (W/m^2)
- k is the **thermal conductivity** (W/m·K)
- ∇T is the **temperature gradient** (K/m)

3.4. Numerical Model Set Up

As was mentioned in the previous sections the model was created in COMSOL Multyphysics. A 3-dimensional model was designed to represent with accuracy the existed system. In that section, the details of the model designed will be presented in detail.

3.4.1. Geometry

The geometry of the system is illustrated in the Figure 3.3. It is important to mention that the surrounding soil needs to be large enough so the boundaries won't interfere with the energy piles operation. It can be seen that the energy piles are divided into 3 circuits which consists of 3 energy piles each and they are connected each other. The fluid is injected through the first pile of each circuit, flows through the middle energy piles and exits from the last energy pile of each circuit. Each pile follows the configuration of a W-shaped tube as it is presented in the Figure 3.4.

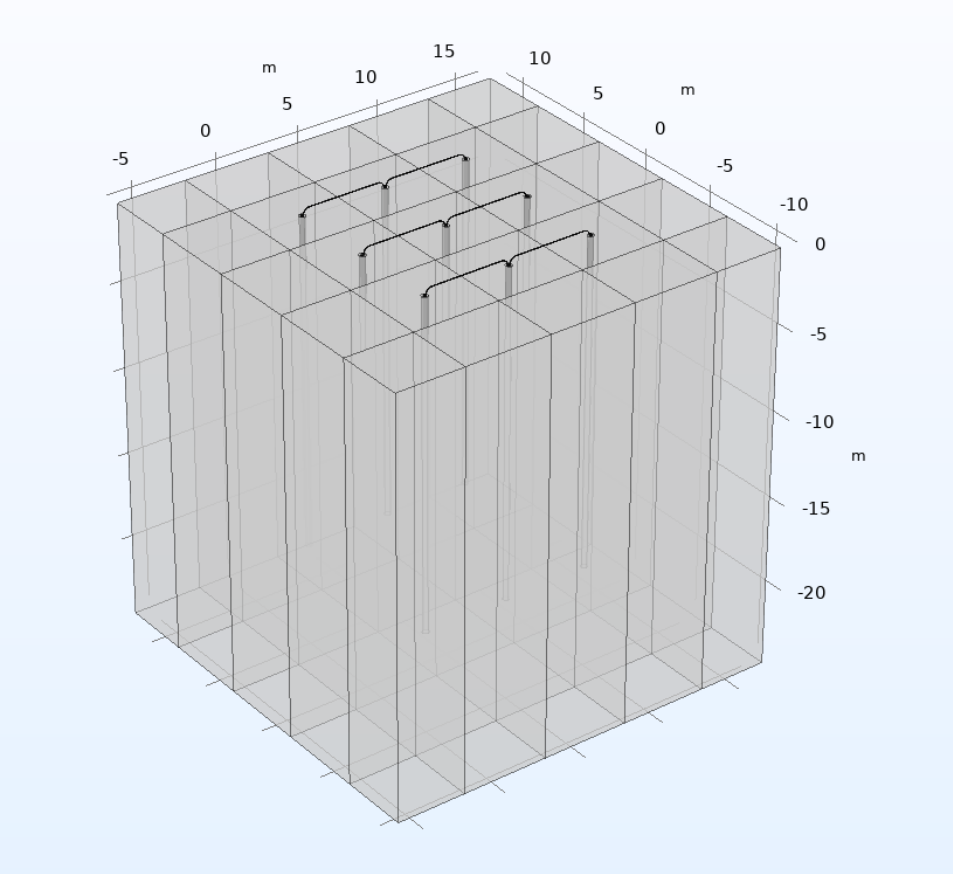

Figure 3.3: Geometry of model

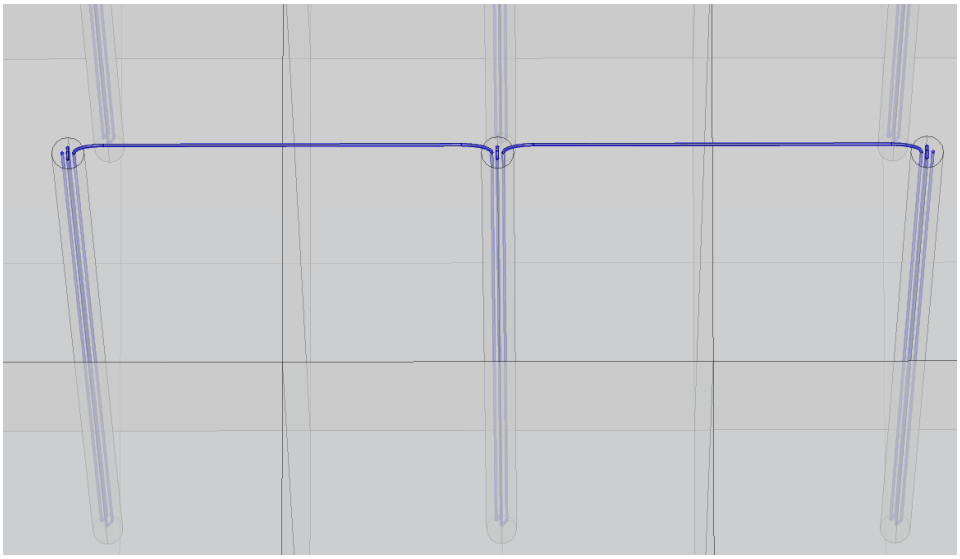

Figure 3.4: W-shaped tube configuration circuit

3.4.2. Materials Properties

Working Fluid

The working fluid circulating in the energy piles is a mixture of water and 20 % ethylene glycol. The ethylene glycol is added to the water for anti-freezing effects. According to [30], the freezing point of the selected mixture is approximately -7.9°C. Considering a safety margin for the operating conditions,

the working fluid is assumed to withstand temperatures as low as –4°C. The table below summarizes the hydraulic and thermal properties of the fluid.

Table 3.1: Thermal and hydraulic properties of the working fluid.

Property	Value
Density (ρ_{fluid})	1089 kg/m^3
Specific heat capacity ($c_{\text{p,fluid}}$)	4180 J/(kg·K)
Thermal conductivity (λ_{fluid})	0.4 W/(m·K)
Dynamic viscosity (μ_{fluid})	0.005 Pa·s
Freezing point	7.9 °C

Pipes
High density polyethelene (HDPE) pipes are used in the system. HDPE are preferred in BTES systems due to their chemical resistance, flexibility, thermal durability and long expected lifetime ensuring efficiency and reliable subsurface heat exchange. The Table below shows the properties of those pipes.

Table 3.2: Thermal properties of high-density polyethylene (HDPE) pipes [29].

Property	Value
Density (ρ_{HDPE})	940 kg/m^3
Specific heat capacity ($c_{\text{P,HDPE}}$)	2300 J/(kg·K)
Thermal conductivity (λ_{HDPE})	0.4 W/(m·K)

Concrete - Grouting Material
In energy pile applications, reinforced concrete is commonly used as the grouting material between the soil and the embedded pipes. This is primarily due to its dual role: it provides the necessary structural support to withstand building loads, while also offering favorable thermal properties. Specifically, reinforced concrete exhibits relatively high thermal conductivity and thermal mass, both of which enhance heat conduction within the ground. These characteristics make it a preferred material for energy pile systems. The table below summarizes its key thermal and mechanical properties.

Table 3.3: Thermal properties of the concrete grouting material.

Property	Value
Density (ρ_{concrete})	2400 kg/m^3
Specific heat capacity ($c_{\text{p,concrete}}$)	880 J/(kg·K)
Thermal conductivity ($\lambda_{\text{concrete}}$)	1.7 W/(m·K)

Surrounding Soil
The subsurface soil beneath the building consists of layers of clay and sand. A borehole profile near the Co-Creation Center, retrieved from Dinoklet, is presented in Figure 3.5. In this study, the soil is assumed to be fully saturated, meaning that the voids within the soil matrix are filled with water. This assumption is supported by the presence of a pond surrounding the area where the Green Village is located. The properties of the saturated soil have been determined through both measurement and estimation, and are provided in the Appendix A. The table below summarizes the soil properties used in the model.

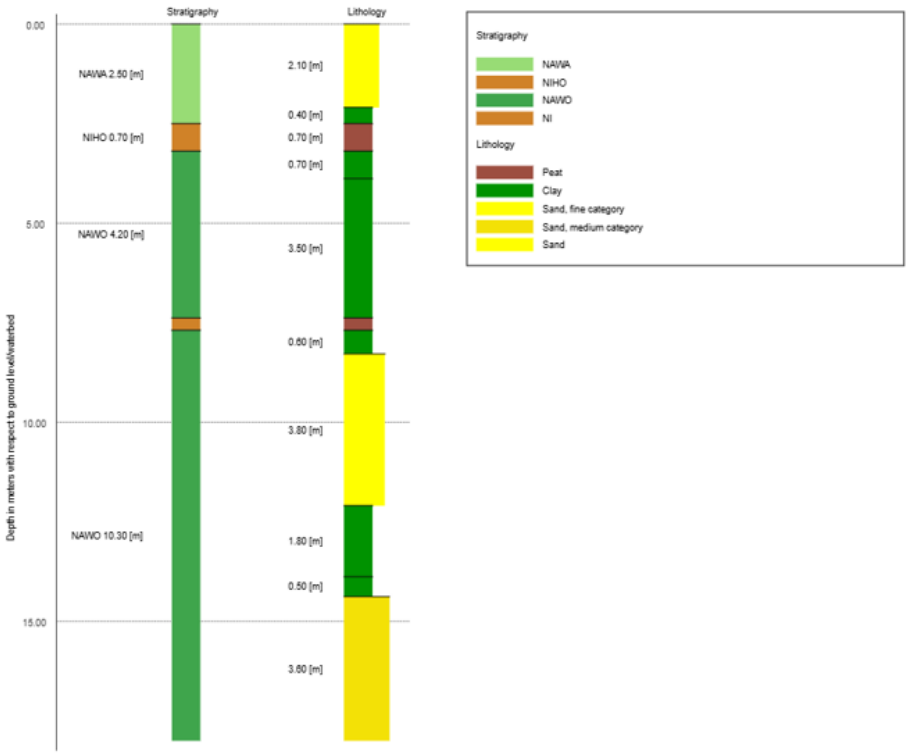

Figure 3.5: Borehole Profile Measured 18 meters depth [32]

Table 3.4: Thermal properties of the subsurface surrounding soil (see Appendix A).

Property	Value
Density (ρ_{ground})	1500 kg/m^3
Specific heat capacity ($c_{\text{p,ground}}$)	2000 J/(kg·K)
Thermal conductivity (λ_{ground})	1.6 W/(m·K)

These are the main materials that the heat storage system consists of and were defined to realistically represent the existing configuration of the building.

3.4.3. COMSOL Multiphysics Modules

The Conjugated Heat transfer module was selected to simulate the physics around the model with a selection of Laminar Flow. By selecting that module COMSOL divides the physics into 3 main sectors. The first one is called Heat transfer in solids and fluids and simulates the heat conduction from soil to concrete piles, pipes and water. Also, this module simulate the heat convection due to the movement of the working fluid inside the pipes and takes into account other heat transfer phenomena that may be occuring on the surrounding boundaries. Secondly, the Laminar Flow module is activated to simulate the movement of the fluid inside the pipe and the profile of the flow which in this case is laminar. Lastly, the Non-isothermal Flow multiphysics coupling allows for simulating fluid flows where fluid properties may change due to the increase or decrease of temperature. In some cases the change in the thermal or hydraulic properties of the fluid can be large enough to have a substantial influence on the flow field and the surrounding environment [6].

3.4.4. Boundary Conditions

Energy piles are considered to be a swallow geothermal system which is mainly affected by the thermal gradient between the ground and the air temperature, which dictates the heat transfer direction in the domain. Seasonal variations in ground temperature are largely depth-dependent and progressively decrease with greater distance from the surface. Initially, the whole domain that has been created it is assumed to have a temperature for 12°C. However, in the (preconditioning chapter) the method to create a realistic thermal gradient based on the seasonality and ground depth will be presented.
The boundaries of the system that they are thermally insulated can be seen in Figure 3.6 as they are highlighted as blue. The energy piles and the soil above those are considered to have no heat flux because the building exists above them. Also, the vertical boundaries of the system considered adiabatic and thus no heat flux occurs between those surfaces. The perimeter zone that surrounds the square that energy piles exists at the top boundary is assumed to be open to the ambient air temperature which fluctuates throughout the year depending on the season. This boundary condition will be discussed in further detail in the following chapters.Lastly, the bottom boundary of the domain is set to a constant temperature of 12°C throughout the whole year, due to its relatively high depth. This boundary is at 24 meters depth and the temperature does not fluctuates at these depths and it is not affected by the seasonality.

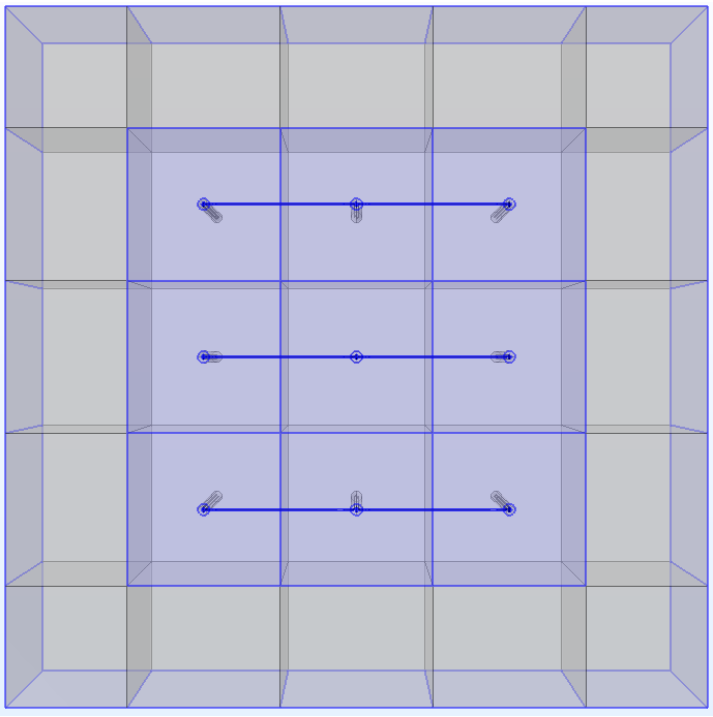

Figure 3.6: Top View of Energy Piles - Insulated Boundaries

Regarding the boundary condition of the inlet flow, a fully developed flow condition was imposed at the inlet boundaries, assuming a steady-state profile for laminar flow. The boundary condition was defined based on a prescribed volumetric flow rate which is measured at m^3/s.The option 'Apply condition on each disjoint selection separately' was enabled to ensure the flow rate is independently applied to each inlet face. A pressure outlet condition was applied at the outlet boundaries. The outlet pressure was set to zero Pascal static pressure, representing atmospheric reference pressure and the 'Suppress backflow' option was enabled to prevent reverse flow at the outlet, reflecting the unidirectional nature of the system's flow.

3.4.5. Operational Principle

The developed model represents a heat storage system coupled with a ground source heat pump (GSHP),which is operating to provide heating or cooling to the building.To accurately simulate the ther-

mal behavior occurring during these processes over the course of a year, a control logic framework was implemented within the model. Specific variables have been created which are defined by the user while other variables are calculated from the system based on a specific equation.
The energy demand of the building is determined by an interpolation function which draws data from the appropriate file that has been created. So, the user can set the heating or cooling demand that the system needs to provide. Furthermore, the outlet temperature of the fluid was defined as a variable over time and measures the average temperature over outlet boundaries. This variable integrates the temperature field across the specified boundaries. The inlet temperature of the fluid is calculated from the system based on the following energy balance equation.

$$T_{\text{in}} = T_{\text{out}} - \frac{Q(t)}{\rho \dot{V} c_p}$$

where:

- $Q(t)$ is the energy demand defined by the user, imported as an interpolated function.
- $\dot{V}$ mass flow rate of the fluid [m^3/s]
- ρ density [kg/m^3]
- c_p specific heat capacity at constant pressure [$\text{J}/(\text{kg} \cdot \text{K})$]
- T_{out} outlet average temperature which is introduced to the system as a variable over time [$^\circ\text{C}$]

This modelling approach enables a dynamic representation of the system's thermal behaviour by connecting the potential heating or cooling load that needs to be delivered with the injection temperature of the fluid. Specifically, the model calculates the appropriate injection temperature based on the outlet temperature and the thermal load. This is a realistic approach of how the system is working and allows it to adapt on each load every hour. It is based on the performance of the system over time and adapts to it accordingly.

3.4.6. Meshing

Mesh quality significantly influences the accuracy of numerical simulation results. Coarse meshes reduce computational time but often compromise accuracy, while fine meshes improve accuracy at the expense of increased computational cost. To balance precision and efficiency, a hybrid meshing strategy was employed in the energy pile (EP) model, combining different mesh densities to optimize both accuracy and simulation time. All the domains of the model were meshed using COMSOL Multiphysics and the features that were used and will be analyzed are 'Free Tetrahedral', 'Corner Refinement' and 'Boundary Layers'.
The strategy used for time-efficient and accurate meshing was to create a dense mesh in the domains where heat transfer phenomena occur, and gradually use coarser meshing in regions further away from them. The domain of working fluid has a fine mesh and the elements was calibrated for fluid dynamics. The pipes and the concrete piles have a normal mesh while the surrounding soil has a coarse mesh. Furthermore, the corner refinement module was used for the pipes and the working fluid to create smaller elements at the sharp angles that have been created in the model. Lastly, the boundary layer module was used to accurately capture the steep gradients in the near-wall region. Especially for heat transfer and flow phenomena at solid-fluid interfaces a boundary layer is applied to improve the numerical accuracy where thin boundary layers are formed near the no-slip boundaries. The complete model mesh consists of 575,683 domain elements, 102,511 boundary elements, and 39,640 edge elements. In the Figure 3.7 below the meshing sequence of an energy pile (EP) is illustrated.

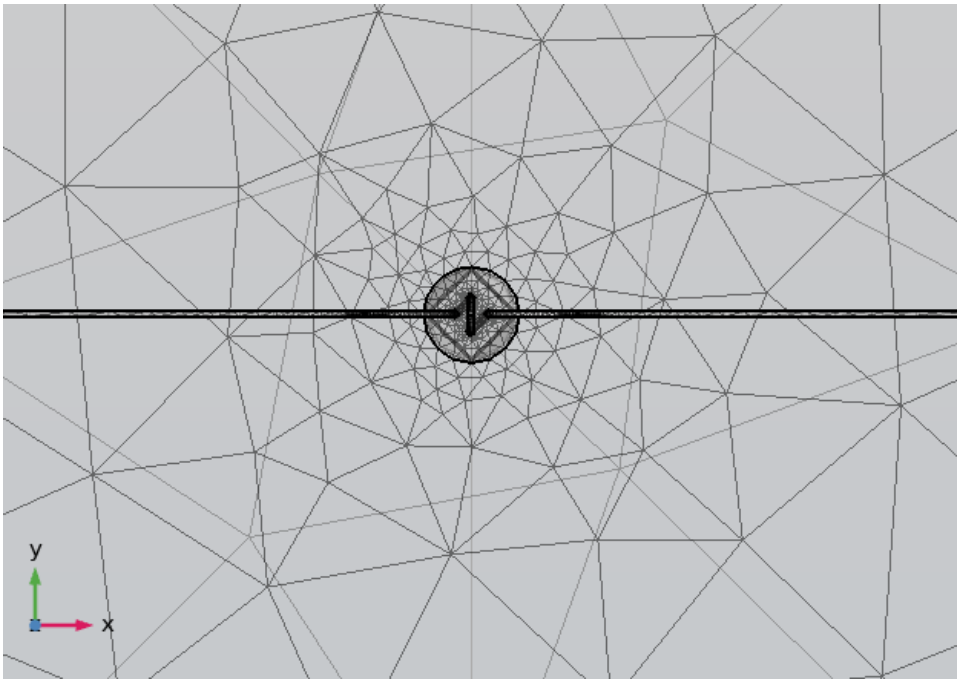

Figure 3.7: Top View of energy piles meshing

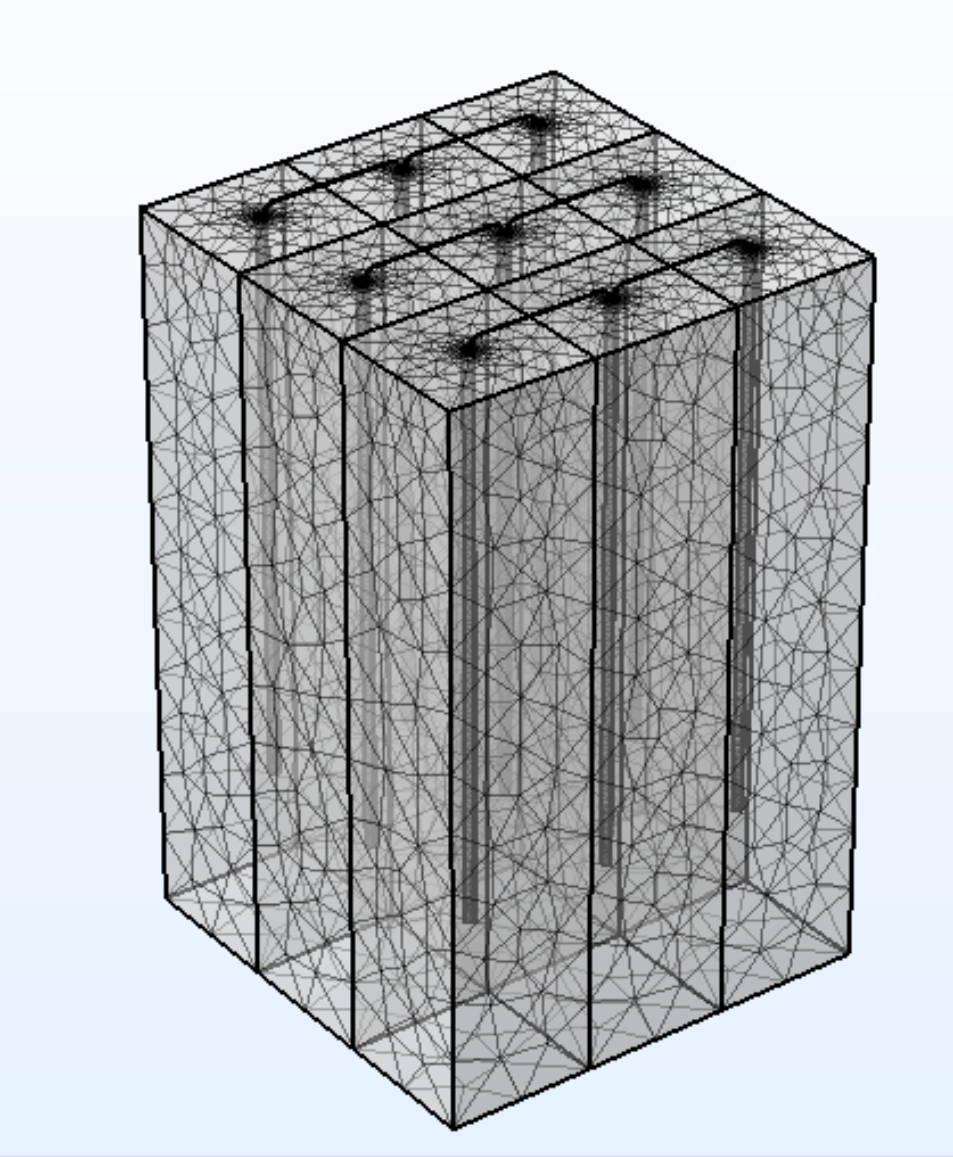

Figure 3.8: Model complete meshing sequence

3.4.7. Solver Configuration

The solver configuration consisted of a combination of stationary and time-dependent steps to simulate the physical behavior of the system. Initially a stationary solver is used to simulate the steady-state velocity and pressure fields that are formed in the Laminar Flow module of the model. The results of this study are stored and used as initial conditions for the subsequent time-dependent analysis.The time-dependent study step focused on solving the thermal behavior of the system using the Heat Transfer in Solids and Fluids interface, in conjunction with the Nonisothermal Flow multiphysics coupling. The time for this study was selected to be hours and the time step is every hour. The relative tolerance needed to be adjusted to minimize the error from hour to hour to 10^{-3}. The accuracy in the system is very important and hard to be kept in balance as the energy loads can significantly vary from hour to hour. This phenomenon can increase the deviation from the schedule and the tolerance needs to be re-adjusted if it is needed. The solver configuration uses the Fully-Coupled time dependent solver utilizing a direct method that is specifically applied to the heat transfer variables.This approach permitted the accurate and computationally efficient determination of the thermal field over extended simulation periods. A fully coupled solver was used in the time-dependent study to capture the strong dependence between thermal and fluid flow phenomena in the system. This approach solves all the governing equations

simultaneously and it is the appropriate one for multiphysics problems where variable such as velocity and temperature are linked. It enhances the robustness and numerical stability of the simulation, especially when nonlinear or transient conditions over time are applied and rapid changes into the field occur. Furthermore, it reduces the risk of iteration lag and ensures more reliable convergence when the model has steep gradients or complex interactions. On the other hand, the fully coupled solver it is computationally expensive compared with a segregated solver however the overall efficiency of the solver is higher due to fewer total iterations that are required to reach convergence.

3.5. Model Verification

In this section, the numerical model that has been designed is verified with an analytical model. The analytical model is based on theory, which will be explained. Comparison graphs and plots will be presented and analyzed.

3.5.1. Analytical Model

In order to secure that the model that has been created in COMSOL Multyphysics represents the physical phenomena and heat transfer mechanisms that occuring with accuracy. It will be verified with the analytical theory. The analytical equation that the model was compared is based on the Infinite Line Source (ILS) model, which was originally introduced by Ingersoll et al. (1945) [14] and Carslaw and Jaeger (1959) [5]. The ILS model describes the radial heat conduction that happens from an infinitely thin line source which is embedded in an infinite homogeneous medium (soil-ground). The heat conduction equation is linear and thus the superposition principle can be applied. The analytical equation allows both the spatial superoposition - in order to investigate multiple boreholes - and temporal superposition - in order to simulate for variable heating/cooling loads - to be simulated. The temperature at any given distance from the infinite line source can be calculated using the following analytical equation :

$$T(t,r) \approx T_0 - \sum_j \left\{ \sum_i \left(\frac{Q_i}{4\pi\lambda l} \left[\ln\left(\frac{4\lambda t_i}{r_j^2 C} \right) - \gamma_E \right] \right) \right\}$$

where:

- $T(t,r)$ is the temperature at time t and radial distance r,
- T_0 is the initial ground temperature (K)
- Q_i is the heat injected during the time interval i (W)
- t_i is the time since the heat injection has started
- r_j is the radial distance from the j-th borehole to the evaluation point
- λ is the thermal conductivity of the ground (W/m·K)
- l is the length of the borehole (m)
- C is the volumetric heat capacity of the ground (J/m³·K)
- $\gamma_E \approx 0.577$ is the Euler–Mascheroni constant.

Based on this equation, which can be used for an array of boreholes, the verification of the model will be presented.

Initially, the physical properties that the equation used need to be defined and they are presented in the Table 3.5.

Table 3.5: Soil physical properties and borehole dimensions.

Physical property	Value
Initial temperature T_0	12 °C
Thermal conductivity λ	1.6 W/(m·K)
Volumetric heat capacity C	2.9 $\times 10^6$ J/(m^3·K)
Borehole length	18 m
Borehole radius	0.19 m

The grid and the configuration of the borehole arrays were defined by specifying the coordinates of each borehole directly within the analytical function code. It is important to note that, for the purposes of verification, the 9 energy piles were assumed to operate individually, without being connected to form a circuit as previously shown and discussed. This assumption was necessary because the analytical model treats each pile as an independent heat source and does not account for hydraulic or thermal connections between them. The modified model is illustrated in Figure 3.9

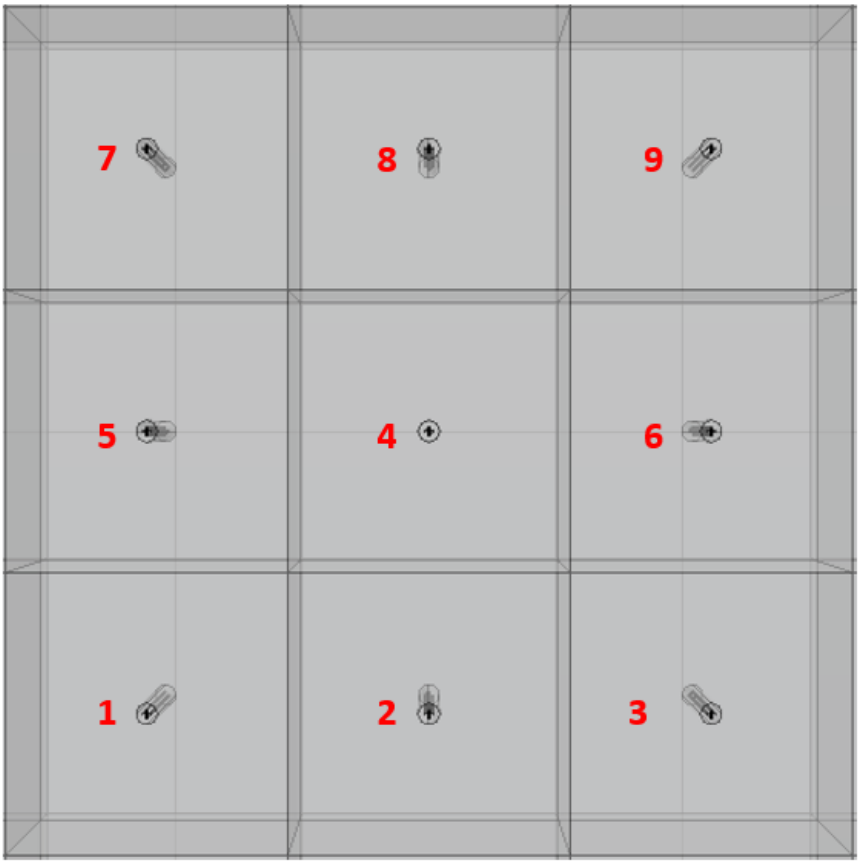

Figure 3.9: Energy piles configuraton

Subsequently, the profile for the heating or cooling demand were created Figure 3.10 for 5 years which will be the simulation time for the verification. During the winter months, the system extracts thermal energy from the ground to provide space heating, whereas in summer, it injects excess heat into the ground to enable cooling. In the transitional periods between seasons, the system remains in resting mode, with no active heat exchange.In the heating and cooling profile of the Figure below it was

selected the system to operate in heating mode for 5 months and in cooling for 4 months. Each energy pile follows the profile shown below which consists of 2 periods of heating, 1 period of cooling and 2 periods of resting mode in between as it can be seen.

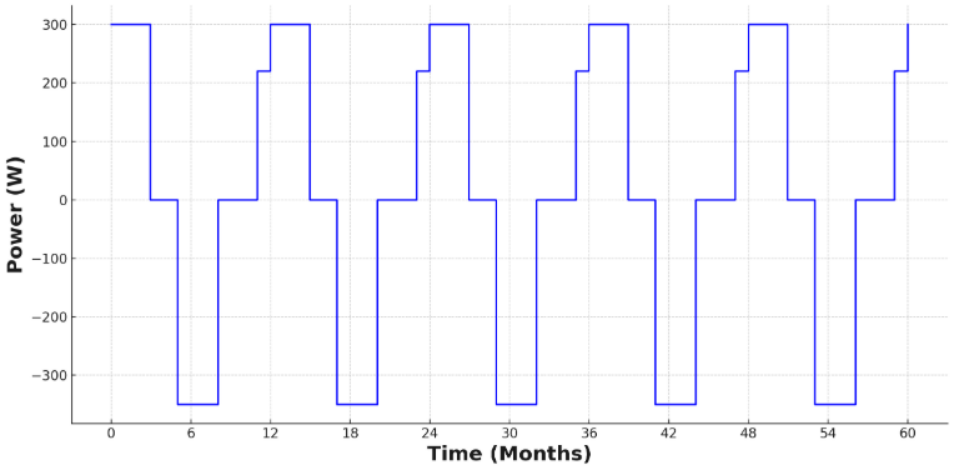

Figure 3.10: Profile Demand for 5 years

It is important to note that in both the analytical and numerical models, the input is prescribed as power. In both cases, the load profile was defined by the hourly injected or extracted energy over the entire five-year simulation period. However, the variable used for comparison between the models was the temperature at specific points within the domain. This approach produced a set of temperature–time curves, which directly reflect the effect of the hourly and seasonal thermal loads. By comparing the temperature evolution obtained from the two models, the consistency and accuracy of the numerical model were evaluated. A close agreement between the analytical and numerical temperature predictions at different locations confirmed that the numerical model accurately represents the heat transfer mechanisms of the system.
In order to verify the accuracy of the model developed in COMSOL, six monitoring points were selected to record temperature throughout the entire simulation period using an hourly time step. A variety of points were selected in different radial distances from the boreholes to check the temperature profile. Due to the limitations of the analytical solution, which assumes an infinite medium with no boundary conditions and accounts only for horizontal (radial) heat conduction, the temperature in the COMSOL model was monitored at a depth of 9 meters - corresponding to the midpoint of the energy pile. This location was chosen because it is equidistant from both the top and bottom boundaries of the model, thereby minimizing the influence of imposed boundary conditions on the temperature field. This allows for a more appropriate and direct comparison between the numerical and analytical results. Figure 3.11 illustrated the points that were selected and the Table 3.6 shows the exact location of the points in the grid.

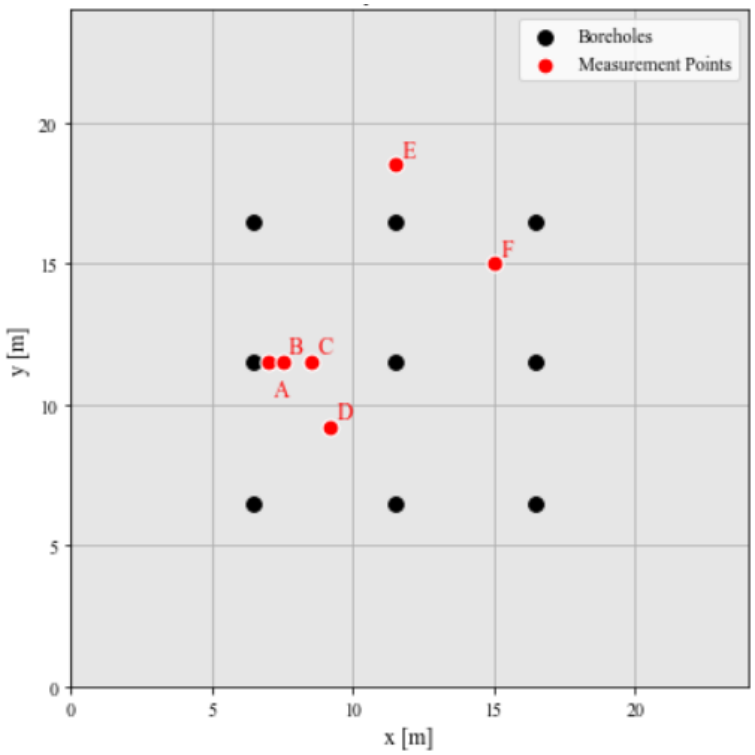

Figure 3.11: Grid configuration and measurement points

Table 3.6: Coordinates and distances of measurement points.

Measurement point	Coordinates (x, y, z)	Distance from borehole (m)
A	(7, 11.5, –9)	0.5
B	(7.5, 11.5, –9)	1.0
C	(8.5, 11.5, –9)	2.0
D	(9.2, 9.2, –9)	2.5
E	(11.5, 16.5, –9)	2.0
F	(15, 15, –9)	2.12

The simulations conducted both in COMSOL model and the model based on the analytical theory for 5 years. For each point a temperature comparison plot has been created and can be seen in the Figure 3.12 below.

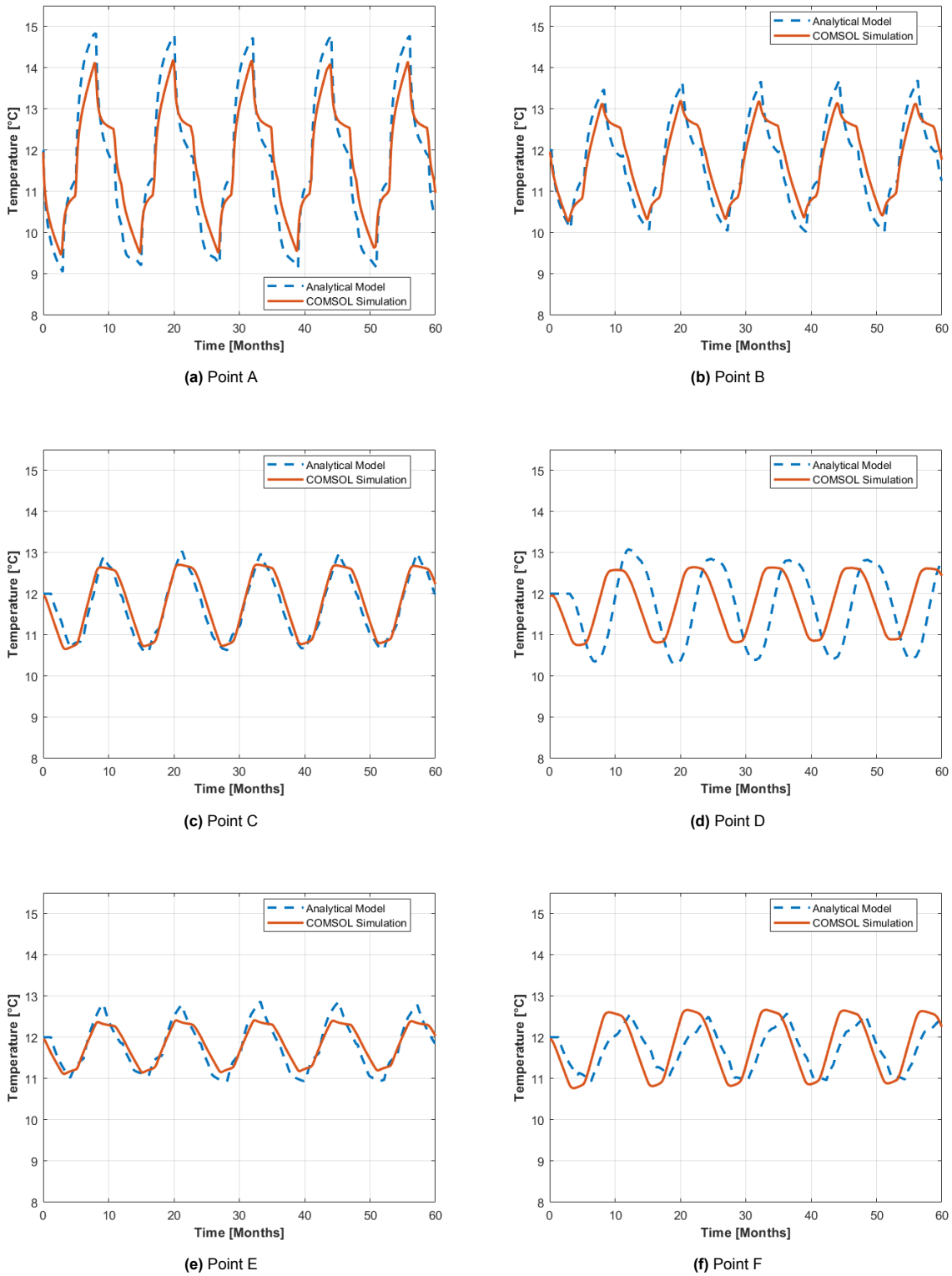

(a) Point A

(b) Point B

(c) Point C

(d) Point D

(e) Point E

(f) Point F

Figure 3.12: Temperature comparison at measurement points A–F for 5 years

As observed from the plots, most of the measured points exhibit similar temperature fluctuations. However, some locations show greater deviations between the analytical and numerical results. To quantify these differences, the average absolute percentage temperature error for each point was calculated on a yearly basis, as well as the overall average error across all points for each year. The

equation that was used can be seen below.

$$\textbf{Average Absolute Percentage Error } [\%] = \frac{1}{n}\sum_{i=1}^{n}\left|\frac{T_{\text{analytical},i} - T_{\text{COMSOL},i}}{T_{\text{analytical},i}}\right| \times 100 \tag{3.5}$$

where n is the number of time steps in a given year, and $T_{\text{analytical},i}$ and $T_{\text{COMSOL},i}$ represent the analytical and numerical temperatures at time step i, respectively. This metric captures the magnitude of deviation without considering its direction, providing a reliable measure of the model's accuracy over time.In the Table 3.7 the results are presented.

Table 3.7: Yearly average absolute percentage error per point and total average.

Year	A	B	C	D	E	F	Total average
1	4.52	2.83	2.01	6.36	2.36	2.98	3.51
2	4.95	3.28	1.46	8.55	2.18	3.70	4.02
3	4.68	3.28	1.47	8.37	2.28	3.48	3.93
4	4.71	3.69	1.44	8.03	2.31	3.49	3.95
5	4.66	3.64	1.39	7.99	2.17	3.36	3.87

Based on the results presented above, it can be observed that the error at each point fluctuates from year to year but remains below 5 %, with the exception of Point D. The highest errors were observed at Points A and D. Point A is located 0.5 meters from the energy pile; thus, the analytical model, due to its assumptions and inherent limitations, is unable to predict the temperature with high accuracy at such close proximity. Conversely, Point D is situated at the greatest distance from the energy pile, where the highest error in temperature measurements was observed. This is also attributed to the limitations of the analytical model, which will be discussed in the following section. The most accurate approximations were obtained at points located between 1 and 2 meters from the energy pile and at those distances seems to have the best prediction. Overall, the average annual error remains below 4%, indicating that the numerical model represents the physical phenomena with a high degree of accuracy.

To further evaluate the accuracy of the analytical model, a series of contour plots are presented comparing the temperature distributions simulated from both the numerical and analytical models. These plots illustrate the spatial variation in temperature around the energy piles at selected time intervals. By visually comparing the two sets of results, it is possible to assess the extent to which the analytical model replicates the thermal behavior predicted by the numerical model. In Figure 3.13 below, 4 sliced isosurface plots at 9 meters depth are presented in different time stamps.

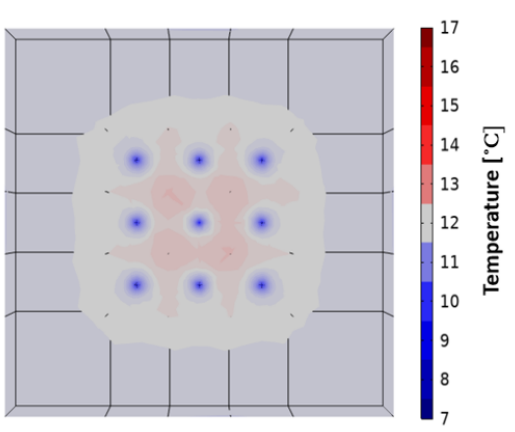

(a) 1 Year Numerical Model

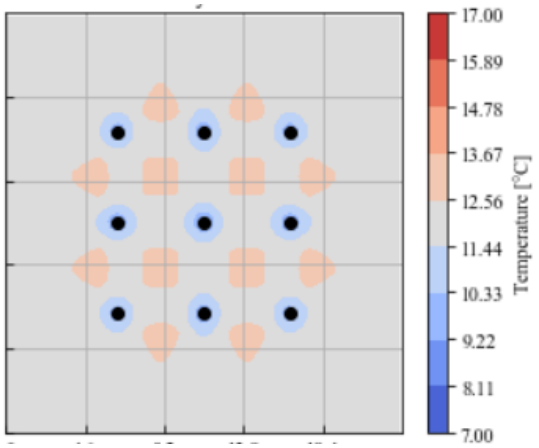

(b) 1 Year Analytical Model

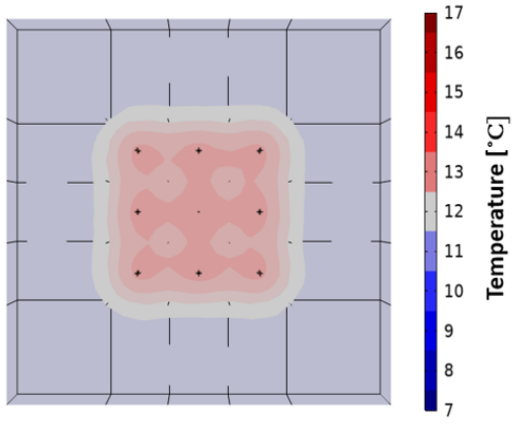

(c) 2.75 Year Numerical Model

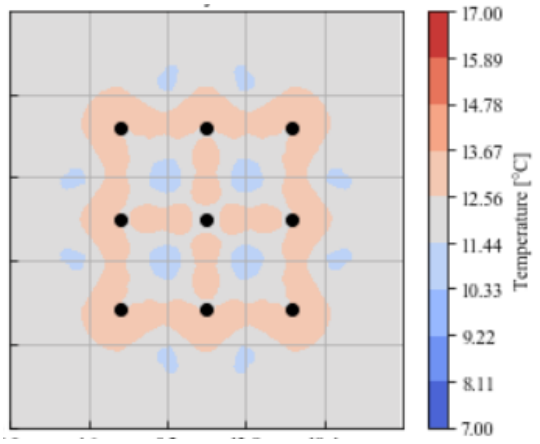

(d) 2.75 Year Analytical Model

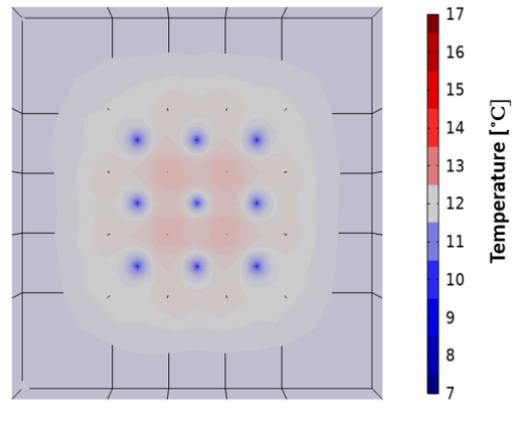

(e) 3 Years Numerical Model

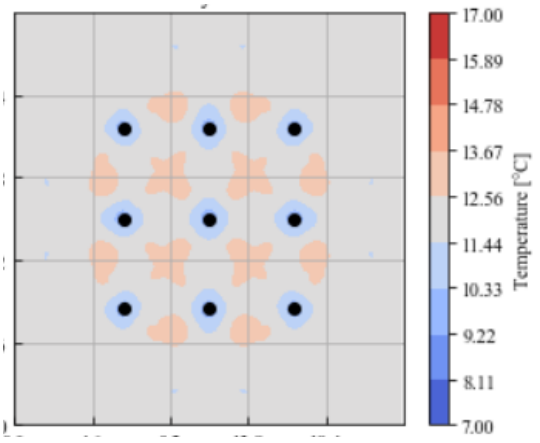

(f) 3 Years Analytical Model

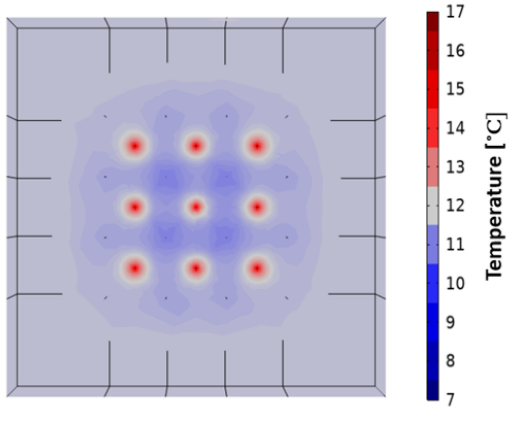

(g) 4.5 Year Numerical Model

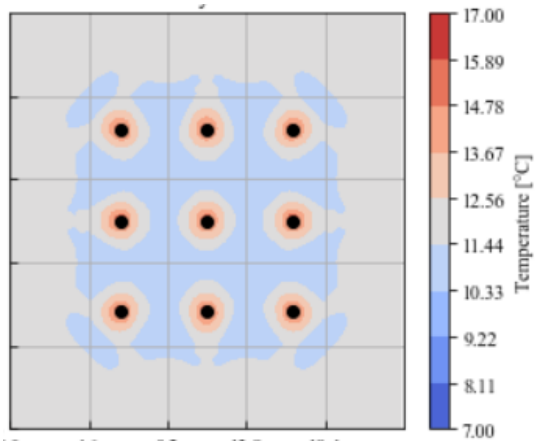

(h) 4.5 Year Analytical Model

Figure 3.13: Isosurface plots comparison of numerical and analytical model over time.

The plots presented at different time intervals show that the analytical and numerical models exhibit many similarities. The isosurface plots extracted from the numerical model closely follow those of the analytical model, with the thermal plumes displaying comparable rates of expansion and contraction. In most cases, the plume sizes are also very similar.

Limitations and Deviations
The analytical model that was used to verify the numerical model is based on the Infinite Line Source (ILS) model. Firstly, the numerical model assumes infinitely long piles and neglects the effects of the top and bottom boundaries and thus introduces inaccuracies close to those boundaries. It also considers an infinite medium with homogeneous properties throughout the entire domain. Usually the significant errors occur in very short or long distances from the pile and also when the simulation time is relatively short.

On the other hand, the numerical model even though can overcome some of the limitations mentioned above can be the one that introduces some inaccuracies as well. The heating/cooling demand changes smoothly in transition zones as the COMSOL can not handle rapid changes, while the analytical model can change the load instantly when this happens.

The errors that have been measured in those six different points that were selected are created due to different limitations of the analytical model and will be explained.
Point D has the highest measured error and it is depicted in 3.12d. The graph shows that the analytical model exhibits a delayed response of approximately four months at the beginning of the simulation. However, after this initial period, the magnitude of the temperature curve closely matches that of the numerical model. This deviation arises from the presence of the Euler–Mascheroni constant in the analytical equation. The effect of this constant is to smooth out or neglect small temperature variations occurring at the start of the simulation, which results in the apparent delay in the initial response.

In contrast, Point A 4.3a is located closest to the energy piles, and the second-highest error is observed at this location. This discrepancy arises from a combination of factors. First, as previously mentioned, the analytical equation does not account for the top and bottom boundaries and their influence on heat transfer mechanisms. Second, the analytical model assumes that the entire domain consists of a homogeneous material (soil). In reality, however, the piles are constructed of concrete cylinders with a diameter of approximately 0.4 m, which possess different thermal properties. This material difference affects the heat transfer processes and contributes to the observed deviation.

3.6. Operational Scenarios Design

This section describes how the heating and cooling demand of the Co-Creation Center was defined in order to construct different operational scenarios. The developed scenarios are then analyzed in detail, including the variable adjustments and the strategies underlying them. Overall, this section represents the second part of the methodology, aimed at investigating the limits, capabilities, and overall behavior of the system, and at extracting useful insights from the results.

3.6.1. Heating and Cooling Demand

The heating and cooling demand of the Co-Creation Center, the building in which the energy pile system is located, was designed for a five-year simulation period from 2020 to 2024. To generate these demand profiles, it was necessary to define the building's material properties, as well as external conditions such as outdoor temperature, indoor temperature setpoints, solar gains, and internal gains from occupants.

Material Properties of Building
The Co-Creation Center consists of glass façades on all four sides of the building. The heat losses and gains from the outdoor environment were calculated by considering the thermal behavior of the four glass walls as well as the rooftop. Based on the documentation provided for the building materials, the overall heat transfer coefficient U ($W/(m^2 \cdot K)$) for the walls and the ceiling was calculated. The heat losses and gains through the walls—comprising triple-glazed window facades—and the ceiling were determined using the calculated thermal properties, as summarized in the Table below.

Table 3.8: Overall heat transfer coefficient of materials

Parameter	Value U
Triple-Glazed Facades	0.75 W/(m^2·K)
Ceiling	0.25 W/(m^2·K)

Assumptions & Limitations

In that section the main assumptions that were taken into consideration will be presented and the physical limitations that must not be neglected.

Modelling

Initially, it is assumed that the flow rate of the system remains constant throughout its operation. It is set at 0.00017m^3/s, which corresponds to approximately 85% of the system's maximum flow capacity. A relatively high flow rate is desirable to ensure a high convective heat transfer coefficient, enabling efficient heat extraction or injection. The calculated Reynolds number is close to 2000, placing the flow at the boundary between laminar and transitional regimes. Additionally, for safety reasons, the water injected into the energy piles must not fall below −4°C to prevent freezing, and should not exceed 40–50°C, particularly for extended periods, as elevated temperatures may compromise the structural integrity of the concrete piles.

Indoor Temperature Setpoints - Ambient Air Temperature

In general, the indoor temperature for the winter in all the scenarios was 18 °C while in summer a temperature of 23 °C were selected. Those temperature setpoints are crucial to be able to measure the heat losses or gains to the ambient environment due to the temperature difference that exists between the inside part of the building and the outside ambient air temperature. To calculate the heat losses or gains of the building, hourly ambient temperature data from the KNMI weather station were collected for the period 2020 to 2024. [26]. The following Figure 3.14 shows the hourly air ambient temperature of those years.

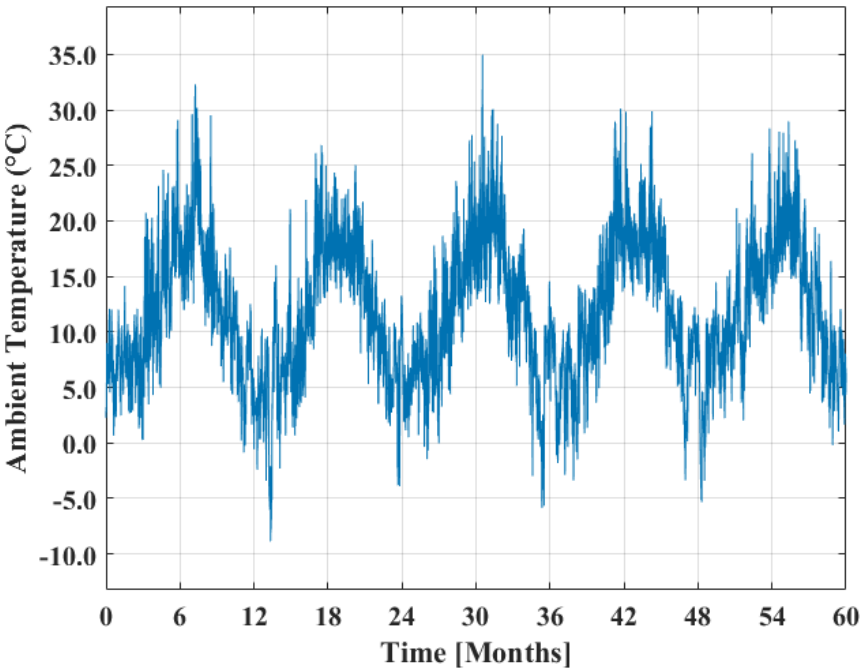

Figure 3.14: Hourly ambient air temperature for 5 years

Heating - Cooling Profile Design

To create the heating and cooling demand profile of the building, as mentioned above, it is necessary to calculate the heat losses and gains to and from the ambient environment, as well as the solar and internal gains from occupants. In this section, the corresponding graphs are presented.

Based on the equation below the heat losses or gains due to the heat transfer from the air ambient temperature are calculated for the glass walls and the ceiling and presented in the Figure for 5 years. The positive values are heat losses to the environment while the negative represent the gains from the environment.

$$Q = U \cdot A \cdot \Delta T \tag{3.6}$$

where:

- Q = Heat transfer rate (W)
- U = Overall heat transfer coefficient (W/m^2·K)
- A = Heat transfer surface area (m^2)
- ΔT = Temperature difference (K or °C)

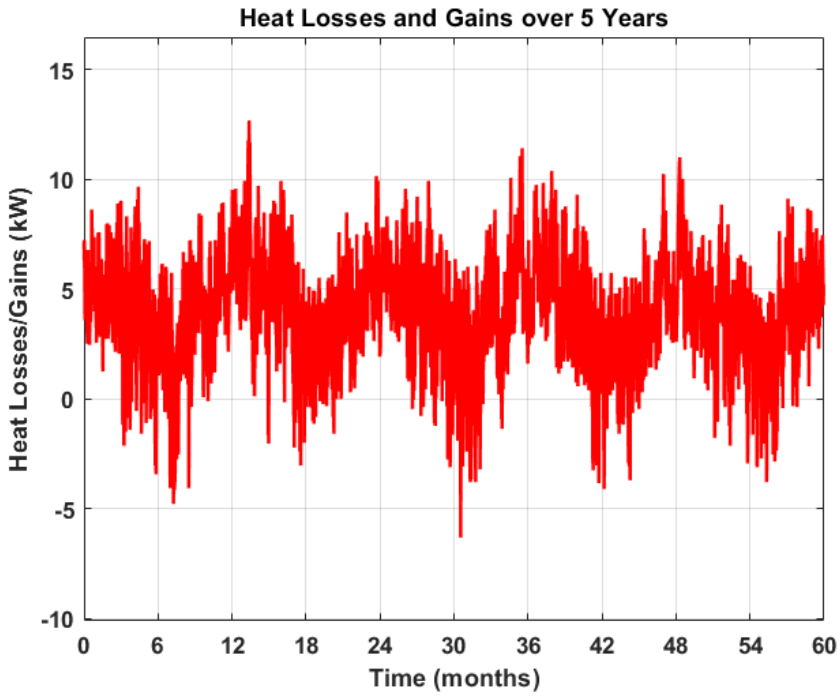

Figure 3.15: Heat Losses/ Gains of the building

The solar gains and internal gains from occupants were obtained from software that measures these values for the building and it is called Priva. Data were available for a two-year period, and the remaining years were constructed accordingly by taking into account the global irradiation data from KNMI and the provided event schedule. Figure 3.16 and Figure 3.17 illustrate the solar and people gains respectively.

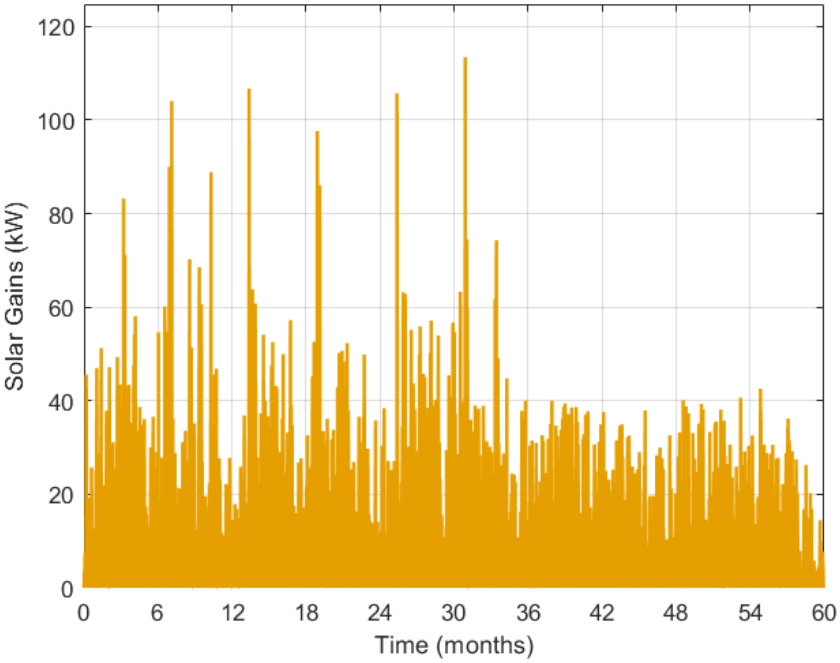

Figure 3.16: Solar gains

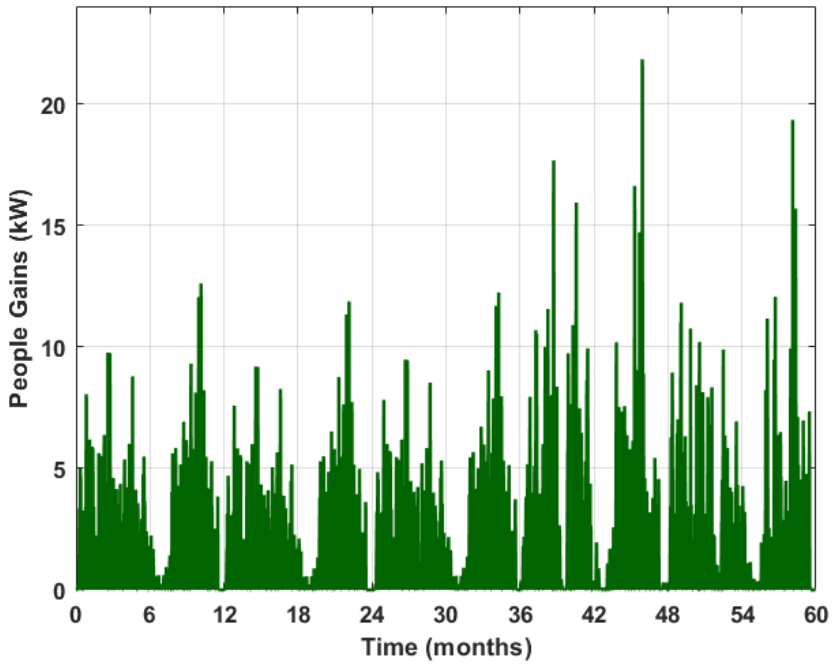

Figure 3.17: People gains

Using all the data presented above, the five-year heating and cooling demand of the building can be constructed by algebraically combining the heat losses/gains, solar gains, and internal gains from occupants. It is important to note, for clarity, that positive values correspond to heating demand, while negative values correspond to cooling demand. The base heating and cooling load assumes that heating is required from November to March, cooling from May to September, and that the system remains inactive during the transitional months in between. This base profile is later modified in certain scenarios through adjustments of variables and the introduction of new factors; however, it serves as the initial reference demand profile.Lastly, the maximum capacity for heating or cooling is assumed to be 20 kW in order for the working fluid to remain between reasonable temperature limits that have been established. In Figure 3.18 the heating and cooling demand of the Co-Creation Center for 5 years is illustrated.

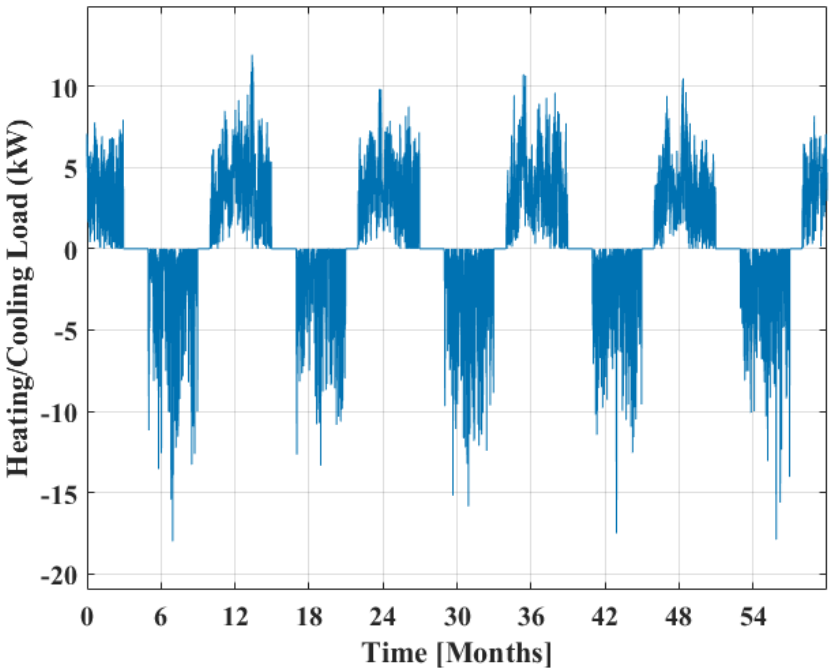

Figure 3.18: Heating/Cooling demand of Co-Creation Center for 5 years 8 hour time step

The heating and cooling demand illustrated above represents the loads that the energy pile system must deliver to the building.It needs to be mentioned that the loads are averages every 8-hours in order to save some time for the simulation and to keep as good precision as possible. Nevertheless, in the numerical model, in order to simulate the ground behavior, the heat transfer mechanisms, and the working fluid temperature at the inlet and outlet, the energy exchanged with the ground (extracted or injected) needs to be defined. It is assumed that the energy pile system is connected to a ground source heat pump (GSHP) operating in both heating and cooling modes. Based on findings in the literature, the system is considered to operate with a COP_{heating} of 4.5 during winter and a COP_{cooling} of 4 during summer [18][28] [19]. Using these values, the power extracted from the ground in heating mode and the power injected into the ground in cooling mode can be calculated from the equations below.

Heating Mode

$$COP_{\text{heating}} = \frac{Q_{\text{out}}}{W_{\text{in}}} \tag{3.7}$$

$$Q_{\text{extracted}} = Q_{\text{out}} - W_{\text{in}} = Q_{\text{out}} \left(1 - \frac{1}{COP_{\text{heating}}}\right) \tag{3.8}$$

Cooling Mode

$$COP_{\text{cooling}} = \frac{Q_{\text{in}}}{W_{\text{in}}} \tag{3.9}$$

$$Q_{\text{injected}} = Q_{\text{in}} + W_{\text{in}} = Q_{\text{in}} \left(1 + \frac{1}{COP_{\text{cooling}}}\right) \tag{3.10}$$

By applying the two equations to the heating and cooling demand profile, a new profile of the injected and extracted power to and from the ground is obtained. This profile is used as input to the numerical model in order to perform the simulations. As expected, the injected and extracted power profile follows

the general trend of the heating and cooling demand; however, it represents the most important input for the analysis, as it is applied in all scenarios and subsequently modified to account for changes in variables, scheduling, and more advanced control strategies that will be introduced and described. To conclude, the extracted/injected power profile is directly linked to the building's heating and cooling demand and represents the corresponding energy exchange with the energy pile system. In Figure 3.19 the profile that is created with the use of the equations above from the heating and cooling demand profile that was presented previously is illustrated.The positive values represent the energy extracted from the ground while the negative values represent the energy injected into the ground. It is a graph that the power extracted or injected is averaged every 8 hours and that technique is implemented in every following graph.

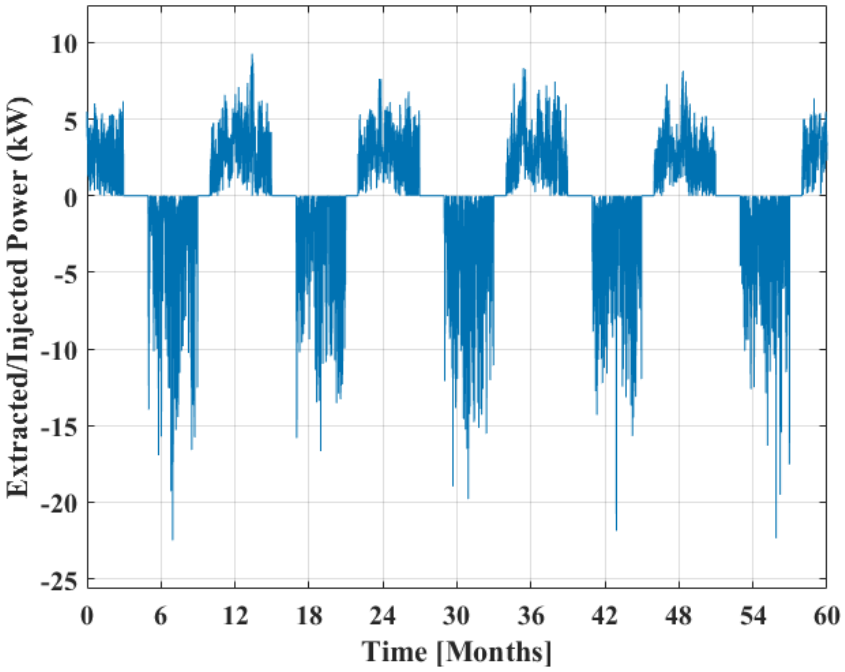

Figure 3.19: Extracted / Injected Power from and to the energy pile system with an 8 hour time-step

The steps described in this section were essential for designing a general five-year heating and cooling demand profile that describes the energy demand of the building. By incorporating the adjustments and assumptions that were made regarding the ground source heat pump (GSHP) and the coefficients of performance (COP), which are considered constant during winter and summer, a new energy profile is created from the demand profile of the building. Based on this, a corresponding profile of the energy extracted from or injected into the ground was created and subsequently used as input for the numerical model and the simulations conducted.

3.6.2. Operational Scenarios

In this section, the operational scenarios that were designed are presented. Their purpose and objectives are analyzed, along with their specific characteristics. In total, eight scenarios were simulated and the results were post-processed. The aim of these scenarios was to address the main research objective: how the efficiency and reliability of the system can be maximized. Accordingly, different strategies were implemented based on the building's heating and cooling demand to achieve this goal. Through these scenarios, the maximum capacity and limits of the energy pile system were investigated, together with its capabilities and the behavior of the subsurface in response to these operations.

Based on the heating and cooling demand profile of the Co-Creation Center (CCC), it was identified that the building experiences significant heating demand from November to March and cooling demand from May to August. The optimum scenario would be for these demands to be fully covered

by the energy pile system while also maintaining the system's energy balance. Energy balance is a critical factor in heat storage systems, as it ensures high efficiency during long-term operation while supporting both the sustainability and longevity of the system. Below, the variables and setpoints of each scenario are presented, together with their purpose, in order to clarify the strategy behind them. Additionally, in the Appendix B the profile that is used as an input in each scenario which is the power extracted or injected to the system can be found.

Scenario 1 - Baseline Performance Assesment

The purpose of this scenario is to observe how the system performs under the calculated heating and cooling demand without any optimization. In this case, the heating demand is covered during the critical months of November to March, while the cooling demand is covered from May to August. The indoor temperature setpoints are 18 °C in winter and 23 °C in summer. This scenario serves to indicate the direction in which optimization should proceed and to quantify the magnitude of the energy imbalance when the system is required to meet the majority of the heating and cooling demand.

Optimization of Operational Parameters

Scenarios 2 3

The research afterwards will move towards the optimization of various parameters in order to reach an energy balanced system. Different indoor temperature setpoints, seasonal schedules and duration of heating and cooling modes were constructed. Those changes were made to be able to improve the efficiency of the system and to achieve an energy balance throughout the thermal energy storage. In Scenario 2, in order to reach an energy balance the heating mode was reduced and was activated from December to March while the cooling mode was extended from May to mid of September. The indoor temperature setpoints were remained as usual. The system was able to reach a balance within a 5% margin that was defined as acceptable. In Scenario 3, a different strategy were implemented. The significant heating demand was able to be covered from November to March and the cooling demand from May to August. However, the indoor temperature setpoint in the summer was reduced to 21 °C in order to be able for the system to store more energy and deliver it in winter. The system was defined as completely balanced. Although both scenarios achieve the important objective of maintaining energy balance, they involve certain compromises. In Scenario 2, the full heating demand is not met throughout the year, while in Scenario 3, thermal comfort during summer may be reduced due to low indoor temperatures. For this reason, more complex strategies must be investigated to ensure that the system can satisfy all defined conditions. In Figure 3.20 the extracted and injected power that was used as an input in the numerical model with a time step of 8 hours is illustrated.

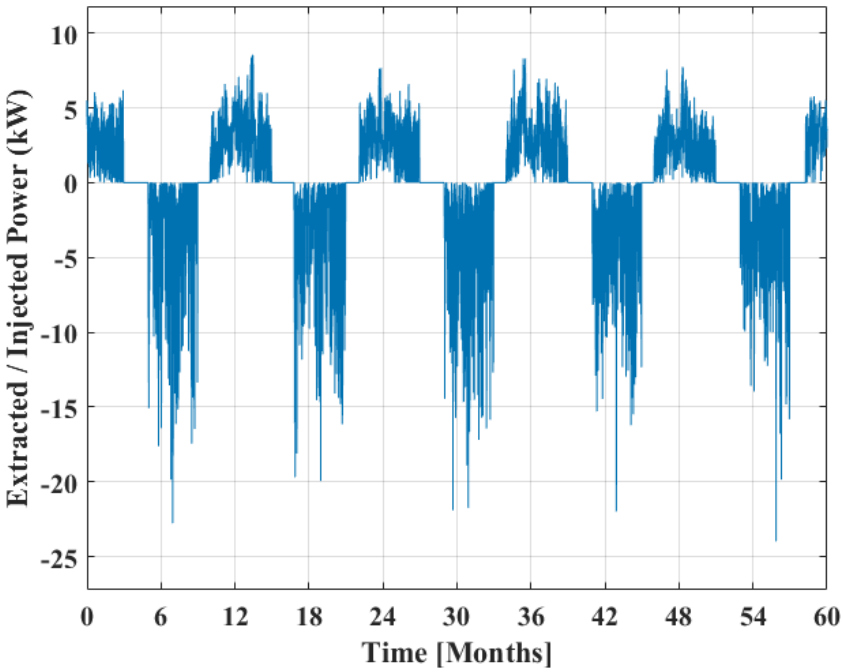

Figure 3.20: Extracted / Injected Power from and to the energy pile system - Scenario 3

Investigation of Passive Solar Strategies

Scenarios 4,5 & 6

The aim of the scenarios that were created and will be presented in that section is to cover the majority of the heating and cooling and achieve an energy balance in the energy pile system. For that reason, passive solar strategies will be implemented in those scenarios that will satisfy the parameters that were stated above while also maintain good thermal and visual comfort in some cases for the occupants of the building. The building has solarblinds in every glass facade that are used to keep outside the excess solar energy and to reduce the cooling demand.In addition to reducing unwanted solar gains, the solar blinds contribute to visual comfort by minimizing glare and preventing direct sunlight from obstructing occupants' vision or interfering with the visibility of screens. Based on data retrieved from the building management platform (Priva), it was calculated that between May and August, the building operates with the solar blinds fully deployed for approximately 1,000 hours which is around 30 % of the total time. The scenarios developed investigate whether energy can be stored by adjusting the solar blinds to different angles and operating them for varying durations. This technique will make able the system to store excess energy from solar gains and provide the appropriate heating demand during winter while maintain an energy balance throughout the year.
Initially, in all scenarios the indoor temperature was maintained 18 °C during winter and 23 °C during summer to secure good thermal comfort for the occupants.Moreover the heating demand is covered for the months that is needed, from November to March. The variables that were changing was the scheduling of the cooling demand and the opening of the solar blinds.
In Scenario 4, the cooling mode is activated from May to August, while the solar blinds are partially opened during certain hours when they would otherwise be fully closed, specifically from June to August. Energy balance is achieved throughout the year, meaning that the energy extracted during winter is reinjected in summer. However, this strategy may reduce the visual comfort of the occupants. According to the people gains data (see Appendix People Gains), the Co-Creation Center hosts events primarily from September to June, while in July—and especially August—the building is largely unoccupied, with few or no events. This implies that opening the solar blinds in June to gain additional solar energy would negatively affect visual comfort when the building is more frequently in use.

Scenario 5 addresses this issue by modifying the solar blind schedule while keeping the same heating and cooling operation periods. In this case, the blinds are opened only from mid-July until the end of August, when building occupancy is low, thereby minimizing any impact on visual comfort. Scenario 6 adopts the same solar blind schedule as Scenario 5 but investigates whether shifting the cooling mode to run from June through September can further improve performance. In Figure B.5 the graph that were used as an input for the Scenario 6 is depicted. Compared with the graph of Scenario 3 presented in the previous section, it can be observed that more energy is stored during summer, allowing it to be distributed in winter to sufficiently cover the entire heating load.

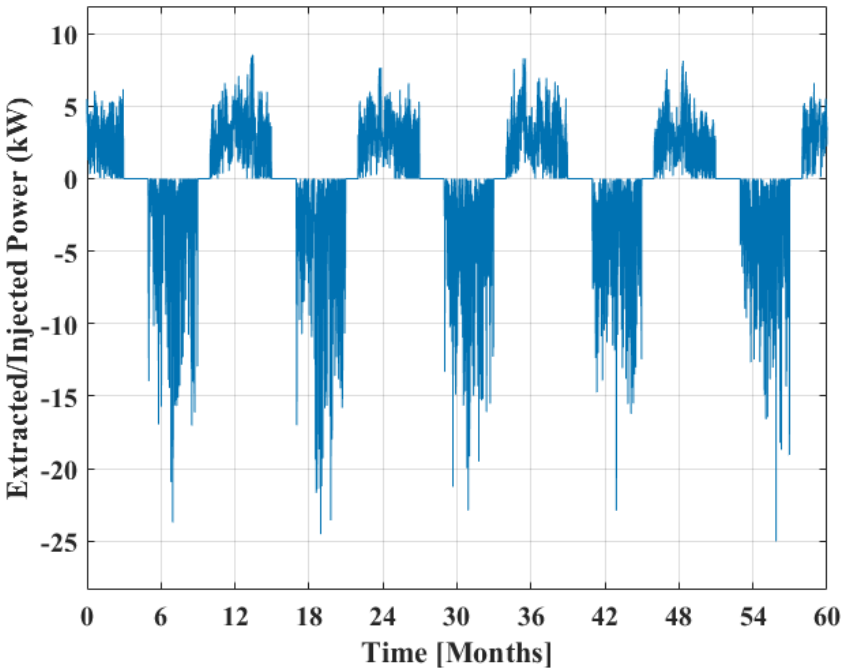

Figure 3.21: Extracted / Injected Power from and to the energy pile system - Scenario 6

In conclusion, in all scenarios the energy balance is satisfied and it is investigated the optimum approach to do that. The detailed results will be presented in the next Chapter.

System Capacity Assesment - Scenario 7

Subsequently, a scenario was designed to stress the system and investigate its limits. This scenario is essential for determining the maximum annual capacity that the system can deliver and for monitoring the inlet and outlet temperatures simulated by the numerical model. The inlet temperature has predefined upper and lower limits to prevent damage to the energy pile system, and these must be maintained within safe boundaries. Moreover, Scenario 7 serves as an initial step toward addressing the final sub-question of the research: whether surplus energy can be stored and supplied to neighboring buildings. By testing the system's limits, it can be evaluated whether the system is capable of handling higher heating and cooling demands. In Scenario 7, the heating and cooling demand of Scenario 5 is multiplied by a factor of 1.5 in order to assess the capabilities of the energy pile system under increased load conditions. It should be noted that the maximum capacity that can be injected into the system is limited to 25 kW. Any values exceeding this threshold are capped to prevent overheating of the concrete in the energy piles and to protect the structural stability they provide to the building.

Surplus Energy Potential - Scenario 8

The aim of that final scenario that will be simulated is to investigate if surplus energy can be gained

from the opening of the solar blindings during summer and be distributed to neighboring apartment during winter. This action will potentially reduce the carbon emissions and the electricity consumption simultaneously. The indoor temperature settings for summer and winter, as well as the building's operational schedule, follow those defined in the previous scenarios, with the solar blinds partially opened during July and August to allow excess energy to be stored in the subsurface system. The aim of this scenario is to investigate whether surplus energy can be stored to fully or partially cover the heating demand of a dwelling of approximately 60–70 m^2. The annual heating energy consumption for such an apartment is estimated at around 6,000–6,500 kWh [22]. Furthermore, it is assumed that this demand would be met using a ground source heat pump (GSHP). Under this assumption, the required surplus energy to be stored during summer is approximately 5,000 kWh, based on a COP of 4 for the apartment. It is also assumed that the energy stored during summer will be fully extracted to meet the required heating demand in winter, while any surplus will be carried over and stored for the following season. Furthermore, the heating demand profile of the neighboring building is assumed to follow the same pattern as that of the Co-Creation Center. In Figure 3.22 the energy extracted or injected into the system is presented. It can be seen that compared to the previous graphs the loads are much higher due to the energy that the system needs to deliver both in summer and winter. Also, it can be seen that the system is operating to its maximum capacity during summer cooling mode when it is storing energy in the subsurface surrounding soil.

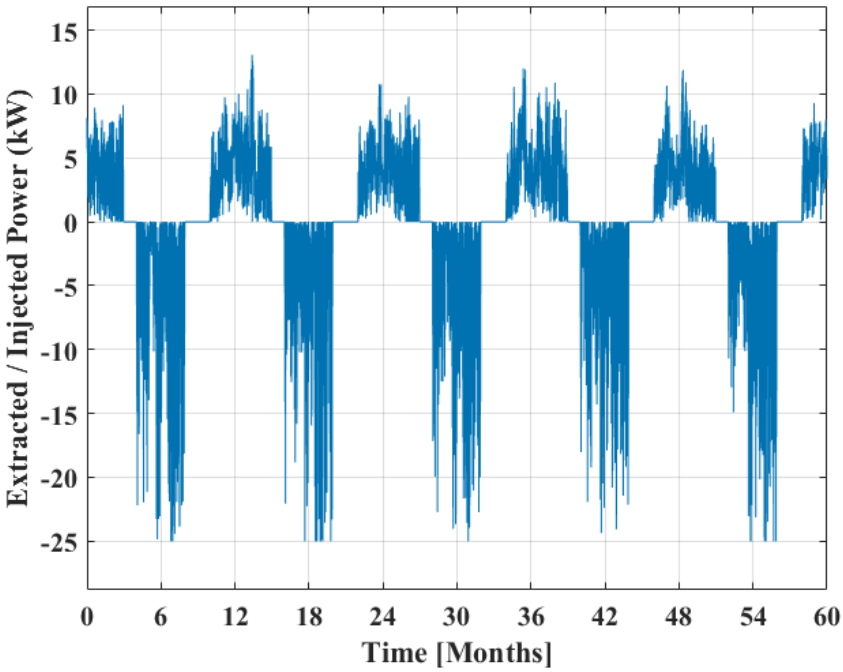

Figure 3.22: Extracted / Injected Power from and to the energy pile system - Scenario 8

4

Results

In this section, the detailed results obtained from the simulations of the scenarios described in the previous chapter are presented and discussed. The main graphs selected for presentation include the ground temperature, cumulative energy balance, average temperature of the energy piles and its deviation, inlet temperature of the working fluid, and the temperature difference between the inlet and outlet. These graphs provide the basis for observations regarding the system's behavior, efficiency, and capabilities. Furthermore, this results chapter also addresses the remaining sub-questions of the research, which are discussed in dedicated subsections.

4.1. Preconditioning Phase

Before simulating the operational scenarios, it is essential to establish a realistic thermal gradient throughout the soil depth. Initially, the entire model domain is assumed to have a uniform temperature of 12 °C, which does not accurately represent real conditions. In reality, the shallow layers of soil experience significant temperature fluctuations due to seasonal variations in ambient air temperature. To address this, a preconditioning phase is implemented. During this phase, a two-year simulation is conducted without any energy injection or extraction from the system. The only active boundary condition is the top surface of the soil, which is exposed to ambient air temperature. This allows natural conductive heat transfer between the ground and the atmosphere, enabling the development of a more realistic initial temperature distribution within the soil domain.In Figure 4.1 the ambient air temperature profile for the two years of simulation is depicted.

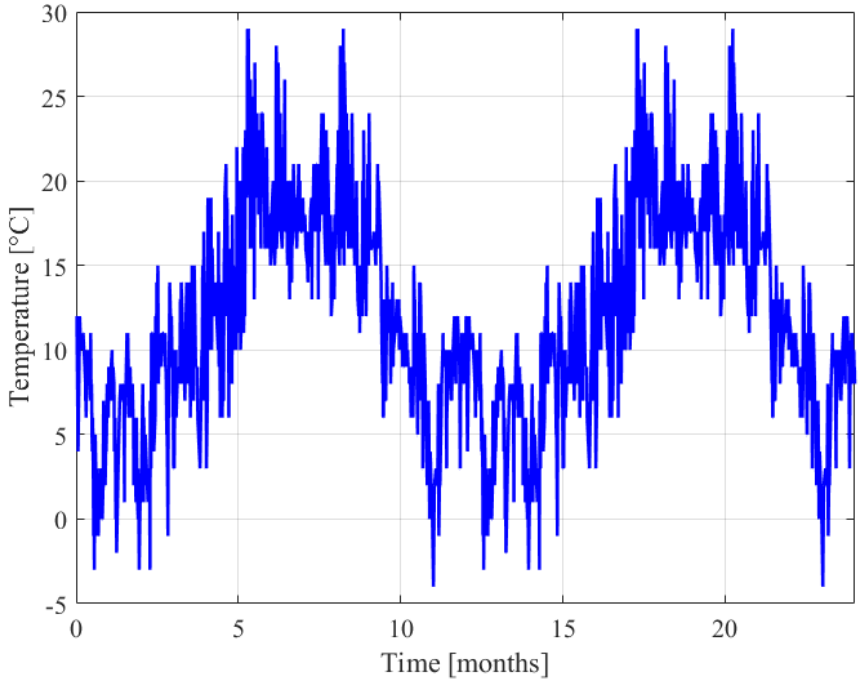

Figure 4.1: Ambient air temperature profile

After this simulation, the aim is for the model to reach thermal stabilization, characterized by minimal temperature variation over time and zero heat flux at the deeper soil boundaries. This condition indicates that no significant heat transfer occurs between the upper and lower soil layers, and a stable thermal gradient has been successfully established. To evaluate these conditions, the temperature difference at the end of each year is measured and isosurface plots are generated to to visualize the isothermal surfaces in the deeper layers of the soil.

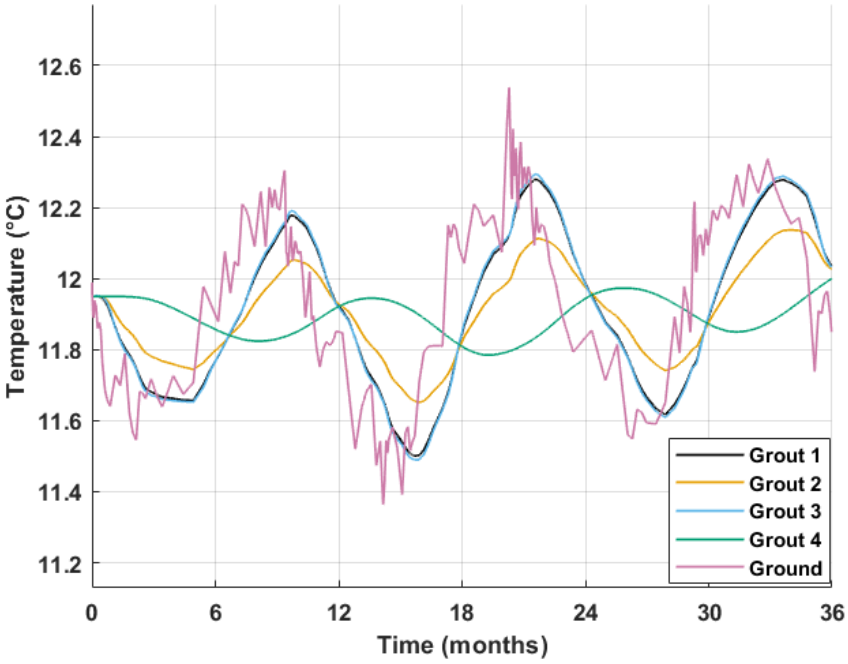

Figure 4.2: Ground and grout temperature in preconditioning phase

In Figure 4.2 the temperature variation of various energy piles and the ground throughout three years of simulation under the same ambient air temperature pattern is depicted. Grout 1 and 2 are the inlet pile and outlet pile respectively while the grout 4 is the middle pile of the circuit. The temperature difference of the ground between the start of the simulation and the end of the first year is - 0.13 °C, afterwards the difference between the end of the first year and the end of the second is 0.02 °C and in the end is again 0.03 °C. This demonstrates that the ground establishes a stable thermal gradient by the end of the second simulation year, which explains the decision to precondition the system for two years instead of three, as extending further does not improve the thermal balance. The ground stabilizes at approximately 11.85 °C, which was taken as the initial temperature for all scenario simulations.

Furthermore, below in Figure 4.3 the isosurfaces plots at the end of those years are presented.The curved isosurfaces indicate that heat flux is occurring between the layers of the soil, either upward or downward. In contrast, the bottom isosurface appears parallel to the boundaries exposed to ambient air temperature, suggesting that the heat flux at the deepest layers is effectively zero. This implies that a stable thermal gradient has been established throughout the soil depth, and no significant heat transfer occurs in those deeper regions.

The bell-shaped isosurfaces that forms between the energy piles is a result of the boundary condition defined as open to ambient air. Since the rectangular domain around the energy piles is insulated, the only pathway for heat transfer is through the open sides. Consequently, the pile located at the center of the configuration experiences the highest thermal delay, as it is the farthest from the open boundaries. This explains the bell-shaped isosurfaces observed in the graphs.

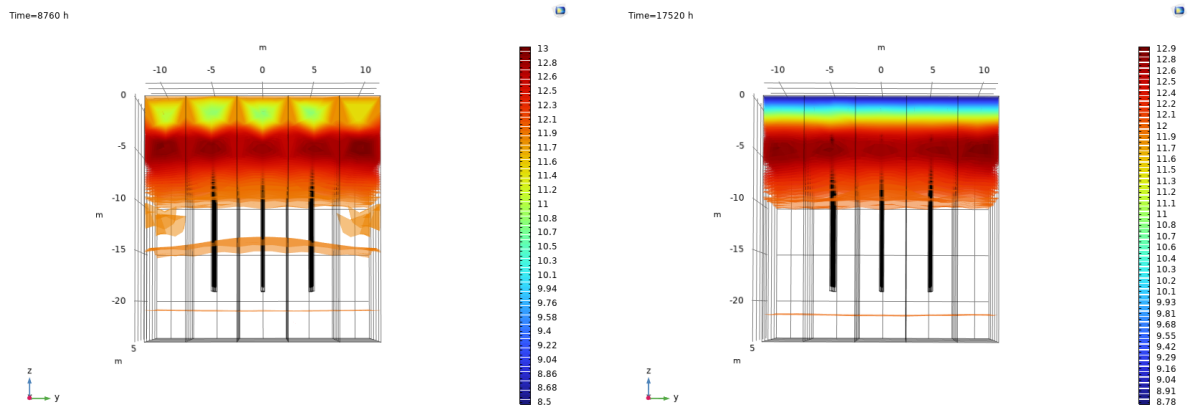

(a) End of first year

(b) End of second year

Figure 4.3: Isosurface plots of the domain

The bell-shaped isosurfaces that forms between the energy piles and is illustrated in Figure 4.4 is a result of the boundary condition defined as open to ambient air. Since the rectangular domain around the energy piles is insulated, the only pathway for heat transfer is through the open sides. Consequently, the pile located at the center of the configuration experiences the highest thermal delay, as it is the farthest from the open boundaries. This explains the bell-shaped isosurfaces observed in the graphs.

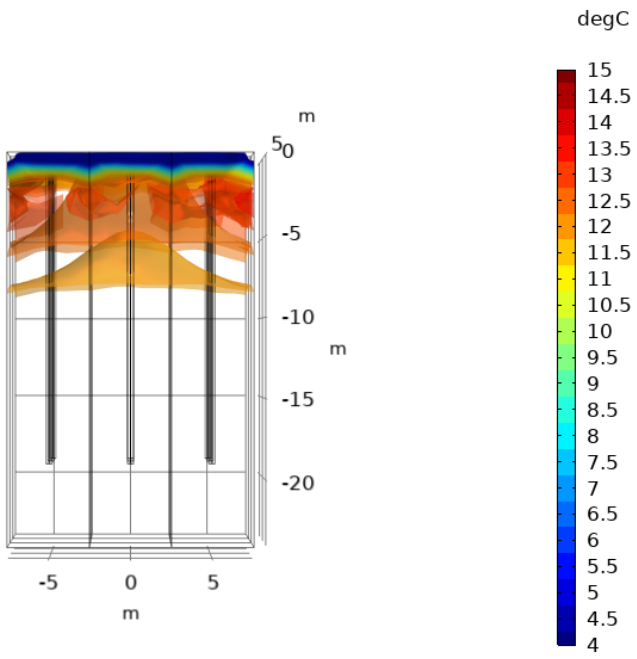

Figure 4.4: Bell-shaped Isosurface plot of preconditioning phase

4.2. Operational Scenarios

In order to be able to answer the main objective question of the research and the sub-question that has been asked 8 scenarios were created. The heating/cooling demand profile will be presented as well as the energy balance of the system. Additionally, the temperature profile of the grouts of the energy piles and soil will be presented in graphs. Inlet and outlet temperatures are going to be pre-

sented and discussed in detail in order to evaluate the performance of the system. The Scenario 1 is named ”Business as usual” as it is a basic scenario to observe how the system behaves under the heating/cooling load that was calculated. In this scenario, the energy is not balanced, and the system is not optimized. In Scenarios 2, 3 adjustments are made to indoor temperature setpoints, the selection of heating and cooling months, and the duration of these periods, in order to maximize the delivered energy and achieve energy balance. Scenarios 4, 5, and 6 take weather conditions into account by investigating the potential to increase solar gains through the controlled operation of solar blinds, allowing them to open for certain hours. Scenario 7 examines the limits and heating/cooling capacity of the system by increasing the thermal load. Finally, Scenario 8 explore whether surplus energy can be stored during the summer and whether this stored energy is sufficient to be distributed to a neighboring apartment.

4.2.1. Baseline Performance Assesment - Scenario 1

As it was mentioned the first scenario is designed without any optimization to show in which direction the system needs to be optimized in order to reach an energy balance. As it can be seen from the Figure 4.5 it is extracted more energy that it is injected annually thus the system was a negative deficit, that increasing with the passage of the years. This means that the heating load is much higher than the cooling load and gives incentives towards the strategies that need to be implemented in order to reach a balance.

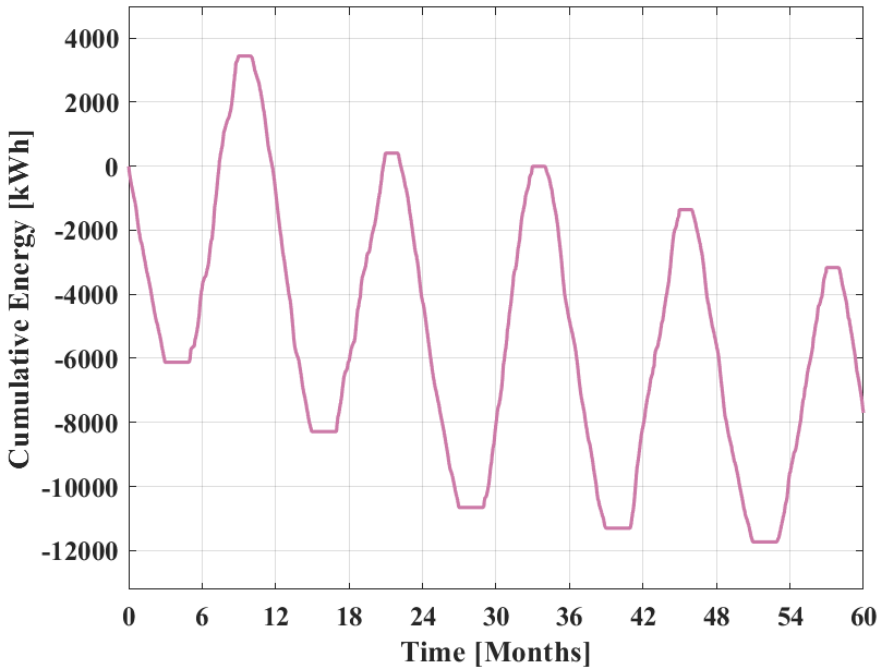

Figure 4.5: Energy Balance - Scenario 1

In Figure 4.6, the evolution of the ground temperature is shown. During the first three years of the simulation, the ground temperature decreases due to the system’s energy imbalance, with more energy being extracted than injected. However, in the fourth and fifth years, the ground temperature appears to stabilize and resist this downward trend. This indicates that the surrounding soil, acting as a thermal buffer, is able to maintain its temperature despite the energy deficit, thereby halting the negative rate of temperature decline. Moreover, Figure 4.7 illustrates the average energy pile temperature along with the maximum deviation from it. The average temperature fluctuates between 5 °C and 21 °C across the winter and summer seasons, while the deviation ranges from approximately +2 °C above the average to –1.5 °C below it. It can be observed that during the summer season, larger deviations occur in both colder and hotter inlet fluid temperatures compared to winter. This can be explained by the greater magnitude of the inlet temperatures during summer operation and their larger difference

from the average ground temperature.

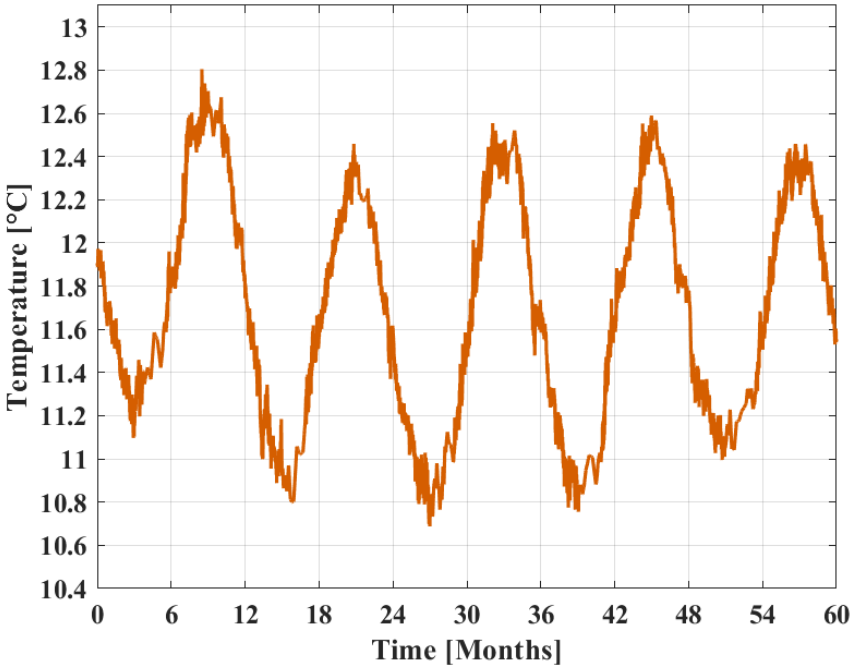

Figure 4.6: Average Ground Temperature - Scenario 1

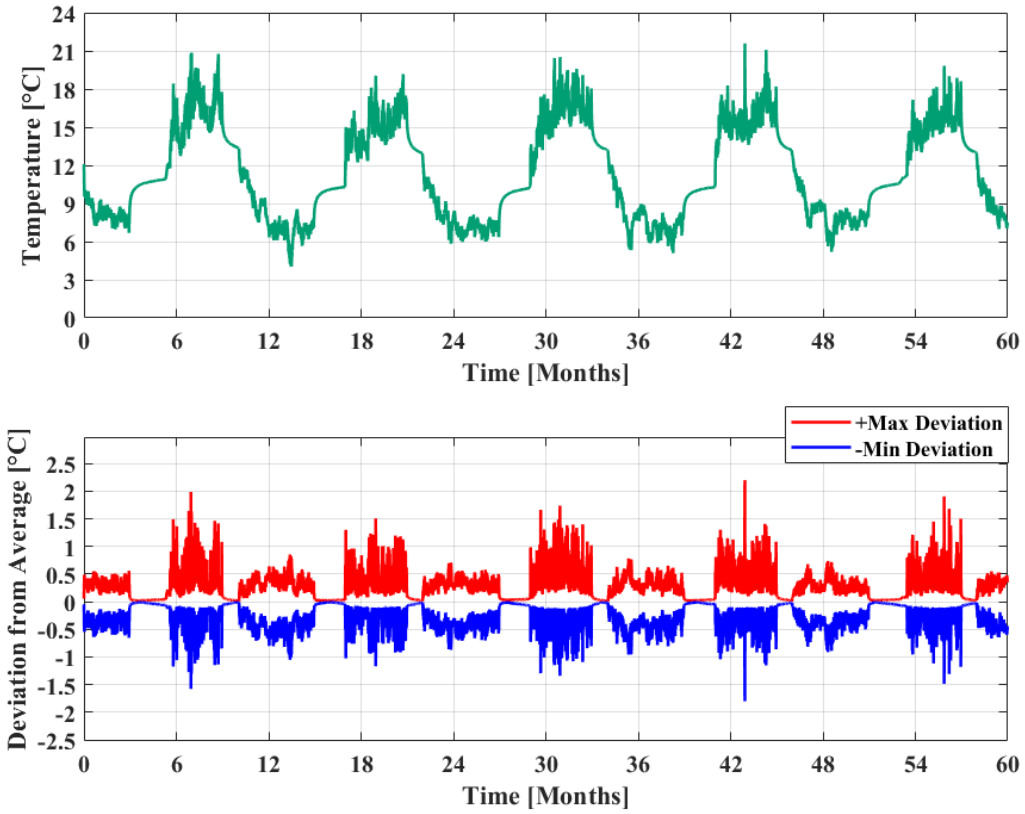

Figure 4.7: Enery piles average temperature and maximum deviation - Scenario 1

In the following, the inlet temperature graph and the temperature difference between outlet and inlet are presented. In Figure 4.8 it can be seen that the inlet temperature of the fluid fluctuates from 2 °C to 30 °C with a minimum observed during winter of 0 °C and a maximum during summer of approximately 34 °C. These values are within the defined limits and are consistent with expectations. Figure 4.9 shows that the ΔT can reach up to 2 °C in winter and up to 8 °C in summer. This occurs because, during summer, the inlet temperature differs more significantly from the ground temperature compared to winter. As a result, the heat flux is higher, and more energy can be transferred during the summer season.

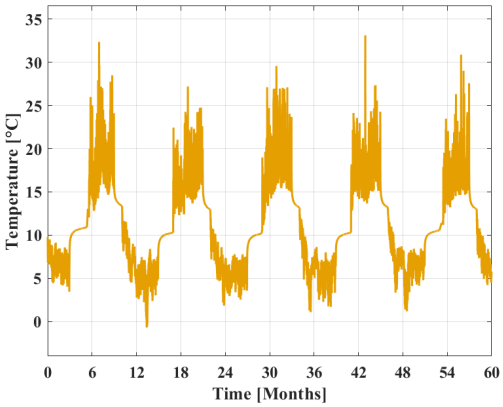

Figure 4.8: Inlet Temperature - Scenario 1

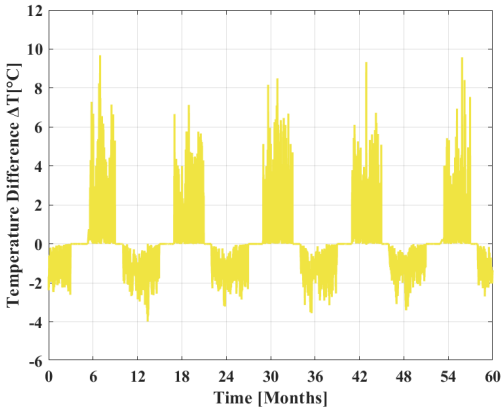

Figure 4.9: Temperature Difference between inlet and outlet - Scenario 1

4.2.2. Optimization of Operational Parameters

This section and the following one are dedicated to answer a main subquestions which is :

4.What control strategies should be used based on the energy demand, weather conditions and seasonality ?

In that section Scenario 2 and Scenario 3 will be presented that were designed by modifying the indoor temperature setpoints, seasonal schedule and duration of the heating or cooling modes as were presented in the previous chapter Those changes were made to be able to improve the efficiency of the system and to achieve an energy balance throughout the thermal energy storage system.

Scenario 2

The accumulative energy balance graph is presented for the simulation of Scenario 2. It can be seen in Figure 4.10 that the system is not perfectly balanced and has a deficit however it is in an acceptable rate of 5 %. A balance is important to be kept in order to achieve high performance throughout the whole operation of the system and also to ensure the longevity of it.

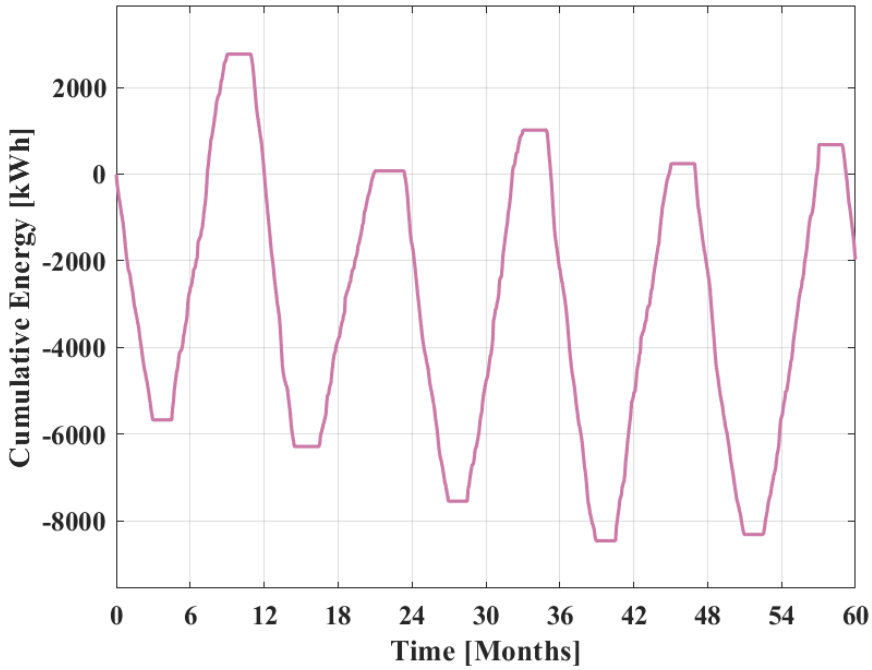

Figure 4.10: Energy Balance - Scenario 2

Table 4.1 , 4.2 shows all the details for the energy that was extracted or injected to the ground while also show the amount of heating or cooling demand that was delivered to the building. The electricity consumption was calculated to be able to determine the season performance factor of the system, which was 4.32.

Table 4.1: System performance in Scenario 2 (heating).

Parameter (Heating)	Value (kWh)
Total energy extracted	43,002
Annual energy extracted	8,600
Total energy delivered	55,131
Annual energy delivered	11,026
Total electricity consumed	12,128
Annual electricity consumed	2,425

Table 4.2: System performance in Scenario 2 (cooling).

Parameter (Cooling)	Value (kWh)
Total energy injected	41,033
Annual energy injected	8,206
Total energy delivered	32,826
Annual energy delivered	6,565
Total electricity consumed	8,206
Annual electricity consumed	1,641

In Figure 4.11 the ground temperature is depicted throughtout the simulation. It can be seen that follows a stable pattern compared to the Scenario 1 because of the energy balance that has been achieved annually. The ground temperature fluctuates from 11.9 °C to 12.8 °C and at the end of the simulation it is observed a small decrease of 0.4 °C due to the 5% imbalance that exists in the system. Moreover in the following Figure 4.12 it can be seen that the average grout temperature has been shifted upwards compared to the Scenario 1.This is explained by the balanced fluctuations of the ground temperature. In Scenario 2, the ground temperature is relatively higher than in Scenario 1. As a result, in winter the system does not need to circulate water at very low temperatures to extract the required power, while in summer it must circulate water at higher temperatures to store the thermal energy from the building.

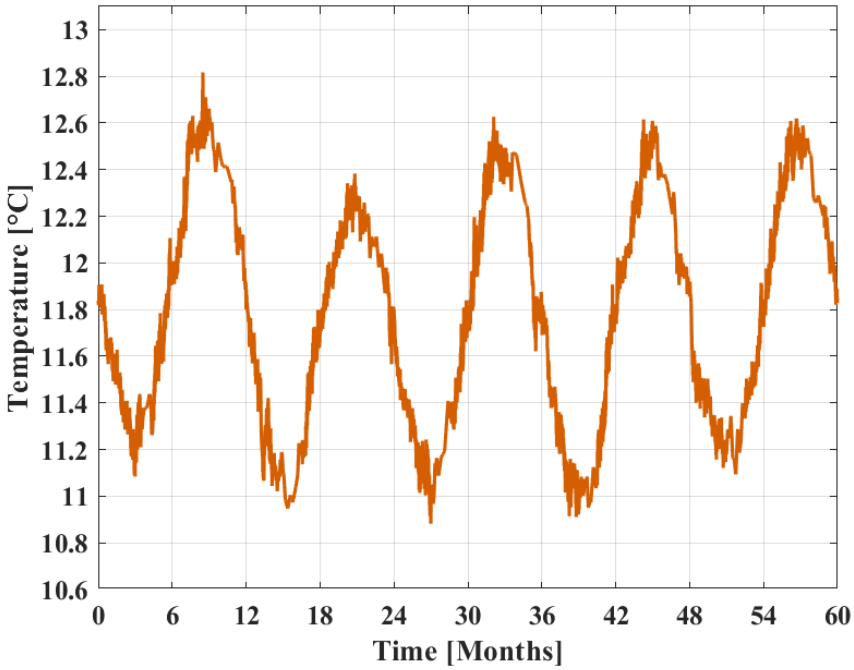

Figure 4.11: Average ground temperature - Scenario 2

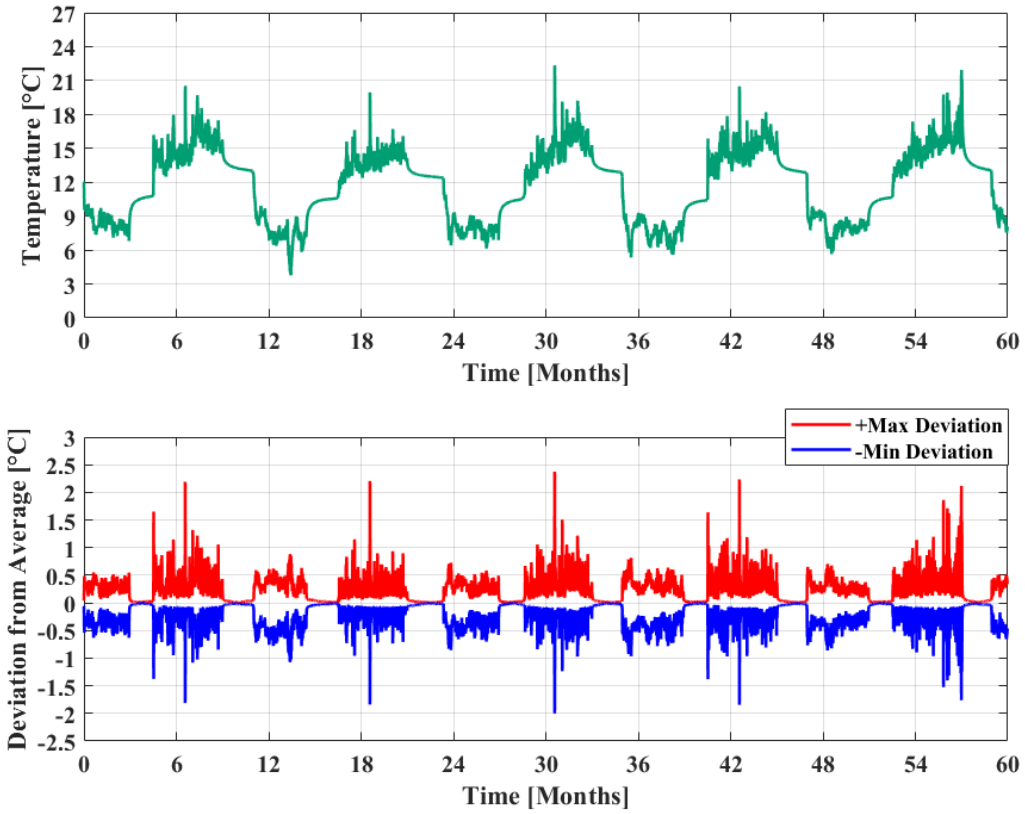

Figure 4.12: Average energy pile Temperature and maximum deviation - Scenario 2

Continuous monitoring and presentation of the inlet temperature are essential to ensure the proper functioning of the system. Furthermore, the temperature difference between the inlet and outlet serves as a key indicator of the amount of energy being extracted from or injected into the ground through the system. Below at the presented graphs this trend that were commented in the previous paragraph can be observed as well, the inlet temperature is higher during summer compared to Scenario 1 and again higher during winter compare to Scenario 1 which showcasing the shift upwards.

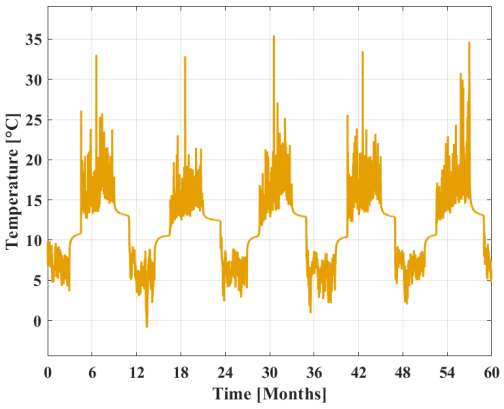

Figure 4.13: Inlet Temperature - Scenario 2

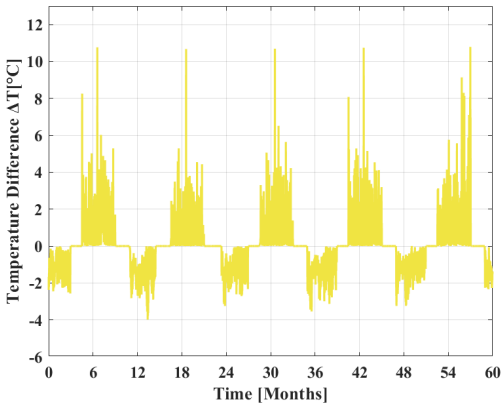

Figure 4.14: Temperature Difference between inlet and outlet - Scenario 2

Scenario 3

In that scenario a different approach was examined. The values that was changed was the indoor temperature during the summer that lowered to 21 °C in order to increase the cooling demand which would increase the energy stored as it was mentioned to the previous chapter. In Scenario 3 the system is completely balanced throughout all the years and the whole simulation, the corresponding graph can be seen in Appendix C. In Scenario 3 more energy is extracted and injected in the system annually and can be justified from the schedule of operations that were mentioned. This scenario satisfies the complete demand that were evaluated as significant and the Tables 4.3 , 4.4 below show the detailed results.

Table 4.3: System performance in Scenario 3 (heating).

Parameter (Heating)	Value (kWh)
Total energy extracted	54,927
Annual energy extracted	10,985
Total energy delivered	70,420
Annual energy delivered	14,084
Total electricity consumed	15,492
Annual electricity consumed	3,098

Table 4.4: System performance in Scenario 3 (cooling).

Parameter (Cooling)	Value (kWh)
Total energy injected	54,853
Annual energy injected	10,970
Total energy delivered	43,882
Annual energy delivered	8,776
Total electricity consumed	10,970
Annual electricity consumed	2,194

The ground temperature is similar to the Scenario 2 however, it seems that in Scenario 3 the ground temperature has shifted upwards which means that the maximum temperature that is observed is around 13 °C and the minimum 11.9 °C. This seems to happening due to the increase of the total load delivered both in winter and summer and also because of the complete energy balance that occurs in that scenario. Moreover, due to this ground temperature effect the inlet temperature is shifted upwards as well while the grouting average temperature remains almost the same for that scenario.

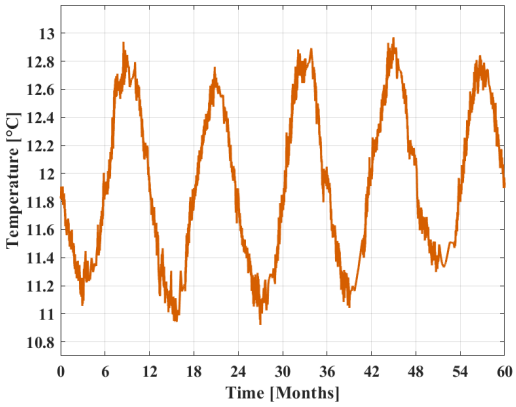

Figure 4.15: Average Ground Temperature - Scenario 3

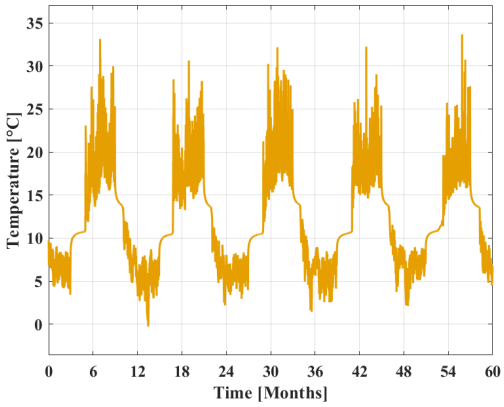

Figure 4.16: Inlet Temperature - Scenario 3

In this section, an initial optimization of the system was explored by adjusting the scheduling and variable setpoints. However, as noted in previous sections, these adjustments involved compromises: in one case the heating load was reduced, while in another the thermal comfort of occupants was affected by low indoor temperatures during summer. For this reason, further investigation was carried out through scenarios that take weather conditions into account. These simulations are presented in the following subsection and aim to fully address the sub-question stated at the beginning of the study.

4.3. Investigation of Passive Solar Strategies

The previous scenarios that were investigated were energy balanced in a reasonable margin and different temperature setpoints and durations of heating and cooling were simulated. However, in order to satisfy the complete demand and achieve a good thermal and visual comfort new strategies were

investigated and applied in Scenarios 4,5 and 6. The strategies and the schedule were presented in the previous chapter. In all the scenarios of that section an energy balance is accomplished however the magnitude of the graph is changing. Those graphs can be found in the Appendix C.

Scenario 4

In this scenario the opening of the solar blindings partially from June to August was simulated and the detailed graphs were extracted and will be presented. Initially, in Tables 4.5 , 4.6 can be seen the details of the simulation in energy terms. It can be observed from the tables below that the reported energy amounts are almost identical to those in Scenario 3. This is because Scenario 3 succeeds in fully covering the heating demand, in contrast to Scenario 2, which does not. In this section, however, all scenarios manage to meet the heating demand of the building while also ensuring both thermal and visual comfort, which may be less satisfactory in Scenario 3.

Table 4.5: System performance in Scenario 4 (heating).

Parameter (Heating)	Value (kWh)
Total energy extracted	55,120
Annual energy extracted	11,024
Total energy delivered	70,666
Annual energy delivered	14,133
Total electricity consumed	15,546
Annual electricity consumed	3,109

Table 4.6: System performance in Scenario 4 (cooling).

Parameter (Cooling)	Value (kWh)
Total energy injected	55,207
Annual energy injected	11,041
Total energy delivered	44,166
Annual energy delivered	8,833
Total electricity consumed	11,041
Annual electricity consumed	2,208

The ground temperature and the grouting average temperature with the deviation are not presenting any significant changes from scenario 3 and can be found in the Appendix C. However, the inlet temperature profile and the temperature difference have some changes in this scenario compared with the previous scenarios. In Figure 4.17 and 4.18 it can be seen that especially in summer the inlet temperature in scenario 4 is slighlty higher than in scenario 3. This is explained by the increase in solar gains simulated in Scenario 4, which is achieved by tilting the solar blinds for several hours during the day when they would otherwise be fully deployed. This strategy allows the system to capture excess energy from solar radiation. To enable this, the inlet temperature is raised, which increases the power absorbed from the building and, consequently, the amount of energy stored in the ground. Additionally, the temperature difference during summmer could reach up to 9-10 °C and represents the peaks of the cooling load as it can be seen from the graph.

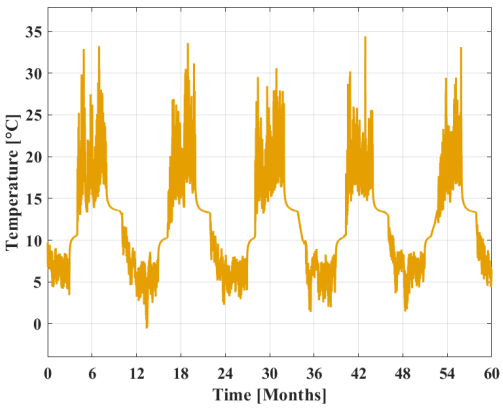

Figure 4.17: Inlet Temperature - Scenario 4

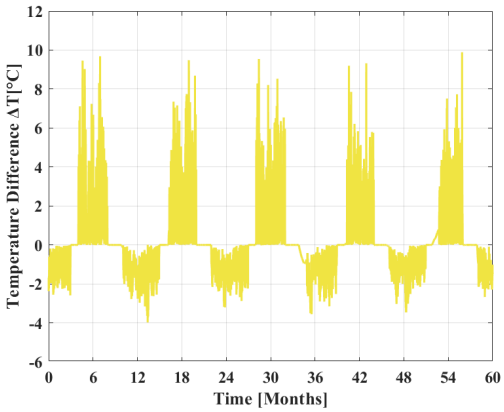

Figure 4.18: Temperature difference - Scenario 4

During the majority of the cooling operation hours, the injection temperature remains below 30 °C. However, during peak cooling demand periods, spikes in the inlet temperature are observed, reaching

up to 35 °C. These values approach the upper limit of acceptable injection temperatures and are permissible only for short durations each year.
Scenario 4 seems to be able to respond in the heating and cooling demand of the building by applying the passive solar strategy. However, opening the solar blinds in June, when the building regularly hosts events, may reduce the visual comfort of the occupants. Therefore, Scenarios 5 and 6 investigate the application of this strategy only in July and August, when the building is least occupied.

Scenario 5

This scenario is very similar with the scenario 4 in terms of energy extracted or injected.The significant change that were investigated is the opening of the solar blindings from mid of July to end of August to preserve high visual comfort when the building is occupied. Thus, scenario 5 is favourable compared with scenario 4. Minor changes are observed between those two scenarios. Especially, in June when the solar blinds are not opening in scenario 5 it seems that the inlet temperature are significanlty lower because the energy that can be stored is lower. This also can be observed in other graphs as the ground temperature and the grouting average temperature. However, because the system is able to store the appropriate excess energy during July and August without being pushed to the limits the differences are difficult observable. Below in Figure 4.19 and 4.20 the ground temperature and the inlet temperature are illustrated.

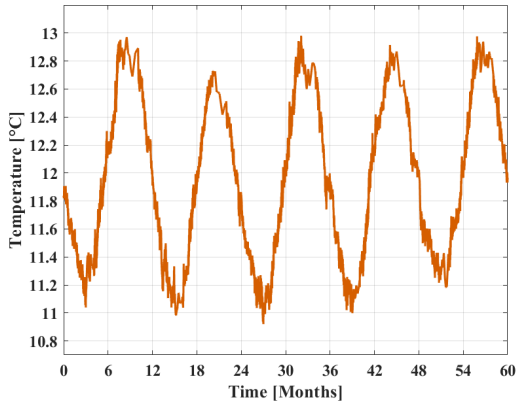

Figure 4.19: Average Ground Temperature - Scenario 5

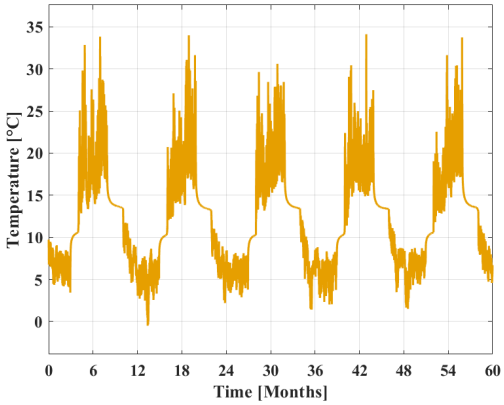

Figure 4.20: Inlet Temperature - Scenario 5

Scenario 6

In that Scenario the cooling mode is operating from June to September instead of May to August. All the other parameters are kept as scenario 5. The energy that is delivered is higher by 2,000 kWh in both heating and cooling sector and as it was stated the system is energy balanced. In Figure 4.21 where the ground temperature is depicted an upward trend is noticed that wasn't noticed in the previous scenarios. This results in the increase of the final ground temperature after those 5 years of simulation by 0.2 °C.

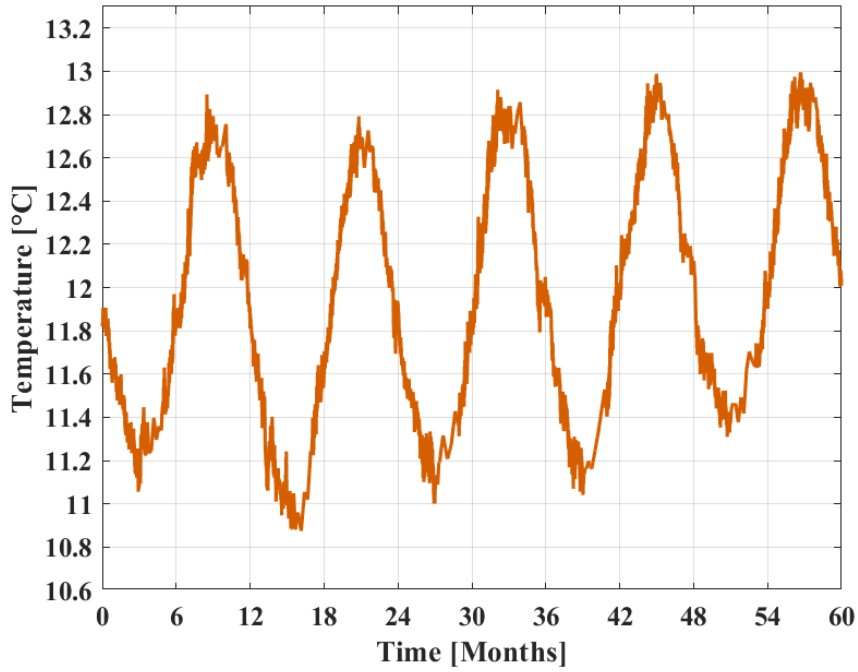

Figure 4.21: Average Ground Temperature - Scenario 6

Additionally, the average grout temperatue and the inlet temperature graph seem to have shifted towards the right hand side because of the changing of the schedule but there is no significant increase or decrease in the temperatures that were noted. Both the graphs are presented below.

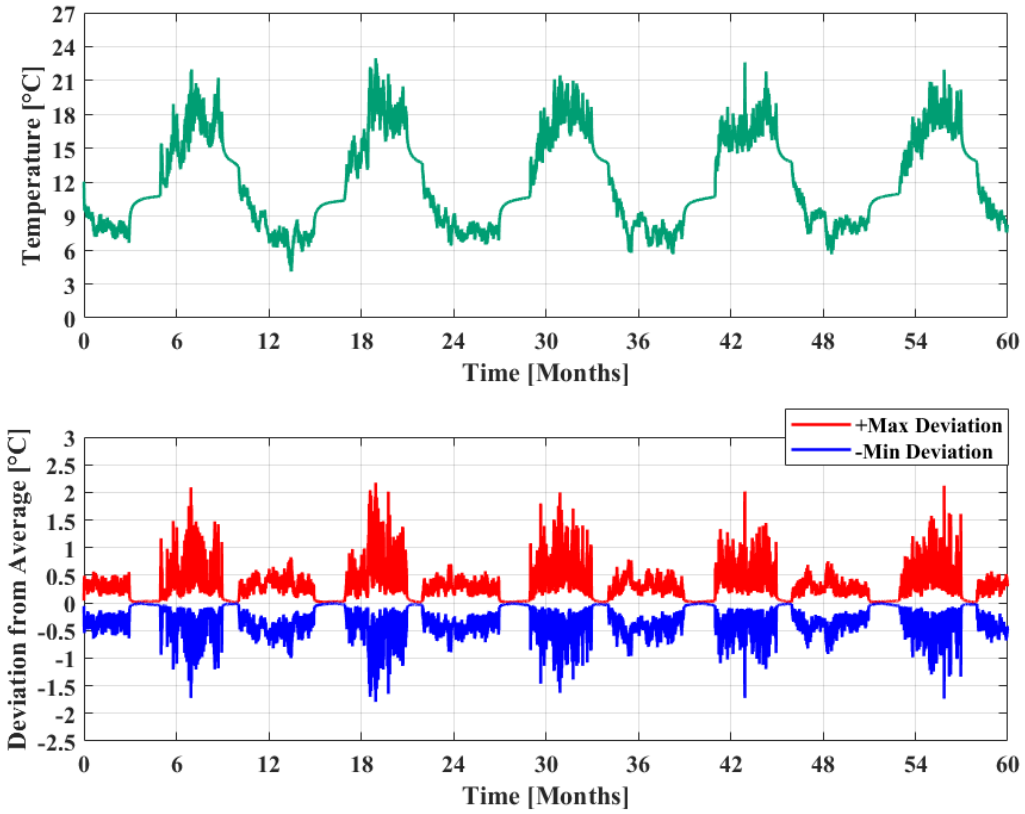

Figure 4.22: Grout average temperature and maximum deviation - Scenario 6

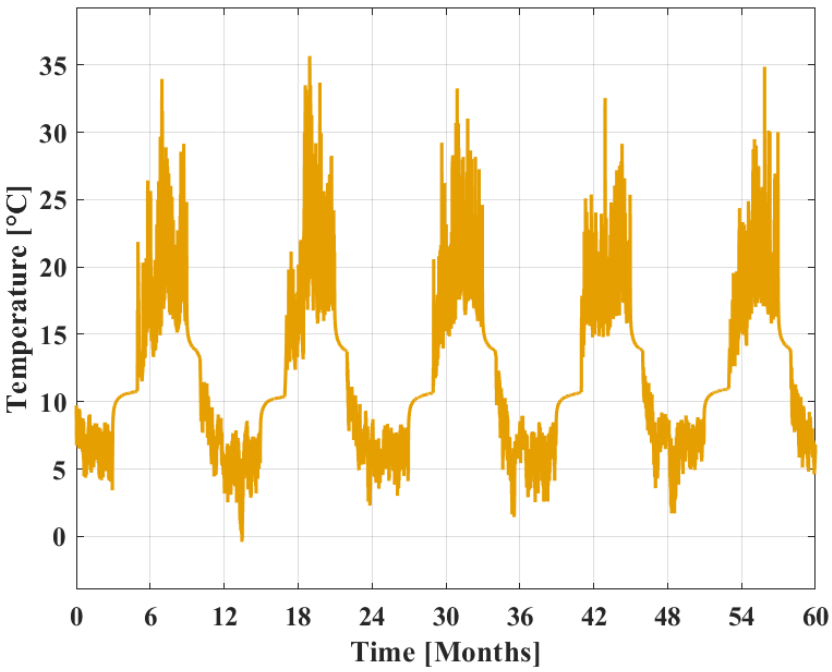

Figure 4.23: Inlet Temperature - Scenario 6

To conclude, in that section passive solar strategies were investigated in order for the system to be able to cover the whole heating and cooling demand while simultaneously having high thermal and visual comfort. Scenario 5 and 6 seem to be the ones that satisfy all those parameters setted. The ground temperature remains constant throughtout the years of simulation while the inlet temperature fluctuates between the boundaries that have been mentioned for safety reasons.

4.3.1. System Capacity Assesment

Scenario 7

In order to explore the limits of the system, even though good indications were extracted from the previous scenarios, a scenario with heating and cooling demand increased by 50 % was developed. Scenario's 6 heating and cooling demand was the one that were increased by 50 %. As it was mentioned earlier the demand is capped to 20 kW so every value that exhibits that limit is lowered to the maximum capacity.A demand of 20 kW of cooling means with an estimated COP of 4 means that the maximum injected power in the system will be 25 kW. Apart from stressing the system, the fluctuation of ground and grout temperature will be investigated as well as the inlet temperature. This scenario also works as a preliminary step to answer the final sub-question.

The system is once again balanced and the only change in that graph is the magnitude that changes due to the higher heating and cooling loads tha the system needs to deliver.In the Tables 4.7 and 4.8 below the energy that was measured for the system is shown. The Seasonal Performance Factor (SPF) is once again at 4.31.

Table 4.7: System performance in Scenario 7 (heating).

Parameter (Heating)	Value (kWh)
Total energy extracted	74,372
Annual energy extracted	14,874
Total energy delivered	95,348
Annual energy delivered	19,069
Total electricity consumed	20,976
Annual electricity consumed	4,195

Table 4.8: System performance in Scenario 7 (cooling).

Parameter (Cooling)	Value (kWh)
Total energy injected	74,334
Annual energy injected	14,866
Total energy delivered	59,467
Annual energy delivered	11,893
Total electricity consumed	14,866
Annual electricity consumed	2,973

In Figure 4.24 the ground temperature is depicted. It can be seen that the ground temperature faces higher fluctuations throughout the years of simulation compared with the previous scenarios. The maximum temperature observed was 13.2 °C, while the minimum was approximately 10.7 °C. The duration of the heating and cooling modes remained the same however, the magnitude of the loads increased meaning that the system was required to extract or inject more energy within the same time frame. Consequently, the temperature decreased more during winter and increased more during summer. In general the ground temperature remained the same from the start to the end of the simulation indicating that the system is in a great balance.

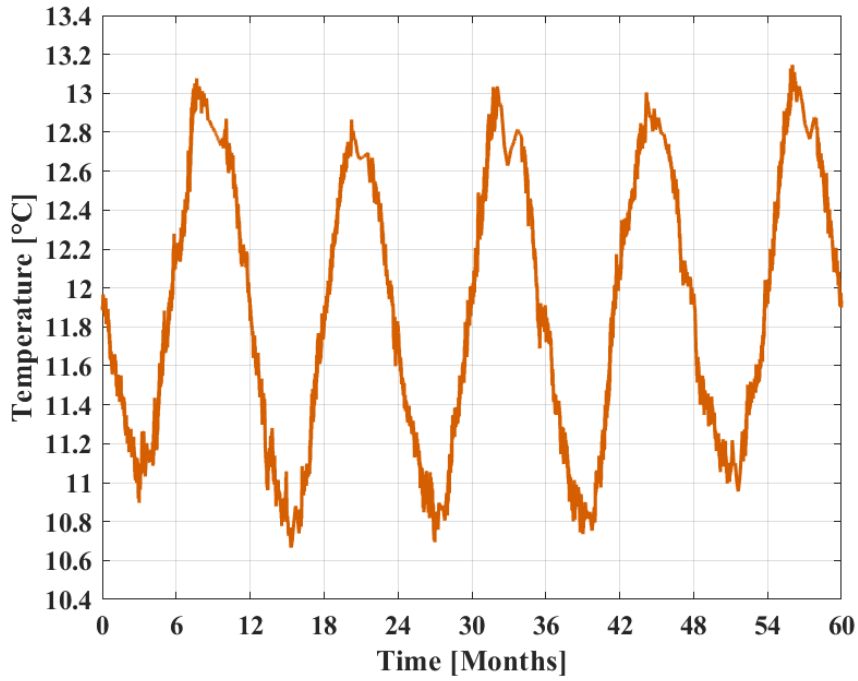

Figure 4.24: Average Ground Temperature - Scenario 7

Moreover, a higher fluctuation in the average grouting temperature is observed. The temperature climbs as high as 24 ° during summer and low to 2-3 ° in some instances as it is illustrated in Figure 4.25. The maximum deviation during summer was 2 ° while in winter was 1.7 ° approximately. The observed grout temperature values remain within the established safe limits. During winter, it is important to avoid temperatures below 0 °C in order to prevent permafrost formation in the ground, which could be detrimental to the stability of the entire building. In summer, grout temperatures should remain below approximately 30 °C to ensure that the structural support provided by the energy piles is not compromised.

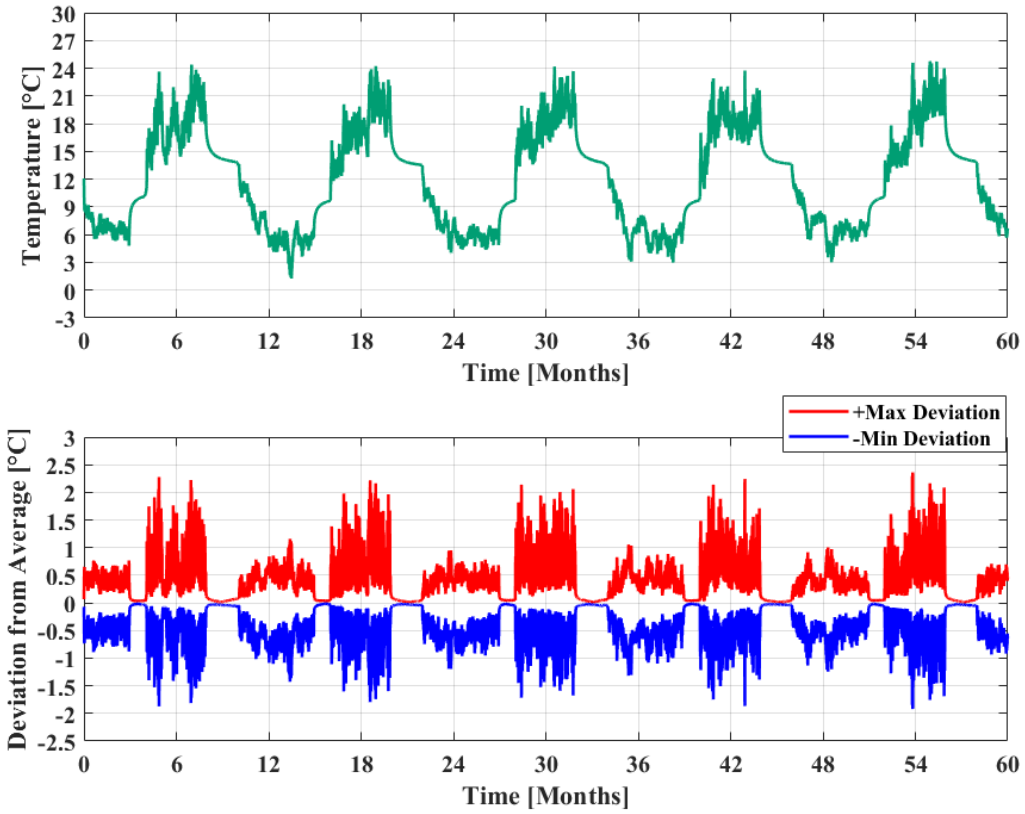

Figure 4.25: Grout average temperature and maximum deviation - Scenario 7

Additionally, the inlet temperature and the temperature difference follow the same trend that was observed. The inlet temperature is lower during winter and higher during summer compared with the previous scenarios and that's because more energy needs to be extracted or injected so a greater temperature difference needs to be formed from the inlet to outlet. In Figure 4.26 and 4.27 those values can be seen. In the inlet temperature graph, the water temperature during winter is significantly lower than in the previous scenarios, frequently reaching 0 °C. In summer, values exceeding 35 °C are observed, which represent relatively high injection temperatures but still remain within acceptable limits. Notably, a value below –4 °C was recorded in winter, which could pose a serious risk to the system despite the freezing point being calculated at –7.9 °C. The temperature difference between the inlet and outlet is greater in this scenario, as more energy must be extracted or injected to satisfy the building's heating and cooling demand, as previously discussed.

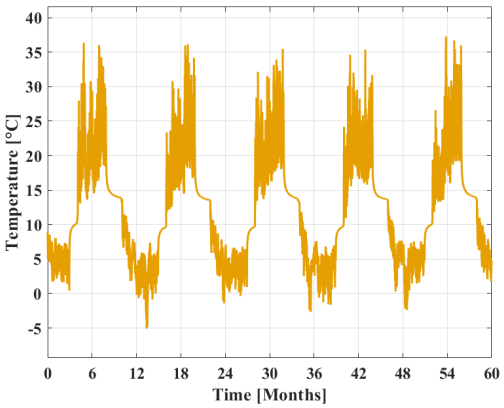

Figure 4.26: Inlet temperature - Scenario 7

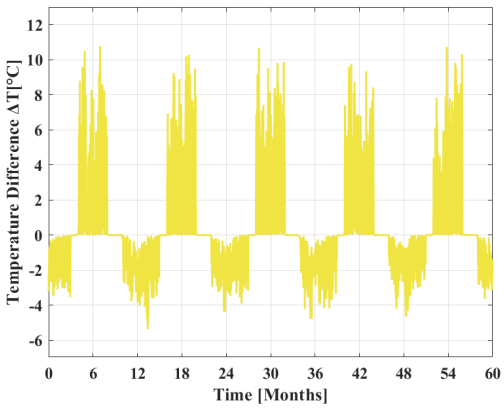

Figure 4.27: Temperature difference between inlet and outlet - Scenario 7

Based on the simulation of Scenario 7, the operational limits of the system were explored. The results demonstrated that the system is capable of delivering higher heating and cooling outputs than the actual demand of the building investigated in the previous scenarios. However, the safe operating limits were effectively reached, and any further increase in load could exceed them. This scenario therefore serves as a preliminary indication of the system's capabilities and its potential to cover the external heating demand of a neighboring building. This question is addressed in the following section.

4.4. Surplus Energy Potential

Based on the analysis conducted thus far, the heating and cooling system demonstrates the capacity to adequately meet the building's thermal demand under typical conditions. In the extreme case represented by Scenario 7, where the system was pushed to its operational limits, results indicate that it can still perform effectively under loads 50 % higher than the average annual demand. This observation raises the question of whether the system could store surplus thermal energy during the summer months and subsequently distribute it to neighboring buildings to support their heating demand during the winter.This possibility could significantly contribute to the decarbonization of heating and cooling in neighboring buildings and play an important role in supporting the energy transition. Scenario 8 is going to answer a main subquestion that has been adressed which is :

6. Can the surplus energy from the system be distributed to neighboring buildings?

It is aiming to investigate whether the system can fully or partially cover the heating demand of a dwelling of approximately 60–70 m^2. The annual energy consumption for such an apartment was estimated to be around 6,000-6,500 kWh as it has been mentioned in previous section. [22].

Scenario 8

Based on the Tables 4.9 and 4.10 it can be seen that even more energy is extracted and injected during each season and also distributed which means that the system is even more pushed to its own limits and this will be depicted on the following graphs. Moreover, in Table 4.11 the annual surplus energy that is being stored during summer is shown. It should be noted that this energy is delivered to a heat pump with a constant COP of 4.5, which is further utilized to cover the heating demand of the neighboring building. However, the target of 5,000 kWh is not achieved in every year. This variation is linked both to the annual heating demand of the Co-Creation Center and to external factors such as global radiation and the availability of sunlight, which influence the amount of surplus energy that can be stored during summer. Nevertheless, the table of results indicates that in certain years surplus energy exceeds the target, allowing it to be stored and redistributed in years with lower availability.

Table 4.9: System performance in Scenario 8 (heating).

Parameter (Heating)	Value (kWh)
Total energy extracted	79,865
Annual energy extracted	15,973
Total energy delivered	102,391
Annual energy delivered	20,478
Total electricity consumed	22,526
Annual electricity consumed	4,505

Table 4.10: System performance in Scenario 8 (cooling).

Parameter (Cooling)	Value (kWh)
Total energy injected	80,026
Annual energy injected	16,005
Total energy delivered	64,021
Annual energy delivered	12,804
Total electricity consumed	16,005
Annual electricity consumed	3,201

Table 4.11: Annual surplus energy stored.

Year	Surplus energy stored (kWh)
1	6,237
2	3,450
3	4,952
4	5,519
5	4,810

In Figure 4.28 it can be seen that the temperature of the ground is fluctuating as the previous scenarios however even higher temperatures are observed during summer and cooling mode. In contrast, during winter some years exhibit lower temperatures than in Scenario 7, while others show higher temperatures. This variation can be attributed to the scheduling. In winter, the heating load includes both the Co-Creation Center and the neighboring building, whereas in summer, years with high global radiation and greater energy availability force the system to store more energy. This leads to elevated ground temperatures, which in turn influence the thermal conditions during the following winter.

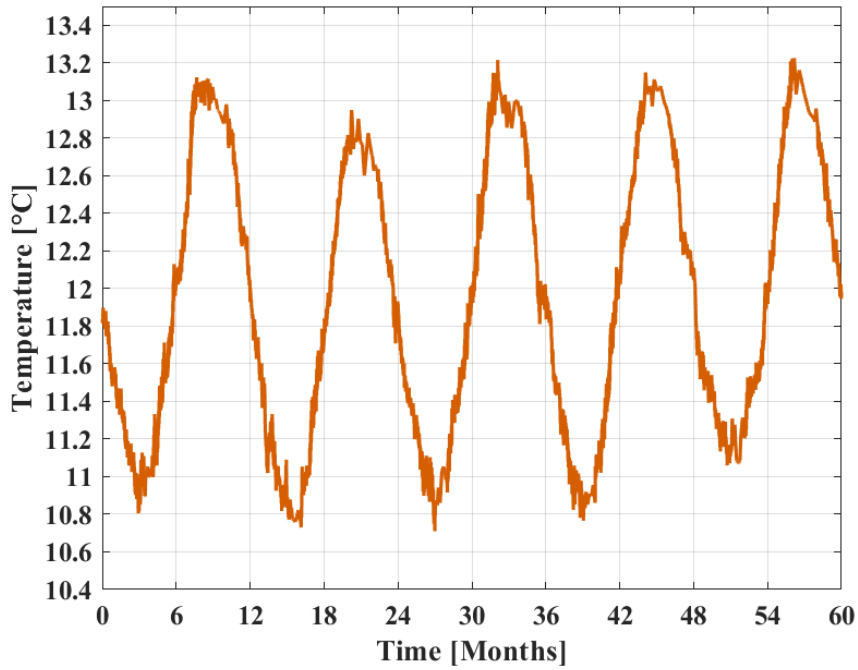

Figure 4.28: Average Ground temperature - Scenario 8

In the Figure 4.29 it can be seen that even higher and lower temperatures are observed compared with scenario 8 which has the same magnitude in energy delivering. Based on the maximums and minimum, it can be said that the grout reaches maximum temperatures of approximately 29 - 30 °C and the lowest temperatures observed were a little higher than 0 °C but for a small period of time.

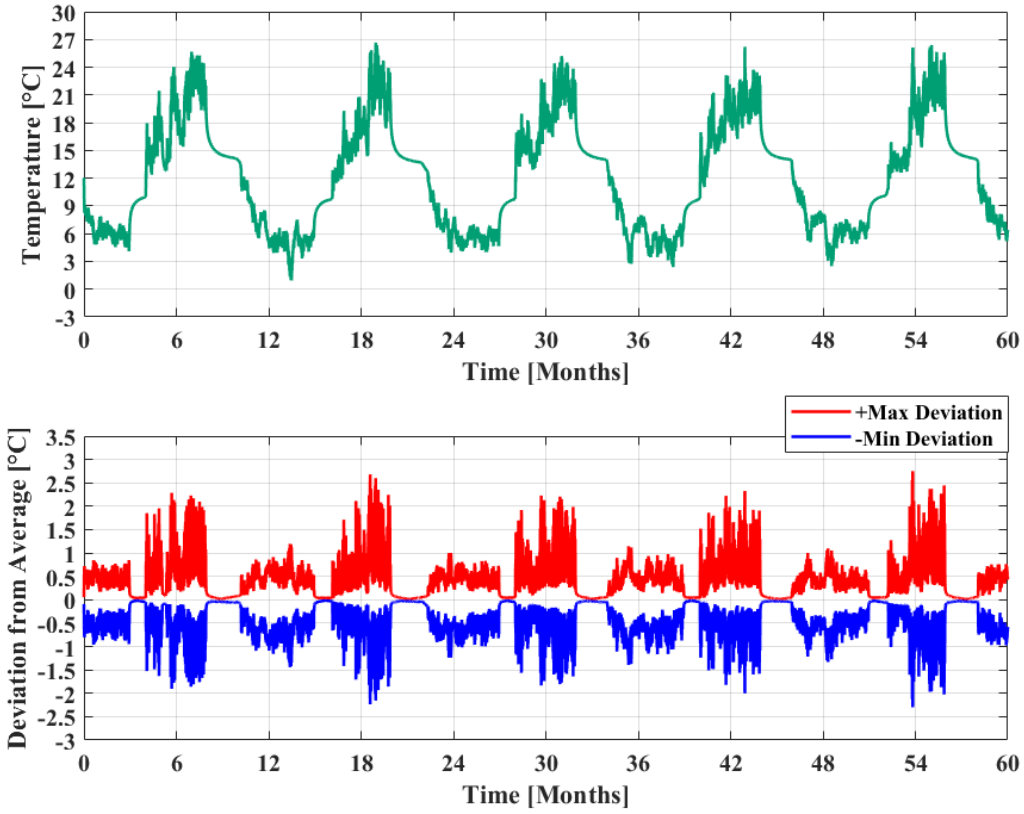

Figure 4.29: Grout average temperature and maximum deviation - Scenario 8

From the graph of the inlet temperature in Figure 4.30 it is illustrated for the first time after all the simulations of the scenarios that the inlet temperature exceed 40 °C during summer and it is many times below 0 °C during winter. The system can be seen that is operating to each own limits however well within the appropriate boundaries that was determined for safety reasons. This high temperatures are observed in summer when the system tries to store as much energy as possible and is operating to the maximum capacity that has been determined for a long period of time for some consecutive days.

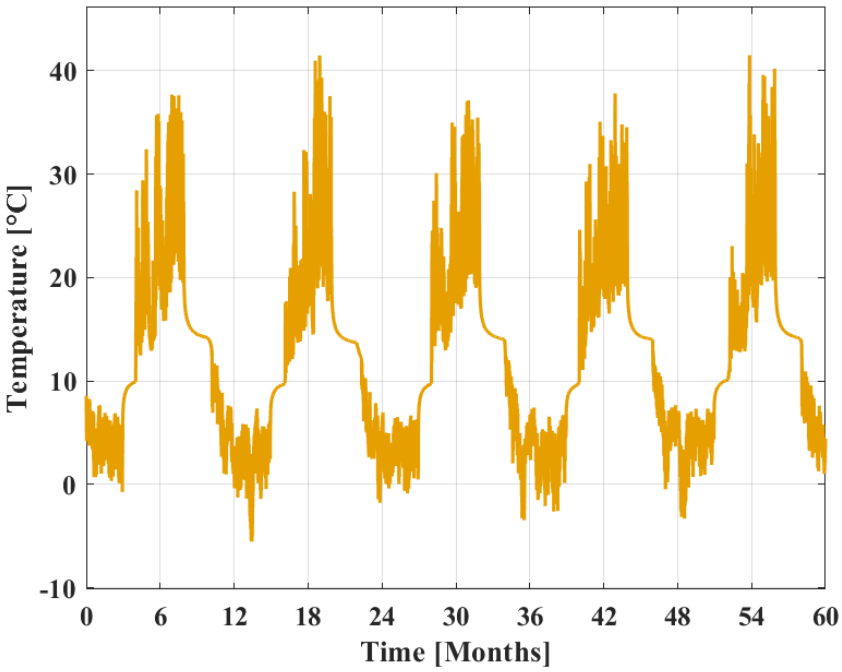

Figure 4.30: Inlet temperature - Scenario 8

To conclude, and in response to the sub-question addressed in this section, the system can fully cover the heating demand of an apartment by implementing passive solar strategies that enable surplus energy to be stored during the summer months. However, the graphs presented also indicate that the system is operating at the limits of the energy it can deliver or store. The amount of surplus energy available each year depends on weather conditions, the heating demand of the Co-Creation Center, and the additional solar energy that can be stored through the partial opening of the solar blinds.

4.5. Thermal plumes interaction

A critical question that must be addressed to gain a deeper understanding of the system's behavior is how thermal plumes interact with each other and with the surrounding soil. These plumes are generated by the injection of fluid at temperatures different from those of the energy piles and the surrounding ground. In this section, these interactions are examined under various operational modes — heating, cooling, and resting. It is essential to recognize and highlight the distinctions observed between these modes. The thermal plumes can expand, contract, or merge depending on the operating conditions. Moreover, this analysis reveals zones of energy accumulation, which appear as elevated temperatures, and areas where energy is depleted. The rate of expansion and contraction will be evaluated using isosurface plots extracted from COMSOL Multiphysics. Different views and plots will be presented however many other supplementary plots can be found in Appendix C.

As previously mentioned, the system comprises three circuits, each consisting of three energy piles. Water enters through the inlet piles, flows into the middle pile, and exits via the outlet piles. In Figures 4.31 and 4.32, a side view and a top view of the thermal plumes are presented, illustrating the system configuration in detail. During this operational phase, the system is delivering heating, meaning that cold water is injected into the ground to extract heat. The extracted heat is transferred through the evaporator of the heat pump, where the water is further cooled and subsequently re-injected into the ground, completing the cycle.

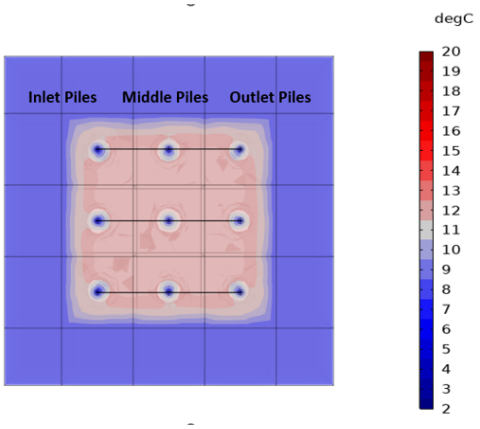

Figure 4.31: Top view of isosurface layers and description of configuration at 104 hours.

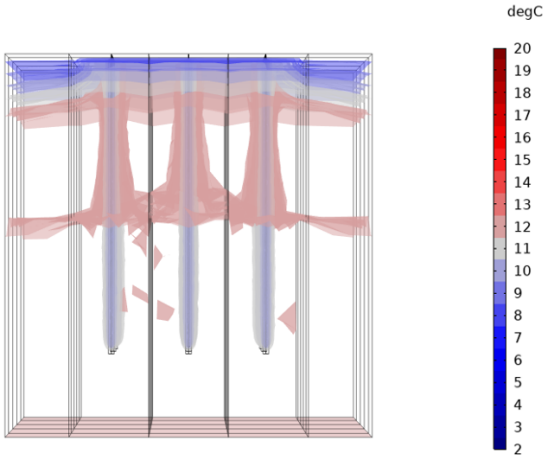

Figure 4.32: Side view of thermal plumes at 104 hours.

The following plots are after some hours of operation in heating mode for the piles. It can be seen that the cold plumes are expanding and they force the hot plume that is trapped in between the piles to shrink. In the side view of the isosurface plot, it can be observed that the thermal interaction between the inlet and middle piles is more pronounced compared to the interaction between the middle and outlet piles. This is because, as water flows through the inlet piles, it gradually absorbs heat from the surrounding ground. By the time it reaches the middle piles, the water is already partially heated, and although it continues to exchange energy with the ground, the temperature gradient is reduced. When the water reaches the outlet piles, its temperature is closer to that of the surrounding soil, resulting in a lower thermal gradient and therefore weaker thermal interaction. Furthermore, it can be seen that the outside squares of the system are open to ambient air temperature and the temperature ofthe upper layers can be seen in the plots below. Finally, the thermal plumes in the top view indicate that heat exchange occurs between the upper parts of the piles and the region exposed to ambient air, as evidenced by the merging of plumes in those areas near the surface.

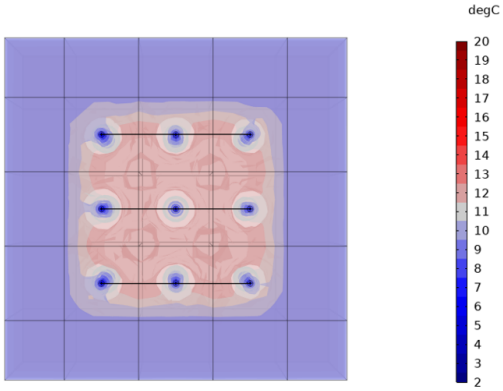

Figure 4.33: Top view of isosurface plots - 280 hours

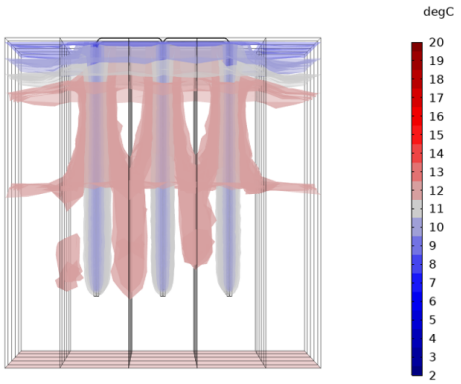

Figure 4.34: Side view of thermal plumes - 280 hours

The following Figure 4.35 serves as evidence that the thermal interaction between the inlet and middle piles is greater than that between the middle and outlet piles. The shrinking hot plumes on the right-hand side appear smaller and more separated compared to the larger, more connected plumes on the left-hand side.

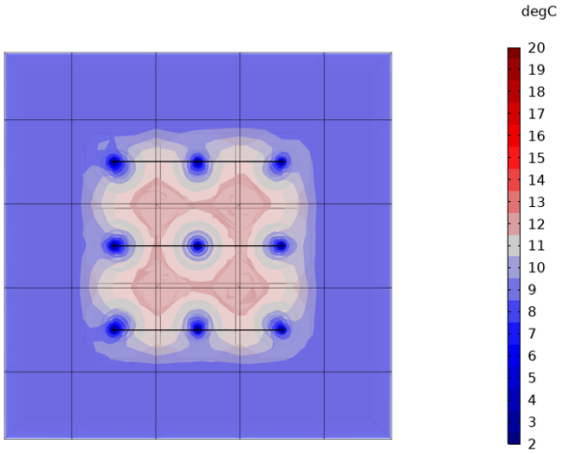

Figure 4.35: Top view at 696 hours of operation

The first cold plumes that are connected each other are the ones that are created from the inlet piles because of the high thermal interaction with the ground the rate of expansion of those plumes is higher than the other piles. Moreover, a side view of those plumes showcased that the plumes are connected from early stages at the upper parts of energy piles, which are closer to the atmosphere. This happens due to the interference with the atmospheric boundaries and the soil temperature at those depths.

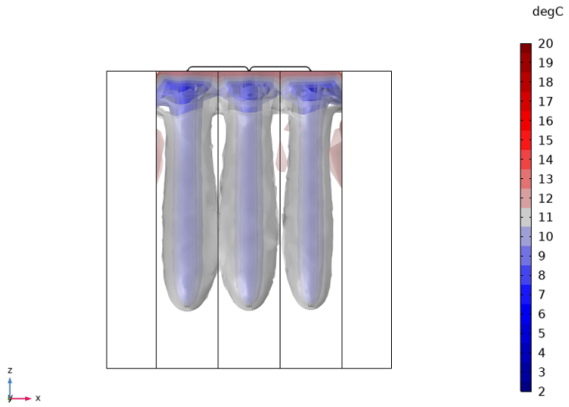

Figure 4.36: Top view of isosurface plots at 1112 hours

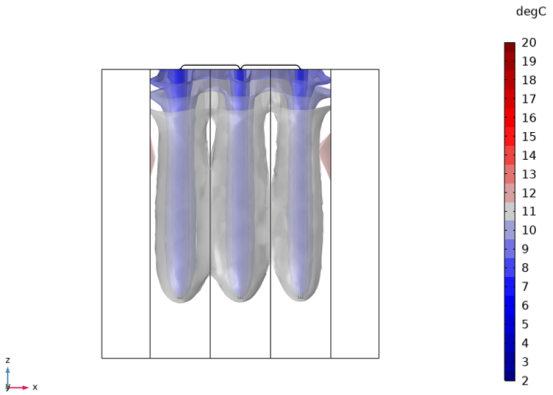

Figure 4.37: Side view of thermal plumes at 1200 hours

As the duration of the heating mode progresses, the thermal plumes expand into the surrounding soil, displacing the hotter regions outward. Simultaneously, colder plumes are formed and gradually expand. When the heating mode ends and the system enters a non-operational (resting) phase, the colder plumes begin to contract from the bottom upward, while the hotter plumes start to expand inward toward the center.

Entering the cooling mode when hot water is injected in the system, the growth of hot plumes is starting. At early stages they start to expand and the entrapped cold plume in between shrinks progressivel. In Figures 4.38 and 4.39 those phenomena are depicted.

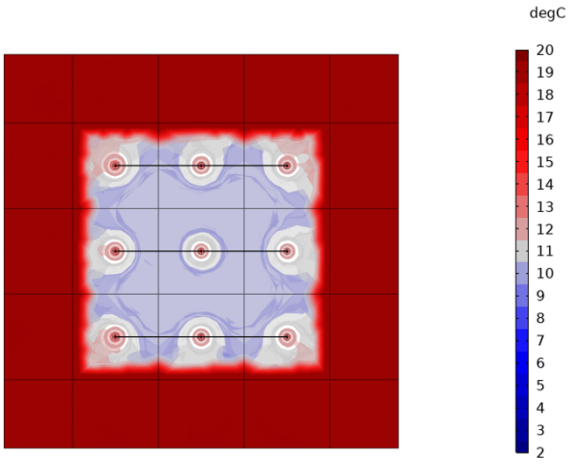

Figure 4.38: Top view of isosurface plots at 4040 hours of operation

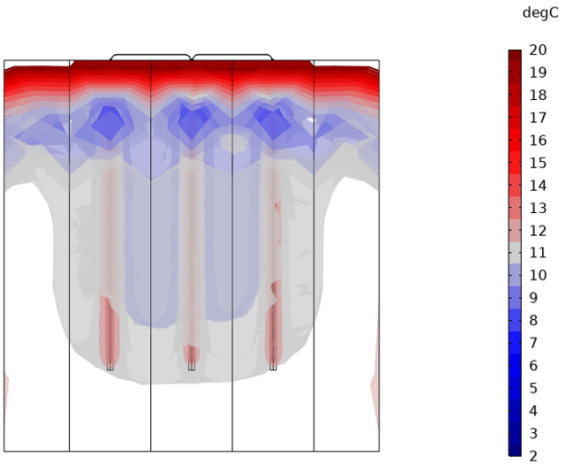

Figure 4.39: Side view of thermal plumes at 4040 hours of operation

Subsequently, the colder plumes shrink and gradually dissipate as the operation continues, while hotter plumes are generated and expand. The connected hot plumes extend into the surrounding soil, indicating that heat transfer is occurring from the injected hot water toward the soil region Figure 4.40 and 4.41. At the end of September the heating mode stops and again a resting period starts where the hot plume that has been expanded starts to contract and dissipates as the time progresses.

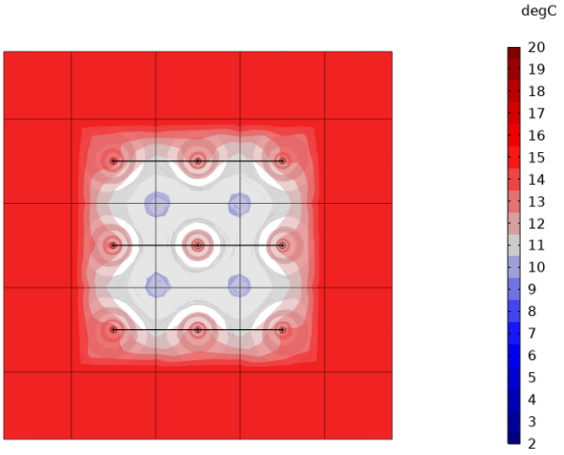

Figure 4.40: Top of isosurface plots - 4688 hours

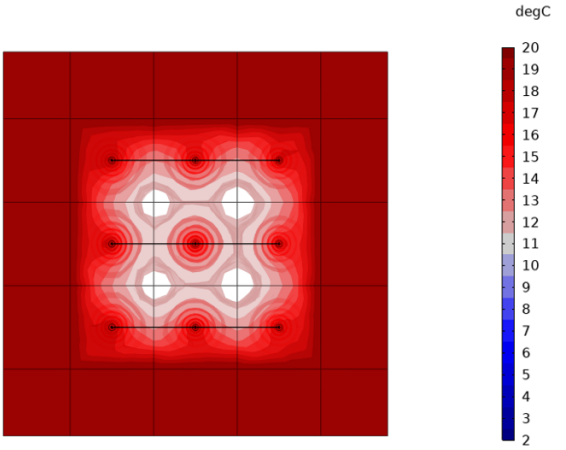

Figure 4.41: Side view of thermal plumes - 4688 hours

During resting period the hot plume behaves similar to the behaviour that the cold plume had during resting mode. However, a hot plume that is created close to the surface of the piles near the insulated boundary was observed. This plume is relatively bigger between the inlet and middle pile compared to middle pile and outlet pile due to the higher thermal interaction of the inlet pile compared with the others. This volume shrinks during that non-operational period. The Figures 4.42 and 4.43 are the same time but from a different view while the Figure 4.44 is 500 hours later and illustrate that remaining thermal plum and its non-symmetrical contraction.

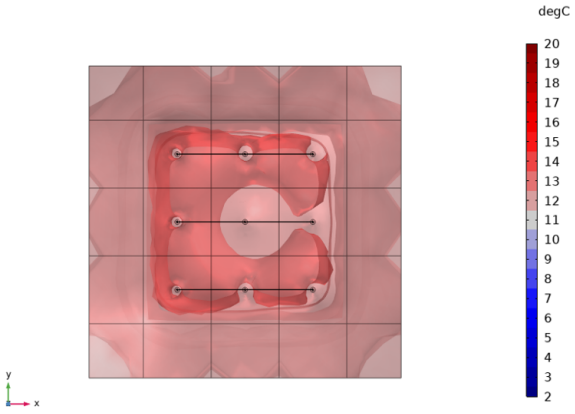

Figure 4.42: Top of isosurface - 7480 hours

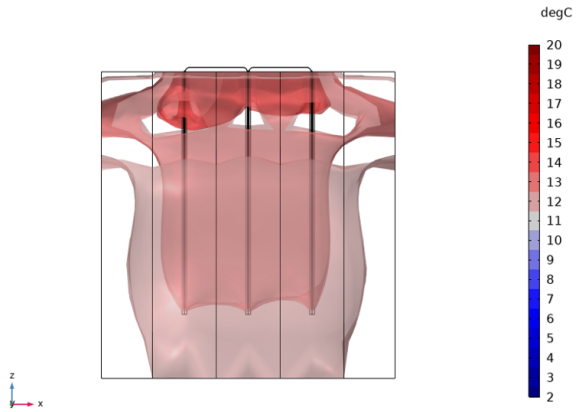

Figure 4.43: Side view of thermal plumes - 7480 hours

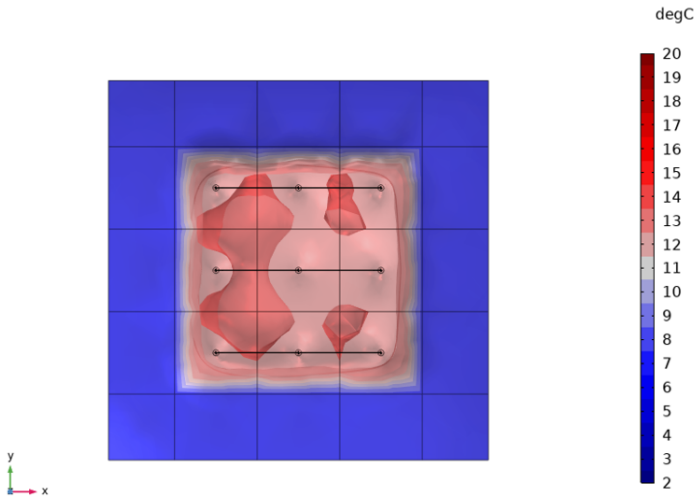

Figure 4.44: 7960 hour top view

When the winter season comes in December and the system starts to working in heating mode the plumes again moving similar to what described in the previous paragraphs. An observation here was that except from the hot plume that is entrapped in between the energy piles because cold plumes start to being developed, cylindrical hot plumes surrounding the energy piles. So a cold plume evolves into a remaining hot plume that slowly dissipates and opens at the bottom and at the top while slowly vanishes completely.

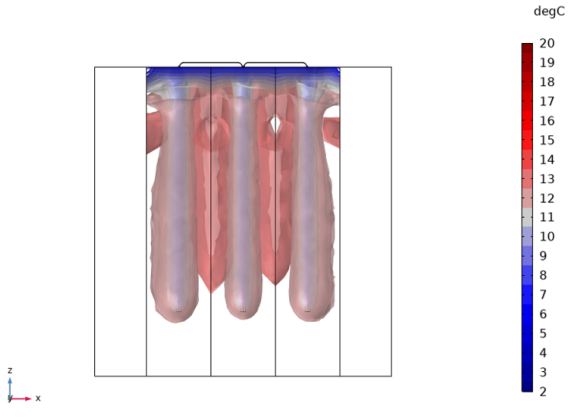

Figure 4.45: Top view of isosurface plots - 8648 hours

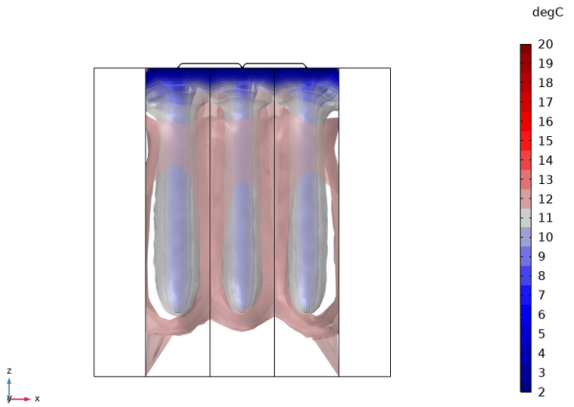

Figure 4.46: Side view of thermal plumes - 8648 hours

A key observation is the asymmetrical expansion of the plumes, which is attributed to the system's design and operational principles. The inlet piles consistently exhibit faster plume expansion due to the greater temperature difference with the surrounding soil, resulting in a steeper thermal gradient. These plumes tend to merge faster however, the heat retained in the plume between the inlet and middle piles causes it to dissipate more slowly compared to the plume formed between the middle and outlet piles.

Finally, the same pattern was observed for every scenario and every year of the simulation, however based on the intensity and the magnitude of the loads the extraction or contraction of the plumes were different in some time-slots. However, the size and the shape the most of the time was the same at each operational mode that was simulated.

4.6. Impact of Ambient Air - Atmospheric Losses/Gains

This section is created to answer once again a main subquestion that was adressed in Chapter 1 which was :

5. How much energy is lost to the atmosphere?

As previously described, the boundary surrounding the energy pile configuration is exposed to ambient air temperature. This boundary exchanges heat with the ambient air only through heat conduction in the simulation, resulting in energy losses or gains depending on the temperature difference between the soil and the surrounding air. Accurately quantifying these thermal exchanges is essential for assessing whether the system experiences a net energy loss or gain over the course of the simulation. The amount of energy that is exchanged will be discussed in that section for various scenarios and the differences will be commented.

During a day can occur both losses or gains as the air temperature fluctuates it can be higher or lower than the top layers of the ground. In Figures 4.47 and 4.48, the arrows represent the direction and magnitude of the heat flux. Larger arrows indicate regions of higher heat flux, while smaller arrows correspond to lower heat flux values.

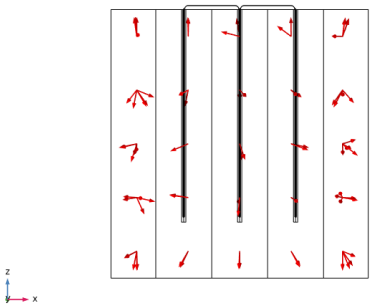

Figure 4.47: Winter heat flux

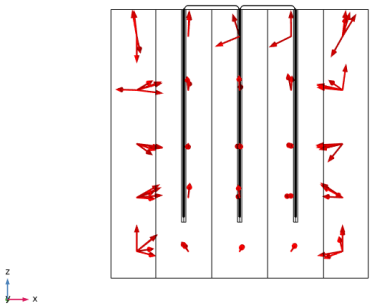

Figure 4.48: Summer heat flux

Initially, the ground temperature is monitored for 5 years of simulation without any operations, which means without any energy extraction or injection and by allowing only heat transfer through conduction with the ambient air. This happens to be able to compare what will be the losses or gains of the soil without any operations and to compare how the operations and each scenario affect those losses. It was found out that the domain of the soil lost in those 5 years of simulation 1,400 kWh of energy. Figure 4.49 shows the ground temperature throughout that simulation and how it was fluctuated. As it can be observed the ground temperature fluctuates from 11.4 °C to 12.5 °C and even though some energy losses were observed it manages to maintain the temperature and a decrease of 0.03 °C was noted.

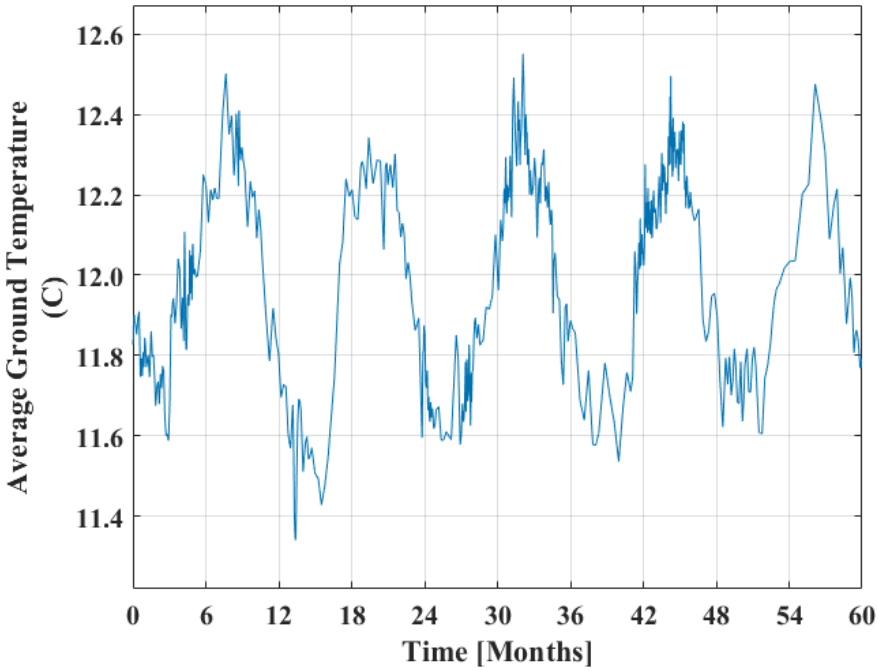

Figure 4.49: Average ground temperature without injection/extraction of energy

In every scenario that was simulated it was observed an energy loss to the atmosphere throughout the time of the simulation. However, it was noted a different magnitude of loss between different scenarios. Table 4.12 shows the detailed results of those.

It was observed that in most cases, the energy losses to the atmosphere were of similar magnitude

and in some instances nearly identical. In Scenario 7, the losses were the lowest, which can be explained by the shift in the cooling mode schedule. Specifically, when the injection of energy into the piles is shifted from May–August to June–September, atmospheric losses are reduced. Conversely, Scenario 8 exhibited the highest losses. This is likely due to the elevated average ground and inlet temperatures recorded in this scenario. The higher ground temperature increases the temperature gradient between the ambient air and the upper soil layers, which in turn enhances the heat flux to the atmosphere and results in greater energy losses.

Table 4.12: Energy loss to the atmosphere for each scenario.

Parameter	Scenario 4	Scenario 5	Scenario 6	Scenario 7	Scenario 8
Total energy loss (kWh)	4,114	4,151	3,516	4,159	4,729
Average annual energy loss (kWh)	822	830	703	831	945
Annual energy loss per m^2 (kWh/m^2)	2.55	2.57	2.18	2.58	2.93

In all scenarios energy losses to the environment were observed as it was shown above. However, the ground temperature based on the graphs presented in the previous section showcased that it is not affected from that energy loss. This can be explained due to several reasons. Initially, the domain is large and it is hardly affected from small annual losses. Afterwards, the bottom boundary which has a constant temperature of 12 degrees gives energy to the system and helps maintain constant temperature. Moreover, the entire ground acts as a buffer where energy is stored during summer and extracted during winter. This process prevents the ground temperature from decreasing significantly. In addition, previous graphs have shown that the ground exhibits resistance to temperature reduction, as already observed and discussed.

5

Discussion

This research focused on the development of a numerical model designed to provide accurate and reliable simulations of the energy pile system located at the Co-Creation Center on the TU Delft campus. The model was then applied to a series of operational scenarios in order to investigate the system's limits, capabilities, and overall behavior.

5.1. Limitations

In that section several limitations of the research will be adressed and discussed.

Modelling

Initially, the model assumed that the surrounding soil was a solid material rather than a porous medium with porosity and permeability. This simplification was applied to reduce computational time and because direct measurements of the subsurface soil properties were available. However, this assumption may have introduced disturbances, causing the simulated domain to behave differently from reality. In addition, certain material properties were assumed constant with respect to temperature, in order to simplify the simulations and because it was evaluated that this would not introduce significant differences. Nevertheless, in real-world conditions such variations occur—particularly in the working fluid—and should be considered in more detailed studies.

With respect to boundary conditions, the top boundary was modeled as exposed to the ambient air temperature. In reality, not all surfaces are exposed to air because the building itself covers part of the domain. This modeling choice introduces a deviation from reality but was selected in order to capture the effect of heat losses through exposed boundaries in a practical way.

It was also assumed that the velocity of the working fluid remained constant throughout the simulation. While such systems typically operate at a constant flow rate during heating or cooling delivery, the flow rate is often reduced or shut down during resting periods. In this case, a constant flow was applied because implementing variable flow rates in COMSOL Multiphysics required very small step changes, which significantly increased simulation time and often prevented convergence. Although this choice introduces some convective heat transfer during resting periods, the inlet and outlet temperatures remain equal, meaning that no significant amount of energy is exchanged. Nonetheless, a deviation from reality can be noted for this reason.

Verification Method

Initially, this research aimed to verify the numerical model using experimental data from the actual energy pile installation in the building. However, due to unforeseen complications, such data were not available within the required timeframe. As a result, verification was instead carried out using analytical theory and an analytical model.

The results demonstrated that the numerical model closely followed the solution predicted by the an-

alytical model, with an average error of approximately 4%. The few cases with higher deviations were identified and their sources explained. Most importantly, it should be noted that the analytical model simulated boreholes as independent units, with loads applied individually. In this case, nine separate energy piles were modeled, each subjected to its own injected or extracted load. To enable verification, the numerical model was modified to replicate this configuration. However, the actual arrangement of the energy piles in the Co-Creation Center, as previously described, consists of interconnected piles forming three circuits, in which water enters through an inlet, passes sequentially through three energy piles, and exits through an outlet. The heat transfer mechanisms in this interconnected configuration differ significantly from those in the analytical model, and consequently the results would also be expected to differ. This represents a limitation that was accepted in order to make verification against analytical theory feasible.

Finally, another important limitation of this stage of the research is that the analytical model was able to adjust the loads applied to the energy piles instantaneously, whereas the numerical model required a gradual transition between load changes to ensure smooth convergence. This difference likely contributed to the discrepancies observed, including the delayed response of the numerical model during load variations.

Operational Scenarios

The operational scenarios were designed using data retrieved from a platform that collects the relevant building parameters. However, the dataset presented two limitations: first, some portions of the data were corrupted and required modification, and second, the data were only available for a two-year period. Consequently, the building loads for the remaining three years were generated by extrapolating patterns based on the two years of available data. This introduced a limitation to the simulations, as assumptions were necessary to construct a complete five-year dataset.

Furthermore, although the original data were provided in hourly time steps, they were averaged over 8-hour intervals to reduce computational demand. This resulted in a simulation time step of 8 hours for the entire study. While this approach compromised the temporal accuracy of the simulation, it was essential in order to significantly reduce the computational time required.

5.2. Research Scope

The goal of this research was to investigate a borehole thermal energy storage (BTES) system, implemented through energy piles, which operates to cover the heating and cooling demand of a building. The study aimed to examine the interaction between the system and the surrounding soil, which functions as its thermal storage, as well as to explore its limits, assess its capabilities, and identify ways to improve its efficiency and reliability.

A numerical model that was created to conduct the simulation was verified with an analytical model that follows the theory. It showcased that the error is relatively low and that the numerical model represents the heat transfer mechanisms correctly.

Based on the constructed scenarios and the simulations conducted, several key observations were made. During winter, the heating demand remains relatively constant throughout the day, with loads rarely exceeding 8–10 kW. In contrast, the cooling demand in summer can drop to zero during the night but peaks sharply during the day due to the influence of solar gains. In several cases, particularly in scenarios where surplus energy was stored, the system was observed to operate near its limits in cooling mode. Furthermore, the ground temperature, even under imbalanced conditions where more energy is extracted than injected, was able to maintain a lower but relatively stable value rather than decreasing linearly as might be expected. Overall, the soil demonstrated a buffering effect, resisting continuous temperature decline.

The simulation results indicate that the system is capable of supporting the building's demands, particularly when passive solar strategies are applied. Implementing such strategies also enables the storage of surplus energy during summer, which can be redistributed to neighboring apartments. In this case, however, the system operates near its limits—specifically the inlet fluid temperature thresholds and the grout temperature limits, which ensure that the energy piles continue to provide adequate

structural support to the building. When the system operates at maximum capacity in cooling mode, the inlet fluid temperature rises along with the temperature of the concrete. Therefore, peak operation must be scheduled with time intervals to prevent overheating and to allow sufficient time for temperatures to decrease.

The system appears to lose energy through the open boundary defined at the environment in every case. This energy loss was quantified and presented; however, it proved to be negligible and did not cause any significant change in the overall ground temperature.

6

Conclusion

This research investigated the efficiency and reliability of energy piles which is a shallow geothermal system that is coupled with a ground source heat pump and it is used to provide heating and cooling. The goal was to investigate a system that will give solutions to energy crisis and climate change. Due to the high COP of it and the sustainability it is an appropriate system that will help to decarbonize a sector that has the highest consumption in households. The system that was investigated was a pre-existed configuration located in a building that is used for events in TU Delft Campus.

A model that represents the energy piles system was created with COMSOL Multiphysics and were used as a tool to enhance the efficiency, optimize the amount of energy extracted or injected and investigate the capabilities of the system. The numerical model was verified with a model that was based on analytical theory and used the Infinite Line Source (ILS) theory. Five years of simulation time was conducted in both models and the results of the temperature in various points of the soil were compared. The comparison showed that the average annual absolute error for every year was less than 4 % in the first year and was reduced by the passing of the years to 3.5 %. This showcases that the model is significantly accurate and can replicate the heat transfer phenomena that are occuring with accuracy. It should be noted that the analytical model provided accurate predictions for distances between 1 and 2.3 meters from the pile, where the lowest error was observed. The measured errors were explained by the assumptions in the analytical model, as well as certain limitations of the numerical model.

The initial scenario that was designed where no optimization of the energy was taken into account or the energy balance of the system the simulation showed that a deficit of - 9,000 kWh is formed into the surrounding soil and the ground temperature drops by 0.5 $^{\circ}$C. Based on this scenario incentives towards the right direction of the optimization were noticed. Subsequently, the Scenarios 2 and 3 were designed in order to optimize the system and create an energy balance of it. Different indoor temperature setpoints, scheduling of operational modes and duration of them were investigated. These scenarios demonstrated that an energy balance can be reached however, the heating demand during winter needs to be reduced or the thermal comfort due to low indoor temperatures during summer will be compromised in order to reach that energy balance.As a result, new strategies that utilize solar gains were developed.

Scenarios 4,5,6 take into consideration the sunblindings and the hours that are fully closed. In order to store more energy during summer to be able to deliver it in winter the sunblindings were opened in those scenarios for several hours in different months. The scenario that achieved the highest levels of both thermal and visual comfort was Scenario 5. In this case, the sunblinds were opened during mid-July and August, when the building was rarely occupied and almost non-operational. The system successfully covered the building's heating demand from November to March and the cooling demand from May to September, thereby maintaining an overall energy balance.

Lastly, a simulation was conducted to showcase if the building can store surplus energy from the sun in order to cover the heating demand for a neighboring building of 60 m^2. The simulation showed that

based on the weather conditions and specifically the global radiation per year the system is capable of delivering 6,000-6,500 kWh to that building and cover completely the heating demand of it. The amount of energy that can be stored during summer strongly depends on the solar radiation and weather conditions of each year. As a result, in some years it was possible to store more energy, while in others the potential was lower. Overall, the results from five years of simulations demonstrated that, with an appropriate strategy, the system can reliably support the heating demand of a neighboring building.

Ground Temperature

The ground temperature was closely monitored, as it is one of the most critical factors in an energy pile system. The ground serves as the storage medium where energy is either injected or extracted, depending on the mode of operation. Monitoring its temperature provides valuable insight into the amount of energy that can be extracted and the extent of energy that is injected. Over an annual cycle, it is essential to maintain the ground temperature at consistent levels to ensure an energy-balanced system. This balance secures high operational efficiency while also supporting the sustainability and long-term performance of the energy pile system.

Even in the first scenario, where no optimization was applied and the energy injected into the ground was insufficient, the average ground temperature showed resistance to further reduction after the first three years. It stabilized at a level lower than the initial value but did not decrease further. In the balanced scenarios, the ground temperature remained close to its initial value, with only small deviations that were explained in the analysis. Overall, the results suggest that the average ground temperature is not significantly affected by energy losses to the atmosphere and does not decrease substantially as a result. When the system delivered higher amounts of energy, the fluctuations in average ground temperature increased, particularly during summer, when peak temperatures rose rapidly due to the intensity of the cooling load.

Inlet Water Temperature

In all the scenarios the inlet water temperature was observed closely as it is significant due to the limits that have been setted. Also, this factor gives an incentive of the maximum capacity that the system can reach. The inlet temperature never exceeded the -4 °C that is the point that has been setted to prevent the working fluid from freezing. However, in many scenarios and especially in those that the system operates on its limits the inlet temperature during cooling mode exceeeds 30 °C. For example, in Scenario 6 inlet temperature was higher than 30 °C for approximately 20 hours every year. On the other hand in Scenario 8 that the system delivered and injected the highest amounts of energy from and to the system the hours above 30 °C were 150-200 hours every year. This is caused due to the magnitude of the cooling load but also it is connected with the frequency of that maximum load. By that is meant that if the system faces extreme cooling loads of 20 kW for an extended period of time it showed that the inlet temperature remains high due to the incapability of the energy piles to cool down the water and this needs to be monitored closely.

Temperature of energy piles

The energy piles average temperature was also closely observed in order to prevent extreme temperatures that might decrease the ability of the pile to support the building. In the most extreme cases that were investigated the average energy pile temperature fluctuated from 0 to 30 °C. This fluctuation can be said that it is on the safe side that a concrete reinforced pile can exceed. However, the inlet piles temperature fluctuation was even higher due to the system design. The inlet piles receive the coldest and the hottest water, as the fluid temperature changes after exchanging energy with the soil while flowing through the system. The highest deviations from the average temperature were observed in these inlet piles 3 °C during summer and - 2.5 °C during winter.

Thermal Plumes Interaction

The expansion and interaction of thermal plumes where investigated and presented in previous sections. The main findings showed the rate of the expansion or contraction and the extend of those during the various operational modes. It was also observed that the thermal plumes initially connect at shallow depths near the top boundary, and subsequently begin to connect progressively from the bottom upwards. In general, across all simulated scenarios, the overall plume behavior was consistent. However, variations were noted in the rate of plume growth or shrinkage depending on the intensity of

heating and cooling. Finally, in each simulated year, the plumes followed the same overall pattern, with only minor variations influenced by the operational schedule.

Impact of Atmosphere

Energy loss was measured throughout the boundary that is open to air ambient temperatur. Initially, a reference simulation without any energy extraction or injection showed that the ground energy losses were approximately 1,400 kWh over five years. In contrast, when simulating the operational scenarios, the calculated losses over the same period increased to around 4,000 kWh in most cases. This indicates that operating the system, by extracting and injecting energy, leads to higher overall losses due to the active thermal interaction with the ground. Moreover, in Scenario 7, these losses were reduced by adjusting the cooling mode scheduling. However, when the system was operated at its maximum capacity—delivering the highest energy in both winter and summer— in Scenario 8 the heat losses increased further. This behavior can be explained by the larger fluctuations in ground temperature, which appear to be influenced more by winter heat losses than by heat gains.

6.1. Recommendations

To enhance the outcomes of this research, several recommendations for further investigation are proposed. There are multiple factors that could be refined or explored in greater depth to improve the understanding and performance of the energy pile system.

Firstly, regarding the numerical model, a normal-to-coarse mesh was used, which satisfied the requirements of this investigation. However, for more accurate results, the mesh could be refined and upgraded. Although this would increase computational time, it would likely improve the precision of the model.

Secondly, the heating and cooling demand profiles were constructed from two years of measured data, with the remaining three years extrapolated using patterns based on global radiation. A more detailed profile could be obtained if the building's event schedule were incorporated, particularly to capture the effect of occupancy-related gains.

Thirdly, the simulations were conducted over a five-year period, which is relatively short for a shallow geothermal system such as energy piles. To properly assess the long-term behavior of the surrounding soil, the system's capabilities, and its efficiency over time, it is recommended that the simulation period be extended to at least ten years in order to observe the evolution of relevant thermal phenomena.

Fourthly, due to certain complications, the model could not be validated with on-site data as originally planned and was instead verified using an analytical model. For greater confidence in the accuracy of the results, validation against experimental measurements from the actual installation is essential to ensure that the model represents the real configuration and heat transfer mechanisms with precision.

Additionally, a more detailed study of atmospheric heat losses could be undertaken to quantify their seasonal variation and to identify strategies for minimizing them.

Finally, it could be valuable to investigate the operation of the three hydraulic circuits individually. Alternating between operating certain circuits while allowing others to rest could reveal opportunities to reduce energy consumption, optimize thermal plume interactions, and improve overall system efficiency. Such an approach might also unlock new possibilities for the building while enhancing both energy savings and operational reliability.

References

[1] E. Abdelaziz et al. “Energy piles: Current practices and future trends”. In: *Journal of Advanced Research* 27 (2020), pp. 15–26. DOI: 10.1016/j.jare.2020.05.001. URL: https://www.sciencedirect.com/science/article/pii/S1110016820303409.

[2] Lazaros Aresti, Paul Christodoulides, and Georgios Florides. “A Review of the Design Aspects of Ground Heat Exchangers”. In: *Renewable and Sustainable Energy Reviews* 92 (2018), pp. 757–773. DOI: 10.1016/j.rser.2018.04.053. URL: https://doi.org/10.1016/j.rser.2018.04.053.

[3] P. J. Bourne-Webb et al. “Energy pile test at Lambeth College, London: geotechnical and thermodynamic aspects of pile response to heat cycles”. In: *Géotechnique* 59.3 (2009), pp. 237–248. DOI: 10.1680/geot.2009.59.3.237.

[4] Alberto Carotenuto et al. “Energy Piles for Ground Source Heat Pump Applications: Comparison of Heat Transfer Performance for Different Design and Operating Parameters”. In: *Applied Thermal Engineering* 124 (2017), pp. 1492–1504. DOI: 10.1016/j.applthermaleng.2017.06.038. URL: https://doi.org/10.1016/j.applthermaleng.2017.06.038.

[5] H. S. Carslaw and J. C. Jaeger. *Conduction of Heat in Solids*. Oxford: Oxford University Press, 1959.

[6] COMSOL Inc. *COMSOL Multiphysics User’s Guide*. Available as a PDF via ETH Zurich blog. COMSOL Inc. May 2020. URL: https://blogs.ethz.ch/ps_comsol/files/2020/05/COMSOLMultiphysicsUsersGuide.pdf.

[7] Cynthia Ann Cruickshank and Christopher Baldwin. *Sensible Thermal Energy Storage: Diurnal and Seasonal*. Ed. by S. Kalaiselvam and R. Parameshwaran. Oxford, UK, 2015.

[8] Ping Cui et al. “Advances in ground heat exchangers for space heating and cooling: Review and perspectives”. In: *Energy and Built Environment* 3.1 (2022), pp. 1–17. DOI: 10.1016/j.enbenv.2022.10.002. URL: https://doi.org/10.1016/j.enbenv.2022.10.002.

[9] Eurostat. *Energy Consumption in Households*. URL: https://ec.europa.eu/eurostat/statistics-explained/index.php?title=Energy_consumption_in_households.

[10] Signhild Gehlin. “Borehole Thermal Energy Storage”. In: *Advances in Ground-Source Heat Pump Systems*. Ed. by Simon J. Rees. Woodhead Publishing, 2016, pp. 295–327. DOI: 10.1016/B978-0-08-100311-4.00011-6. URL: https://doi.org/10.1016/B978-0-08-100311-4.00011-6.

[11] *Green Energy and Technology*. ISSN 1865-3529; ISSN (electronic) 1865-3537. 2023. DOI: 10.1007/978-3-031-24524-4. URL: https://doi.org/10.1007/978-3-031-24524-4.

[12] J. Guimbal. “Lotissement de 16 villas à chauffage solaire intégral”. French. In: *Proceedings of the International Conference on Solar Energy Storage*. Paris, France, 1976.

[13] Ahmet Gultekin, Murat Aydin, and Altug Sisman. “Thermal performance analysis of multiple borehole heat exchangers”. In: *Energy Conversion and Management* 122 (2016), pp. 544–551. DOI: 10.1016/j.enconman.2016.05.086. URL: https://doi.org/10.1016/j.enconman.2016.05.086.

[14] Leonard R. Ingersoll, Otto J. Zobel, and Alfred C. Ingersoll. *Heat Conduction with Engineering, Geological, and Other Applications*. New York: McGraw-Hill, 1954.

[15] Ahmed Khalil et al. “Recent Advancements in Geothermal Energy Piles Performance and Design”. In: *Energies* 17.14 (2024), p. 3386. DOI: 10.3390/en17143386. URL: https://www.mdpi.com/1996-1073/17/14/3386.

[16] Michael Lanahan and Paulo Cesar Tabares-Velasco. “Seasonal Thermal-Energy Storage: A Critical Review on BTES Systems, Modeling, and System Design for Higher System Efficiency”. In: *Energies* 10.6 (2017), p. 743. DOI: 10.3390/en10060743. URL: https://www.mdpi.com/1996-1073/10/6/743.

[17] Fleur Loveridge and William Powrie. “Pile heat exchangers: thermal behaviour and interactions”. In: *Proceedings of the Institution of Civil Engineers – Geotechnical Engineering* 166.2 (2013), pp. 178–196. DOI: 10.1680/geng.11.00042. URL: https://doi.org/10.1680/geng.11.00042.

[18] Jin Luo et al. “Heating and cooling performance analysis of a ground source heat pump system in Southern Germany”. In: *Geothermics* 51 (2014), pp. 143–151. DOI: 10.1016/j.geothermics.2014.04.004. URL: https://doi.org/10.1016/j.geothermics.2014.04.004.

[19] Qijie Ma, Jianhua Fan, and Hantao Liu. “Energy pile-based ground source heat pump system with seasonal solar energy storage”. In: *Renewable Energy* 211 (2023), pp. 1146–1159. DOI: 10.1016/j.renene.2023.02.116. URL: https://doi.org/10.1016/j.renene.2023.02.116.

[20] Zahraa Mohamad, Farouk Fardoun, and Fekri Meftah. “A Review on Energy Piles Design, Evaluation, and Optimization”. In: *Journal of Cleaner Production* 292 (2021), p. 125802. DOI: 10.1016/j.jclepro.2021.125802. URL: https://doi.org/10.1016/j.jclepro.2021.125802.

[21] Emil Nilsson. “Borehole Thermal Energy Storage Systems for Storage of Industrial Excess Heat: Performance Evaluation and Modelling”. Licentiate Thesis. Linköping, Sweden: Linköping University, 2020. ISBN: 91-7929-902-4. URL: https://liu.diva-portal.org/smash/record.jsf?pid=diva2:1394869.

[22] Odyssee-Mure Project. *Heating consumption per m²*. 2024. URL: https://www.odyssee-mure.eu/publications/efficiency-by-sector/households/heating-consumption-per-m2.html.

[23] Farzin M. Rad and Alan S. Fung. “Solar community heating and cooling system with borehole thermal energy storage – Review of systems”. In: *Renewable and Sustainable Energy Reviews* 60 (2016), pp. 1550–1561. DOI: 10.1016/j.rser.2016.03.025. URL: https://doi.org/10.1016/j.rser.2016.03.025.

[24] Manfred Reuss. “The Use of Borehole Thermal Energy Storage (BTES) Systems”. In: *Advances in Thermal Energy Storage Systems: Methods and Applications*. Ed. by Luisa F. Cabeza. Woodhead Publishing, 2015, pp. 117–138. DOI: 10.1533/9781782420965.1.117. URL: https://doi.org/10.1533/9781782420965.1.117.

[25] Gösta Rosenblad. “Seasonal heat storing 1979–83 in Utby ground heat pump project”. In: *Proceedings of the International Conference on Subsurface Heat Storage – In Theory and Practice*. Stockholm, Sweden: Chalmers University of Technology, 1983, pp. 670–678. URL: https://research.chalmers.se/publication/152672.

[26] Royal Netherlands Meteorological Institute (KNMI). *KNMI Weather Station Data - The Netherlands*. https://www.knmi.nl/home. 2024.

[27] Habibollah Sadeghi, Ramin Jalali, and Rao Martand Singh. “A review of borehole thermal energy storage and its integration into district heating systems”. In: *Renewable and Sustainable Energy Reviews* 192 (2024), p. 114236. DOI: 10.1016/j.rser.2023.114236. URL: https://doi.org/10.1016/j.rser.2023.114236.

[28] Zhiwen Sun, Gangqiang Kong, and Hanlong Liu. “Performance of a ground source heat pump with energy piles and borehole heat exchangers under continuous and intermittent operating modes”. In: *Energy* 294 (2025), p. 137910. DOI: 10.1016/j.energy.2025.137910. URL: https://doi.org/10.1016/j.energy.2025.137910.

[29] Ali H. Tarrad. *A 3-Dimensional Borehole Numerical Modeling for Single and Double U-tube Ground-Coupled Heat Pump*. Université de Lorraine, CNRS, LEMTA, Nancy, France. Professor, Ph.D. Mechanical Engineering. . <YEAR>. DOI: <DOI-if-avai lable>.

[30] The Engineering Toolbox. *Ethylene Glycol - Density and Specific Weight*. https://www.engineeringtoolbox.com/ethylene-glycol-d_146.html. 2023.

[31] The Green Village. *Co-Creation Centre*. 2025. URL: https://www.thegreenvillage.org/co-creation-centre/.

[32] TNO Geological Survey of the Netherlands. *DINOloket: Data and Information on the Dutch Subsurface*. https://www.dinoloket.nl/en. TNO Geological Survey of the Netherlands, 2025.

[33] Bastian Welsch et al. “A Comparative Study of Medium Deep Borehole Thermal Energy Storage Systems Using Numerical Modelling”. In: *Proceedings of the World Geothermal Congress 2015*. International Geothermal Association. Melbourne, Australia, Apr. 2015, pp. 1–7. URL: https://www.academia.edu/108841182/A_Comparative_Study_of_Medium_Deep_Borehole_Thermal_Energy_Storage_Systems_Using_Numerical_Modelling.

[34] Tian You et al. “An overview of the problems and solutions of soil thermal imbalance of ground-coupled heat pumps in cold regions”. In: *Applied Energy* 177 (2016), pp. 515–536. DOI: 10.1016/j.apenergy.2016.05.115. URL: https://doi.org/10.1016/j.apenergy.2016.05.115.

[35] Mohamed E. Zayed et al. “Recent advances in geothermal energy reservoirs modeling: Challenges and potential of thermo-fluid integrated models for reservoir heat extraction and geothermal energy piles design”. In: *Journal of Energy Storage* 70 (2024), p. 107456. DOI: 10.1016/j.est.2024.107456. URL: https://www.sciencedirect.com/science/article/pii/S2352710224022897.

[36] Peng Zhang et al. “Simulation and Analysis of the Thermal-Mechanical Response of an Energy Pile”. In: *Lithosphere* 2022.Special 10 (2022), pp. 1–17. DOI: 10.2113/2022/5506908. URL: https://pubs.geoscienceworld.org/gsw/lithosphere/article/2022/Special%2010/5506908/614300/Simulation-and-Analysis-of-the-Thermal-Mechanical.

[37] Li Zhu and Sarula Chen. “Sensitivity Analysis on Borehole Thermal Energy Storage Under Intermittent Operation Mode”. In: *Energy Procedia* 158 (2019), pp. 3133–3138. DOI: 10.1016/j.egypro.2019.01.740. URL: https://doi.org/10.1016/j.egypro.2019.01.740.

A

Energy Piles Details

Single Energy Pile structural details

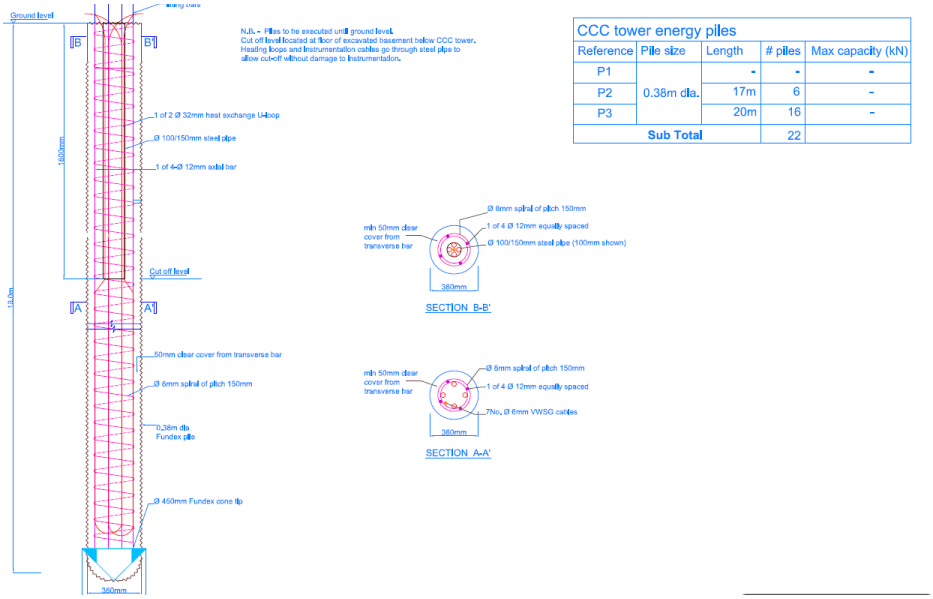

CCC tower energy piles				
Reference	Pile size	Length	# piles	Max capacity (kN)
P1	0.38m dia.	-	-	-
P2		17m	6	-
P3		20m	16	-
Sub Total			22	

Figure A.1: Structural details of energy piles

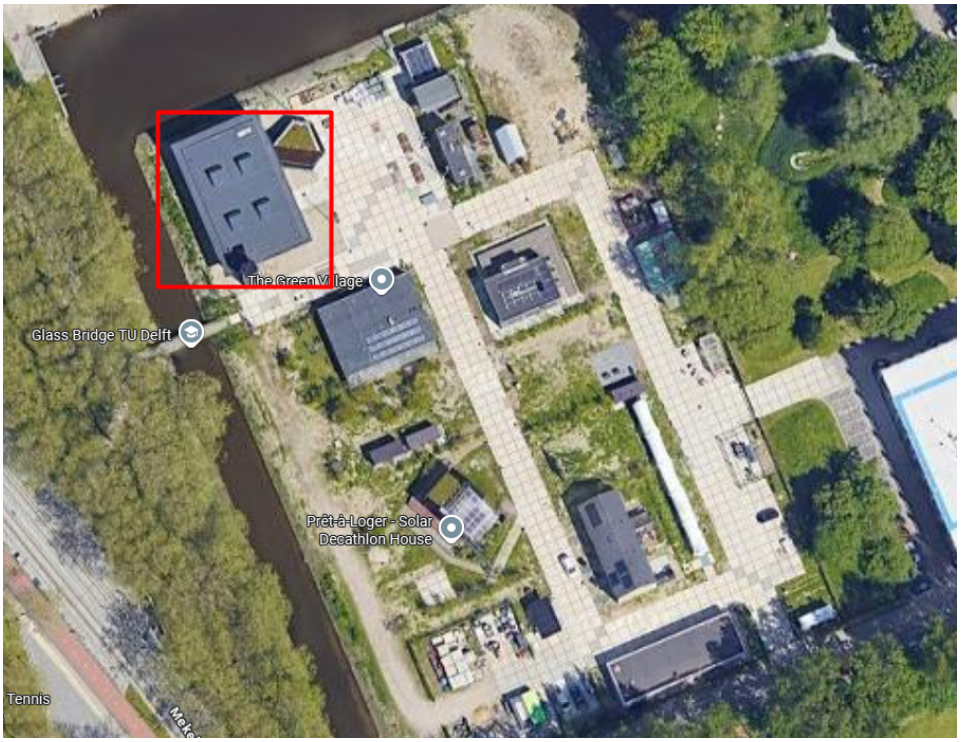

Figure A.2: Location of Co-Creation Center in TU Delft Campus

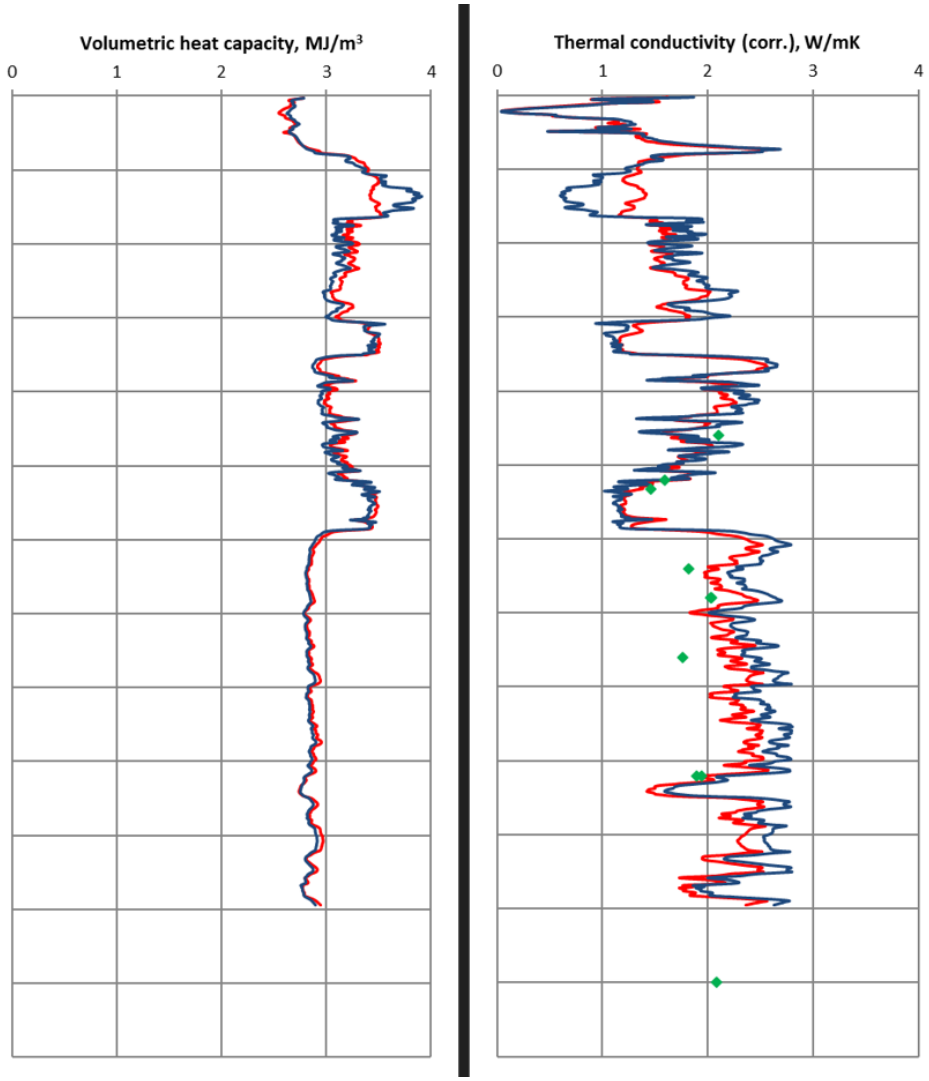

Figure A.3: Estimation of surrounding soil characteristics

B

Operation Scenarios - Input

Below the graphs that were used as an input in the numerical model to be able to conduct the simulations for 5 years with an 8 hour time-step are presented.

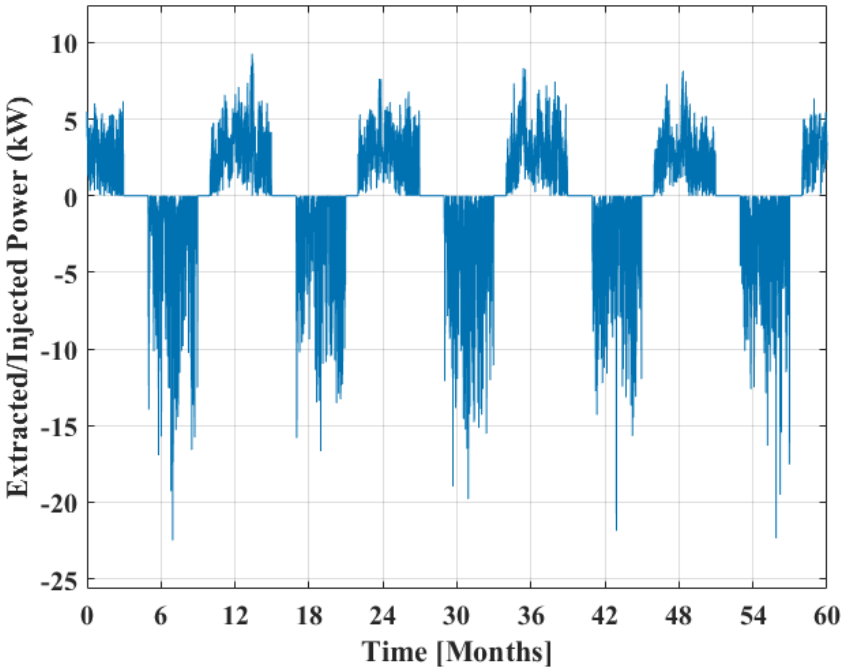

Figure B.1: Extracted / Injected power for Scenario 1 with 8 hour time-step

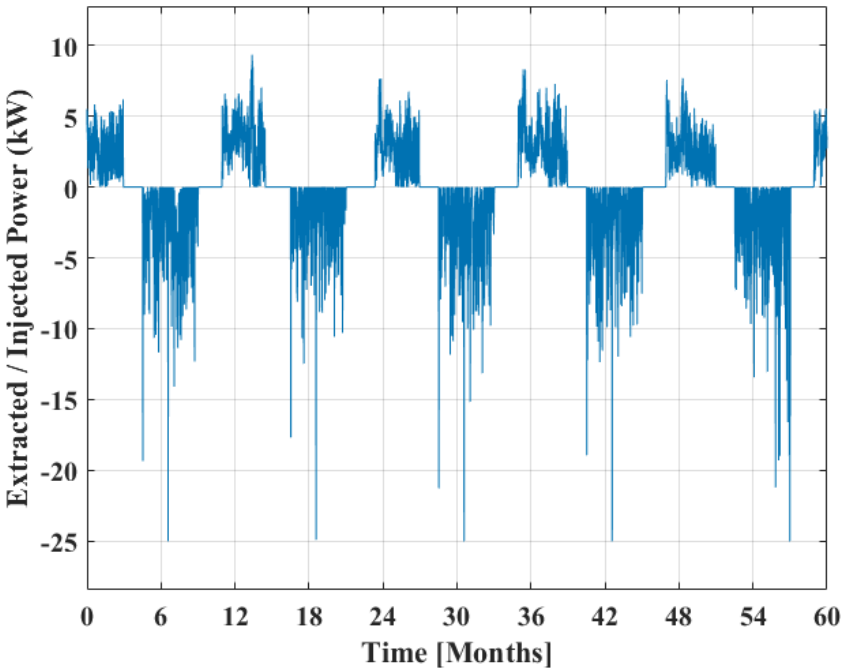

Figure B.2: Extracted / Injected power for Scenario 2 with 8 hour time-step

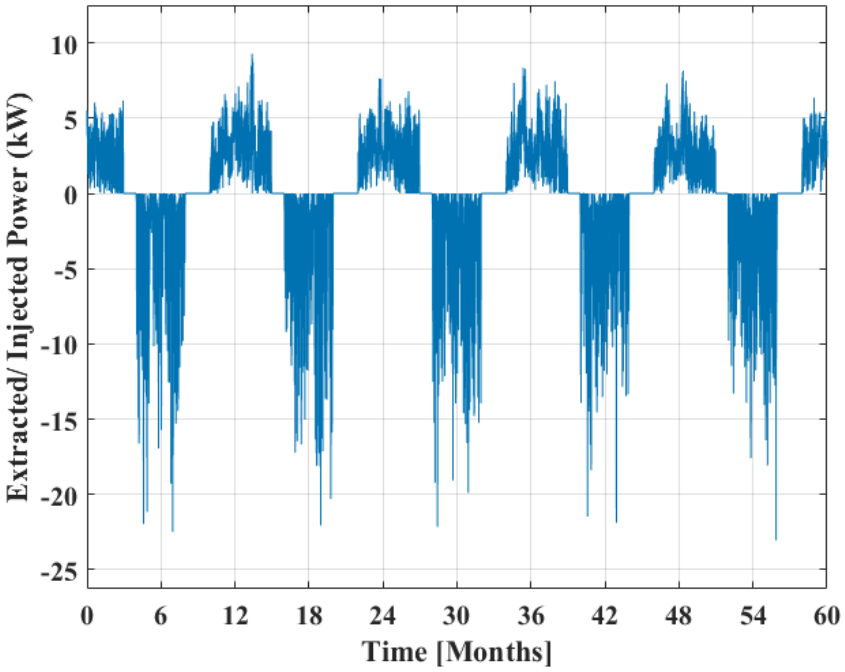

Figure B.3: Extracted / Injected power for Scenario 4 with 8 hour time-step

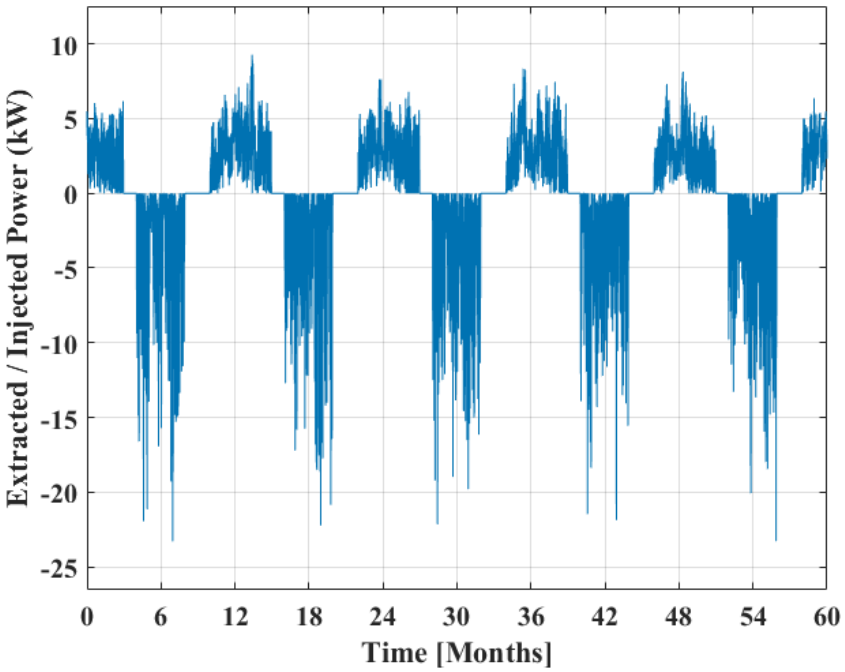

Figure B.4: Extracted / Injected power for Scenario 5 with 8 hour time-step

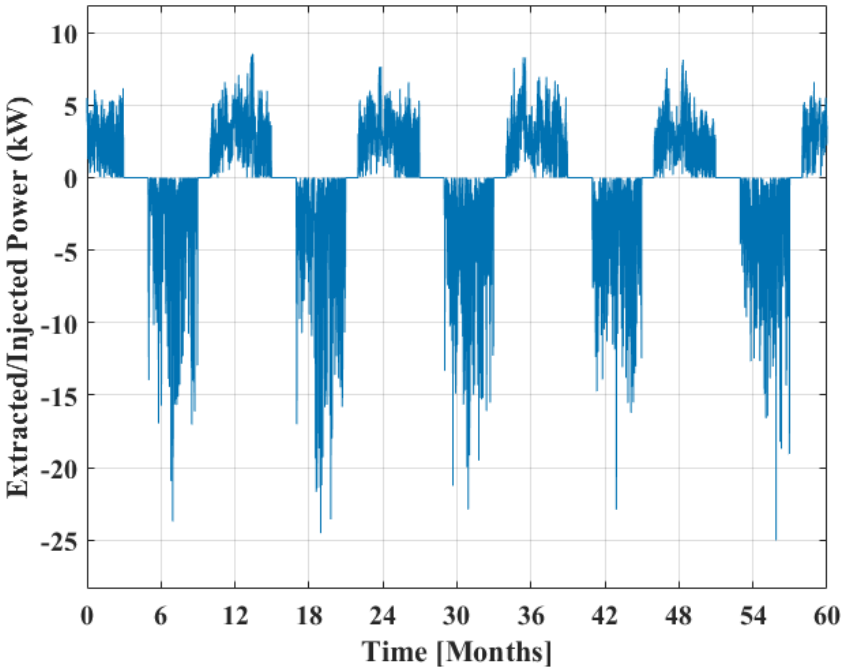

Figure B.5: Extracted / Injected power for Scenario 6 with 8 hour time-step

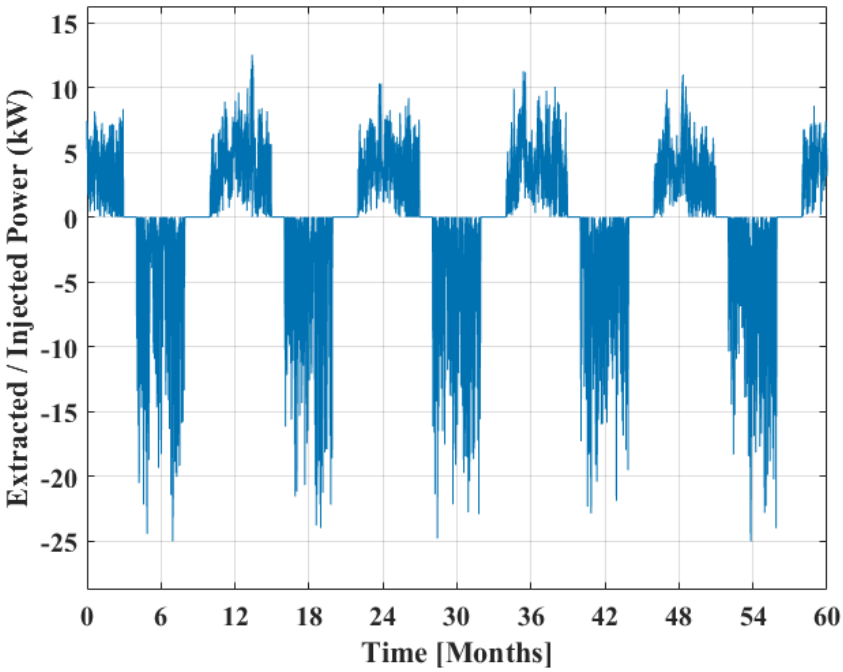

Figure B.6: Extracted / Injected power for Scenario 7 with 8 hour time-step

C

Results of Simulated Scenarios

Below all the explanatory graphs that were not presented inside the text are shown. It needs to be mentioned that every graph follows an 8 hour time-step as it has been mentioned.

Scenario 3

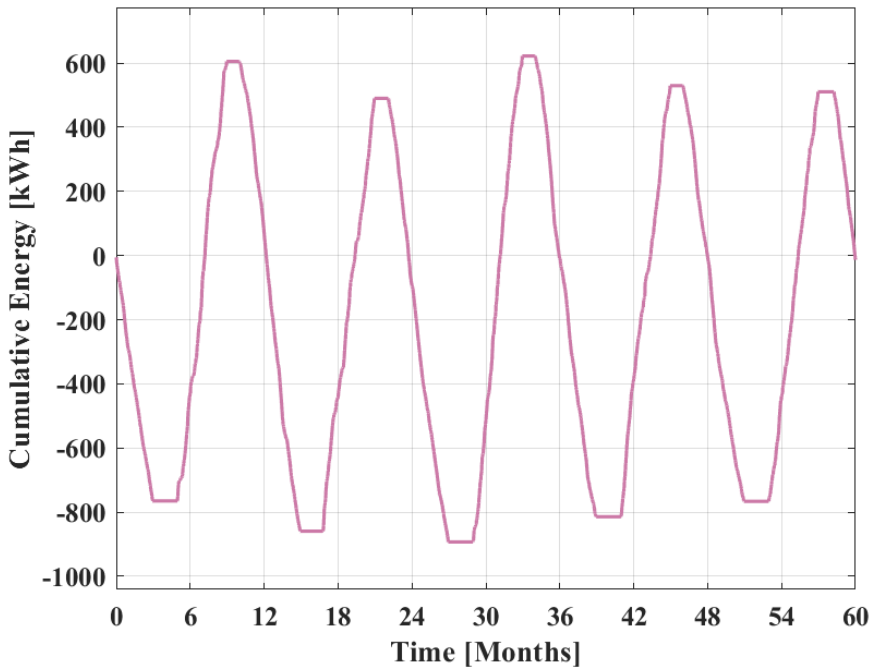

Figure C.1: Cumulative energy balance - Scenario 3

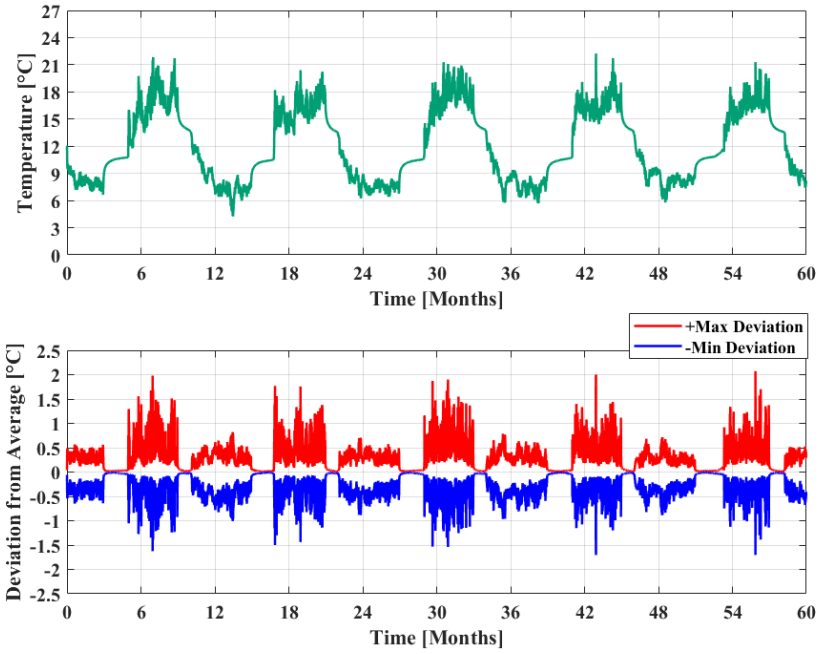

Figure C.2: Average grout temperature and maximum deviation - Scenario 3

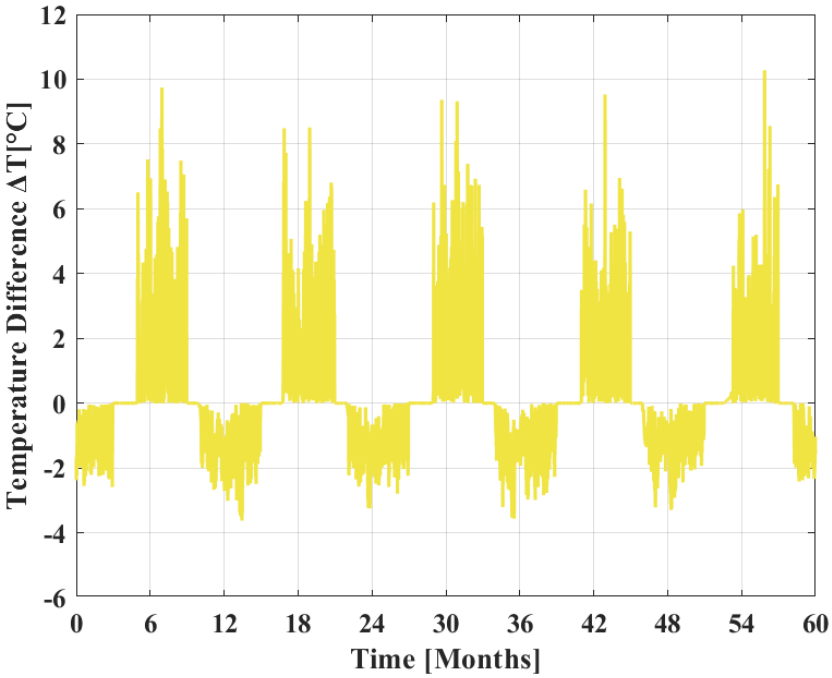

Figure C.3: Temperature difference between inlet and outlet - Scenario 3

Scenario 4

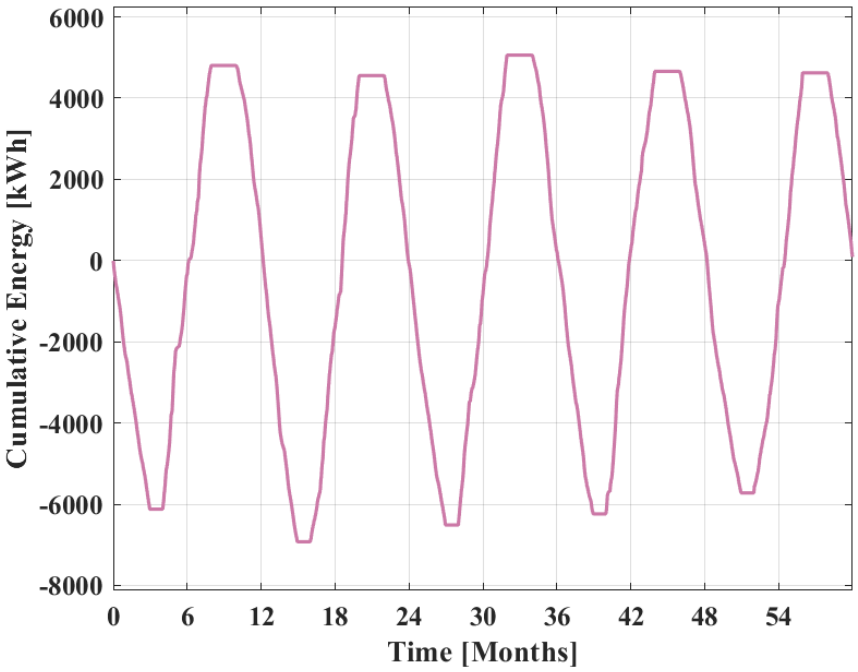

Figure C.4: Cumulative energy balance - Scenario 4

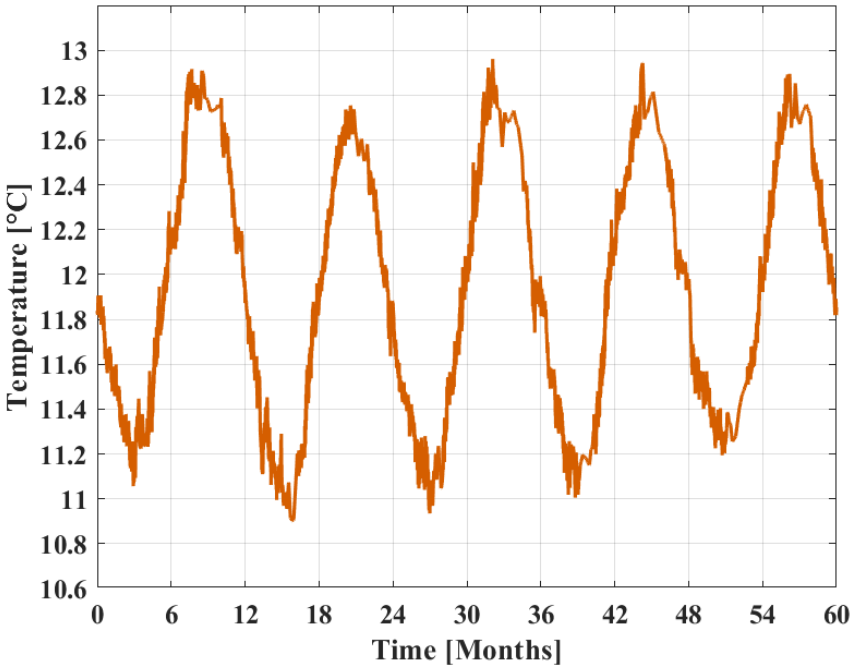

Figure C.5: Average ground temperature - Scenario 4

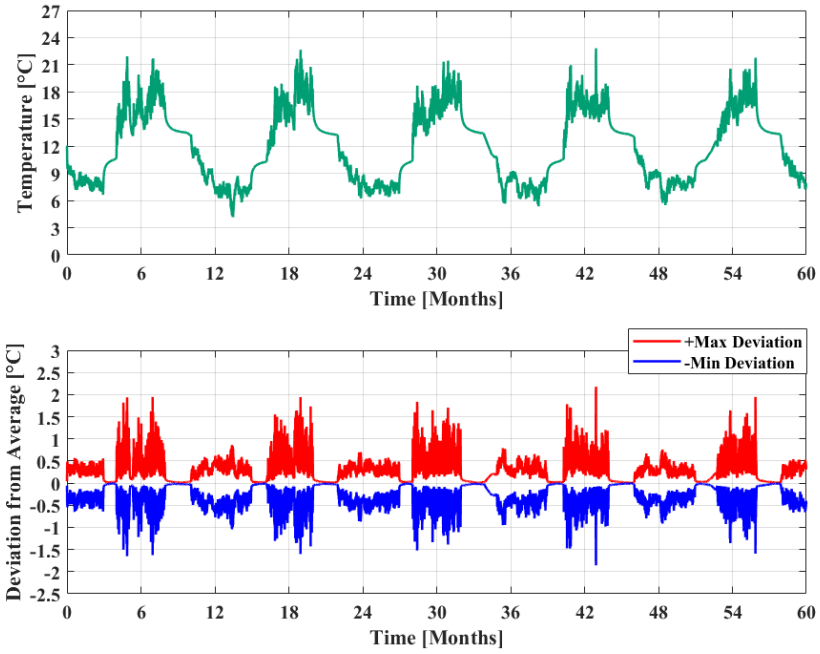

Figure C.6: Average grout temperature and maximum deviation - Scenario 4

Scenario 5

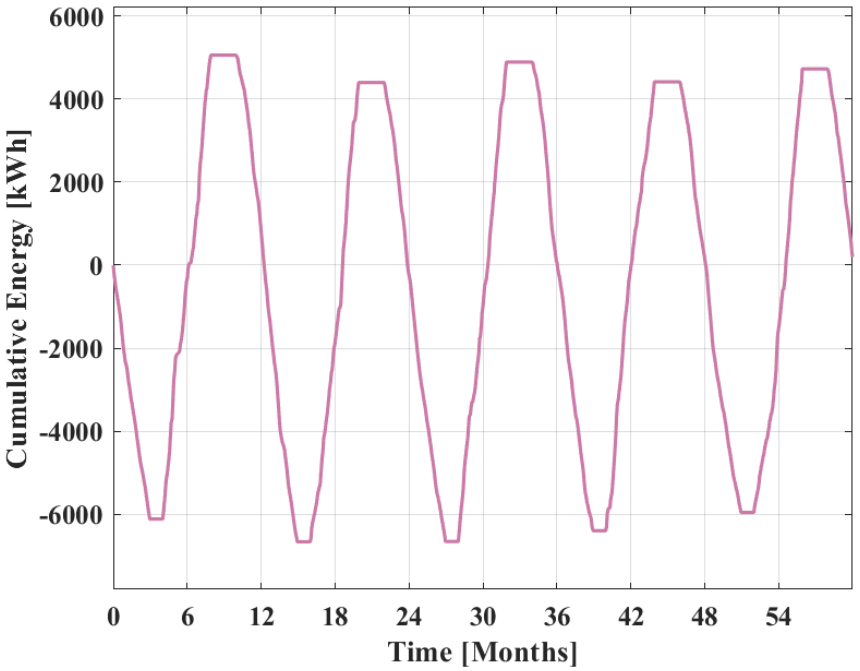

Figure C.7: Cumulative energy balance - Scenario 5

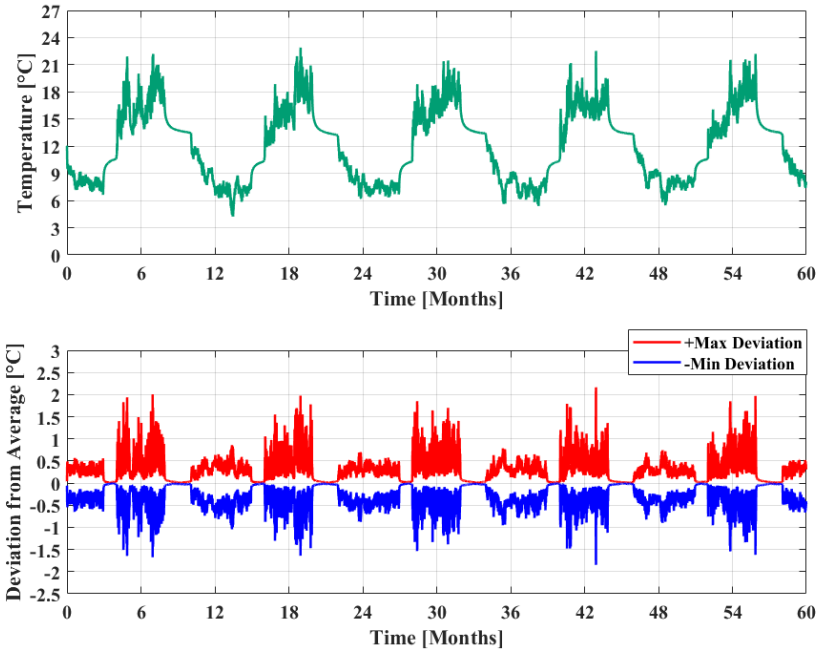

Figure C.8: Average grout temperature and maximum deviation - Scenario 5

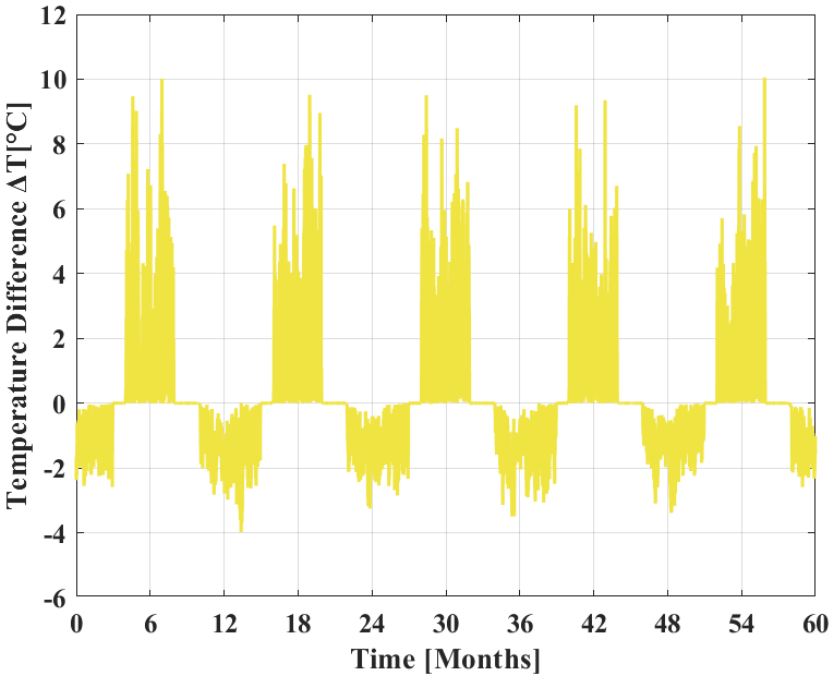

Figure C.9: Temperature difference between inlet and outlet - Scenario 5

Scenario 6

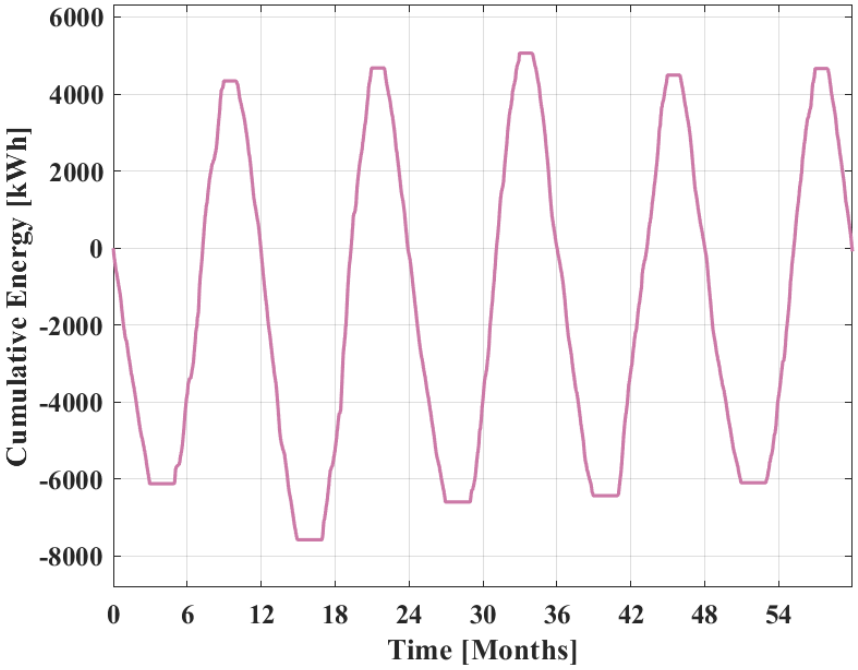

Figure C.10: Cumulative energy balance - Scenario 6

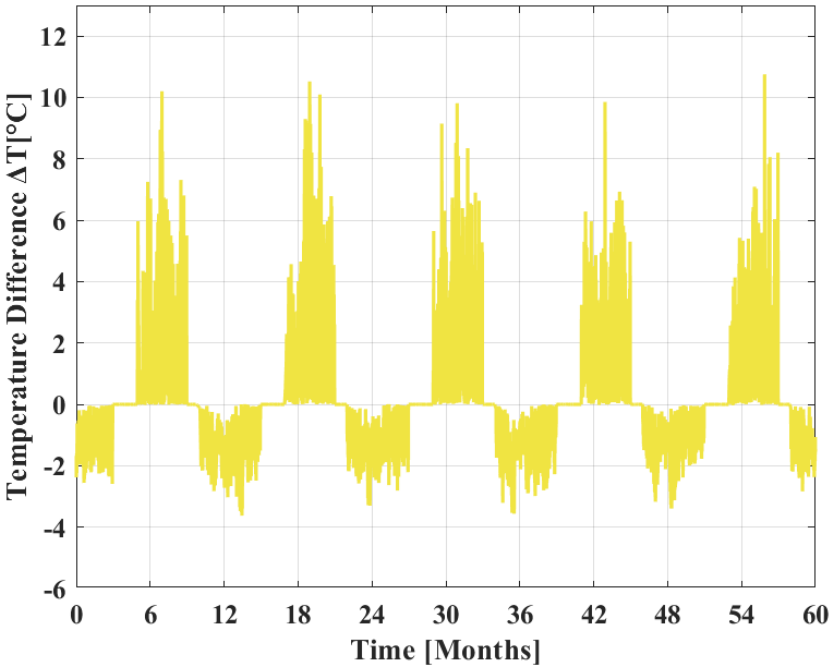

Figure C.11: Temperature difference between inlet and outlet - Scenario 6

Scenario 7

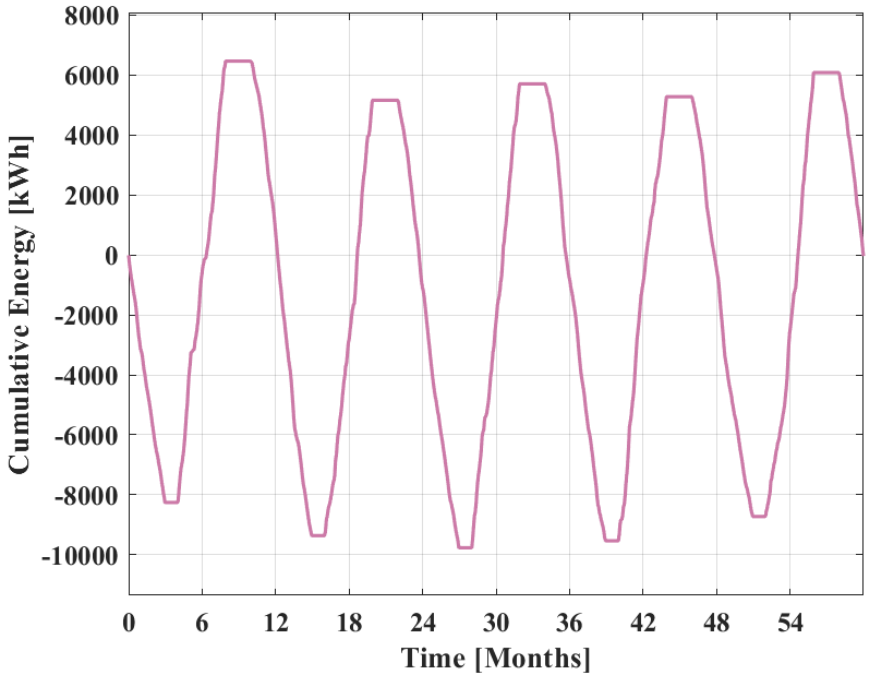

Figure C.12: Cumulative energy balance - Scenario 7

Scenario 8

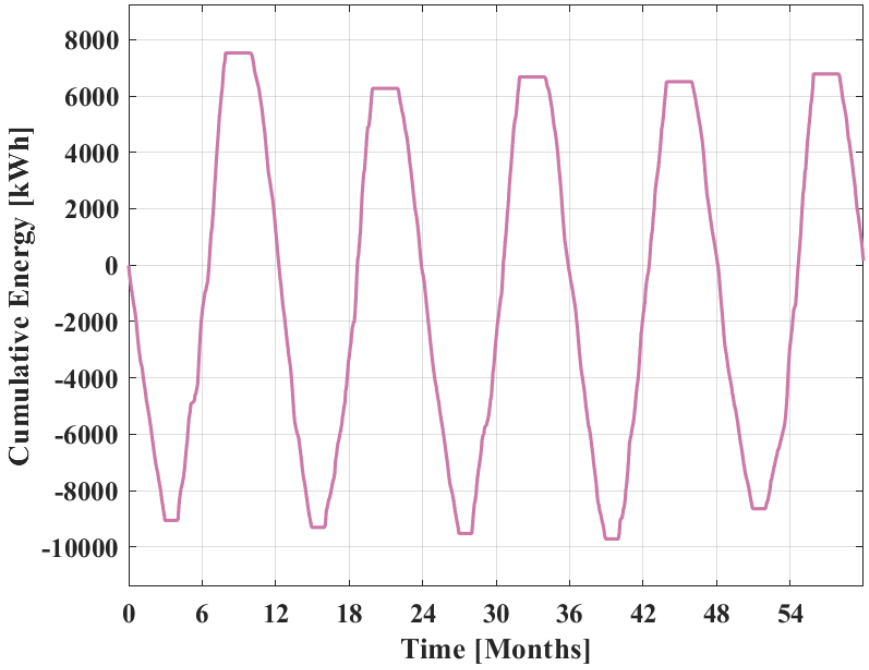

Figure C.13: Cumulative energy balance - Scenario 8

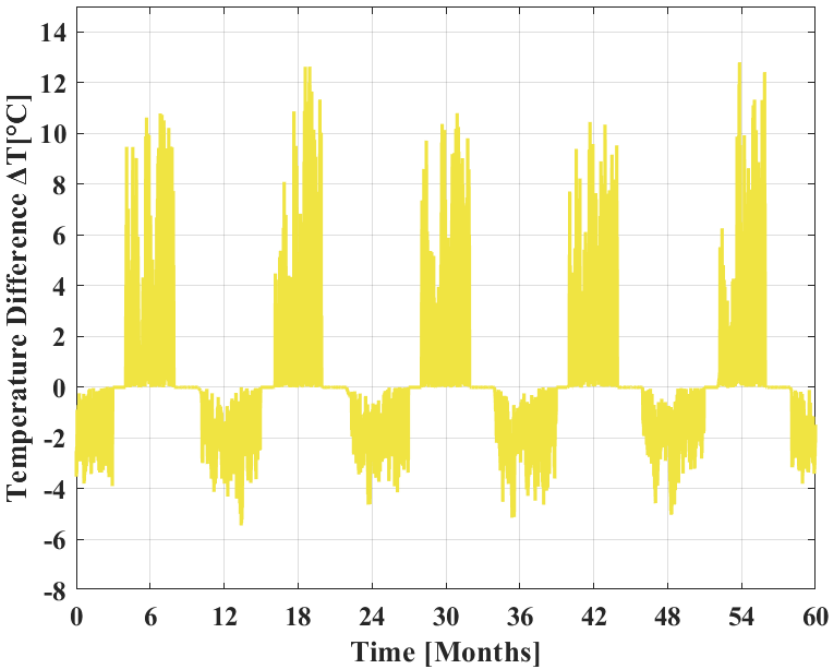

Figure C.14: Temperature difference between inlet and outlet - Scenario 8